Lyle, M., Wilson, P.A., Janecek, T.R., et al., 2002
Proceedings of the Ocean Drilling Program, Initial Reports Volume 199

14. Site 1221[1]

Shipboard Scientific Party[2]

BACKGROUND AND OBJECTIVES

Site 1221 (12°01.999′N, 143°41.572′W; 5175 meters below sea level (mbsl); Fig. F1) forms an equatorial component of the 56-Ma transect drilled during Leg 199 and is situated about three-quarters of the way between the Clipperton and Clarion Fracture Zones in typical abyssal hill topography. On the basis of regional magnetic anomalies, we anticipated the basement age at Site 1221 to be equivalent to Chron C25n (~56 Ma) (Cande et al., 1989), about the same age as Site 1220. At the outset of drilling at Site 1221, our estimate for total sediment thickness was ~150 meters below seafloor (mbsf) (Fig. F2).

Based upon a fixed hotspot model (Gripp and Gordon, 1990, for the 0- to 5-Ma Pacific hotspot rotation pole; Engebretson et al., 1985, for older poles), Site 1221 should have been located about 1° south of the equator at 56 Ma (in an equatorial position at ~50 Ma) and ~2°N at 40 Ma. Thus, Site 1221 should have been situated underneath the South Equatorial Current in the early Eocene. A nearby piston core (EW9709-14PC) taken during the site survey cruise recovered >11 m of red clay with the base of the core containing a calcareous radiolarian ooze dated as early Oligocene age on the basis of radiolarian biostratigraphy (Lyle, 2000).

Site 1221 will be used to study equatorial ocean circulation from the late Paleocene through the late Eocene during the early Cenozoic thermal maximum. Sediment records from this site will help to define the carbonate compensation depth (CCD) during the Paleocene–Eocene and Eocene–Oligocene transitions. In this and other respects, Site 1221 will act as an interesting analog to Site 1220. The two sites are situated on similar age crust and exhibit similar seismic-stratigraphic sequences, but Site 1221 is thought to have crossed the equator ~5 m.y. earlier than Site 1220, during latest early Eocene time (~50 Ma).

F1. Site location map, p. 25.

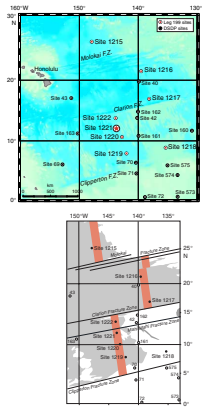

F2. Seismic reflection profile, p. 26.

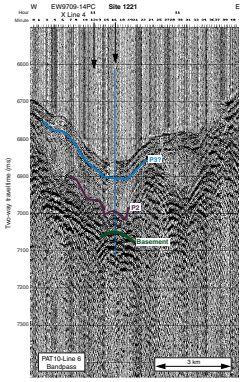

[1]Examples of how to reference the whole or part of this volume.
[2]Shipboard Scientific Party addresses.

SUMMARY

Site 1221 (Fig. F1; 12°01.999′N, 143°41.572′W) forms an equatorial component of the 56-Ma transect drilled during Leg 199. It is situated about three-quarters of the way between the Clipperton and Clarion Fracture Zones in typical abyssal hill topography at a water depth of 5175 mbsl. On the basis of regional seafloor magnetic anomalies, we anticipated basement age at Site 1221 to be equivalent to Anomaly An25n (~56 Ma) (Cande et al., 1989), about the same age as Site 1220. At the outset of drilling at Site 1221, our estimate for total sediment thickness was ~150 m (Fig. F2).

Based upon a fixed hotspot model (Gripp and Gordon, 1990, for the 0- to 5-Ma Pacific hotspot rotation pole; Engebretson et al., 1985, for older poles), Site 1221 should have been located ~1° south of the equator at 56 Ma, in an equatorial position at ~50 Ma, and ~2°N at 40 Ma. Thus, Site 1221 should have been situated underneath the early Eocene equivalent of the South Equatorial Current.

Four holes were drilled at Site 1221. Hole 1221A was abandoned because of a stuck extended core barrel (XCB) that resulted in a pipe trip to clear the bottom-hole assembly (BHA). Hole 1221B recored the Oligocene interval at the top of the sediment column, whereas Hole 1221C was cored to cover the major gaps in the upper sediment column and then cored continuously to basement. Hole 1221D was drilled to obtain a second copy of the lower Eocene and Paleocene sediments.

The heave of the vessel frequently exceeded 5 m while we were drilling at Site 1221. The ship heave compromised the quality and recovery of the core. The uppermost ~20 mbsf encountered severe flow-in problems, whereas in the remaining intervals, the often soupy nature of the sediment (radiolarian ooze) resulted in multisensor track (MST) data that were not suitable for correlation purposes, with the exception of the Paleocene/Eocene (P/E) boundary interval. A continuous sediment column could not be correlated below 19.5 meters composite depth (mcd).

The sediment column is a variation of lithologies seen at other Leg 199 sites. A very thin clay and radiolarian ooze lithologic unit overlies lower Oligocene nannofossil ooze, terminated by an abrupt transition to clay rapidly grading to radiolarian ooze. The abrupt transition is typical of the Eocene/Oligocene (E/O) boundary. At Site 1221, however, shipboard results suggest the latest Eocene and earliest Oligocene time is represented by a hiatus of perhaps 1 m.y. in extent. The middle and upper Eocene radiolarian ooze section is the thickest of any site of Leg 199. Deposition of the radiolarian ooze was highest in the period between 45 and 43 Ma, when sedimentation rates reached 18 m/m.y.

A chert-rich section covering the time interval from ~48 Ma (radiolarian Zone RP11) to 53.8 Ma (nannofossil Subzone CP9a) lies beneath the radiolarian ooze. Although only chert was recovered, coring times were relatively short, suggesting a significant amount of radiolarian ooze or clay is also present. Hole 1221C was drilled somewhat faster than Hole 1221D, indicating some variability in the thickness and areal extent of the chert. In the recovered sediments below the chert unit, clay layers in Hole 1221C can be correlated to clay layers in Hole 1221D. Beneath the chert-rich interval are nannofossil chalks of early Eocene–Paleocene age that comprise the basal sedimentary unit. Within this basal chalk, we recovered two copies of the P/E boundary interval. The P/E boundary interval is recognizable by a multicolored clay-rich

unit remarkably similar in structure to the P/E boundary interval at Site 1220, 206 km to the south. The lowermost chalks above basement were dated at 56.5–57 Ma with foraminifers and nannofossils.

Physical properties of the sediments follow lithology. The densest unit is the lower Eocene chalk (~1.6–1.8 g/cm^3) followed by the upper clays and nannofossil ooze. The radiolarian ooze sediments have the lowest wet bulk densities (~1.14 g/cm^3) and the highest porosities (~84%) as well as the highest velocities of the unconsolidated sediments (1530–1550 m/s).

Biostratigraphic analyses indicate that Site 1221 contains a continuous sequence of radiolarian-bearing sediments from the early Oligocene through the early Eocene. The uppermost sequence contains considerable quantities of reworked middle Eocene radiolarians, whereas the interval from ~7 to 111 mbsf is almost exclusively brown radiolarian ooze with a sugary texture. No radiolarians were recovered in the chert-rich interval except in the core catcher of Core 199-1221C-10X at a depth of 141 mbsf. These radiolarians are from the late Paleocene–early Eocene Zone RP7. No radiolarians are found in the basal chalk.

The sediments of Site 1221 contain calcareous microfossils in only the uppermost and lowermost units. Calcareous microfossils are completely absent in the siliceous sediments between ~7 and ~111 mbsf, and biostratigraphic control through this interval was provided entirely by radiolarians. The carbonate content of sediments increased in the basal reaches of Holes 1221C and 1221D, and nannofossil and planktonic foraminiferal biostratigraphies allow basic zonation of a condensed sequence of lower Eocene nannofossil ooze and chert. Section 199-1221C-11X-3 contains an interval of dramatic and colorful banding, the base of which, as at Site 1220, corresponds to the extinction of Paleocene benthic foraminifers and, therefore, the P/E boundary. Preservation of calcareous microfossils improves below the P/E boundary, and planktonic foraminifers and nannofossils allow a detailed zonation of upper Paleocene nannofossil ooze and clay. Calcareous benthic foraminiferal assemblages are present only in the basal sediments below 140 mbsf. These assemblages are moderately well preserved, but the presence of small calcite microcrystals on the surfaces of the tests indicate some diagenetic alteration.

Interstitial pore water profiles from Site 1220 are very similar to the profiles of all other Leg 199 sites except Site 1219 and primarily reflect minor organic matter degradation, the dissolution of biogenic silica, and minor alteration of underlying basalt. The bulk geochemistry of the sediments from Site 1221 reflect the shifts in lithology between sediments dominated by silica and carbonate.

Highlights

P/E Boundary

The P/E boundary was recovered twice (interval 199-1221C-11X-3; 50–90 cm, and interval 199-1221D-4X-2, 70–125 cm). The two intervals are very similar, with the interval in Hole 1221D appearing slightly expanded relative to that in Hole 1221C and exhibiting more disturbance.

The benthic foraminiferal fauna were examined in small surface scrapes prior to more complete shore-based analysis. The first occurrence of Eocene benthic foraminifers is at 50 cm in Section 199-1221C-11X-3, whereas the last occurrence of Paleocene forms is at ~91 cm in the same section.

The Site 1221 P/E boundary interval appears remarkably similar to that recovered at Site 1220. Distinctive brown, pink, black, and dark brown layering can be correlated between the two sites 206 km apart.

OPERATIONS

Transit to Site 1221 (PAT-10B)

The 144-nmi transit to proposed Site PAT-10B was accomplished in 17.0 hr at an average speed of 8.5 kt. The vessel did not proceed directly to proposed Site PAT-10B because of strong winds (27–31 kt) and wind-driven seas (combined sea and swell >6 m). To avoid heavy pounding, the vessel pursued a course at a reduced speed that exposed the starboard quarter to the elements for most of the transit. The second half of the dog-leg track required the vessel to steer almost directly into the seas. The vessel motion was moderate with maximum pitch and heave values measured at 6°. The modified track added 33 nmi to the transit.

At 0230 hr on 5 December 2001, the vessel slowed to 4 kt, and a short 3.5-kHz survey was made from east to west across the site. Upon conclusion of the 42-min survey, the vessel came about and returned to site as the thrusters were lowered and the dynamic positioning system (DPS) was activated. The Global Positioning System receiver interface to the DPS was employed to situate the vessel over the coordinates of the new location by 0315 hr. A beacon was deployed at 0425 hr. The corrected precision depth recorder (PDR) depth was 5197.4 meters below rig floor (mbrf).

Hole 1221A

After the drill string was deployed to a depth of 5157 mbrf, the driller lowered the bit until the heave compensator appeared to activate, suggesting contact with a firm seafloor. Hole 1221A was spudded with the advanced piston corer (APC) at 1425 hr on 5 December, 2001. The seafloor depth that was indicated by the recovery of the initial core was 5186.6 mbrf. This depth was 10.8 m shallower than the PDR depth.

Piston coring in Hole 1221A advanced to the APC refusal depth of 110.6 mbsf with an average recovery of 102.8% (Table T1). Core orientation began with Core 3H. During piston coring, the heave of the vessel frequently exceeded 5 m and compromised the quality and recovery of the core. It was also difficult to land the APC assembly in the BHA without parting the overshot shear pin. Because of the excessive vessel motion combined with the deep water, it was also difficult to ascertain whether the APC actually fired or was hydraulically pushed into the sediment after the shear pin parted during landing.

T1. Coring summary, p. 49.

XCB operations began with Core 13X, and the interval from 110.5 to 115.6 mbsf was cored in 15 min. Most of the rotating time was consumed penetrating the first 2 m of this interval. Upon retrieval of the core, the core barrel became stuck in the BHA. Efforts to recover the core barrel by alternately applying overpull and upward impacts with the wireline jars were given up after 40 min. The overshot shear pin was intentionally parted, and the wireline recovered. The drill string was pulled out of the hole and tripped to a depth of 3572 m, where another attempt was made to recover the stuck core barrel. This effort was unsuccessful. The BHA reached the rig floor at 0215 hr on 7 December and

the core barrel was removed. Only 0.14 m of chert fragments were salvaged from the core catcher.

A fresh bit seal and lockable float valve were installed, and the BHA was redeployed. Concurrently, the vessel was offset 20 m south of Hole 1221A in preparation for spudding Hole 1221B.

Hole 1221B

Hole 1221B operations were designed to retrieve two cores near the mudline in an interval that contained the E/O boundary. Hole 1221B was spudded with the APC at 1400 hr on 7 December and advanced to 14.2 mbsf (two cores) with 102.3% recovery. The estimated seafloor depth that was calculated from the recovery of the first core was 5186.4 mbrf. The bit cleared the seafloor at 1505 hr on 7 December.

Hole 1221C

Hole 1221C was spudded with the APC at 1640 hr on 7 December, and the estimated seafloor depth that was calculated from the recovery of the first core was 5185.7 mbrf. This hole was spot cored (five cores) with the APC to a depth of 102.5 mbsf to recover material missed in Hole 1221A. The cored interval was 45.4 m with an average recovery of 96.3% (Table T1). The last three cores were oriented.

XCB coring (Cores 6X through 12X) deepened the hole from 102.5 mbsf to a basement contact at 157.3 mbsf. Abundant chert stringers adversely affected recovery. The average recovery over the 45.4-m cored interval was 43.7%. Upon completion of Hole 1221C, the bit was pulled to the seafloor at 1530 hr on 8 December. The vessel was then offset 20 m south in order to spud the last hole.

Hole 1221D

Hole 1221D plans were to drill ahead (in the interest of time) to 132.0 mbsf and then core to basement in the hope of recovery a second P/E boundary at this site. Hole 1221D was spudded with the XCB and a center bit at 1715 hr. After drilling ahead to 132 mbsf, the center bit was recovered and an XCB barrel was deployed. XCB coring advanced from 132.0 to 156.0 mbsf (Table T1). The interval from 144.8 to 151.0 mbsf was drilled ahead with a center bit to reduce penetration time. Basement contact was confirmed by the recovery of the basalt in the last core. The cored interval was 17.8 mbsf with 2.28% recovery. The drilled interval was 138.2 m.

After recovering the drill string, the vessel departed for the last site of the leg at 2100 hr on 9 December.

LITHOSTRATIGRAPHY

The sedimentary section at Site 1221 consists of 156 m of pelagic sediment dominated by Eocene radiolarian ooze and chert, which overlie lower Eocene to uppermost Paleocene chalks. Intervals containing both the E/O boundary and P/E boundary were recovered. The lithologic descriptions are primarily based on Holes 1221A and 1221C because they contained most of the recovered material from the site. The section at Site 1221 is divided into four lithologic units on the basis of sedimentary facies (Fig. F3). Unit I is a thin (1.12 m) clay and radiolarian ooze of

F3. Lithologic summary, p. 27.

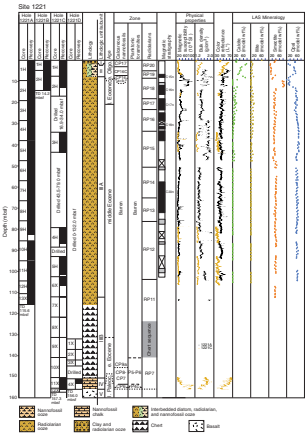

early Oligocene and younger age. Unit II contains 6.28 m of nannofossil ooze and diatom ooze of early Oligocene age. Unit III comprises a 143.10-m-thick sequence of upper and middle Eocene age of radiolarian ooze resting on chert. Unit IV is a 5.50-m-thick sequence that is dominated by nannofossil chalk with clay of late Paleocene–early Eocene age and contains the P/E boundary. Unit V is represented by basalt fragments recovered at the base of the section.

Unit I

Intervals: 199-1221B-1H-1, 0–121 cm, and 199-1221C-1H-1, 0–112 cm
Depths: 0.00–1.21 mbsf (Hole 1221B) and 0.00–1.12 mbsf (Hole 1221C)
Age: early Oligocene through Neogene
Lithology: radiolarian ooze with clay

Unit I is composed of 1.12 m of brown to yellowish brown (10YR 4/3 to 10YR 4/4) radiolarian ooze with clay; abundant black (10YR 2/1) mottling is also present. This unit may reflect an erosional lag and contains an admixture of diatoms, Fe-Mn oxides, and opaque minerals. This unit was not recovered in Hole 1221A due to overpenetration.

Unit II

Intervals: 199-1221A-1H-1, 0 cm, through 1H-6, 100 cm; 199-1221B-1H-1, 121 cm, through 1H-3, 20 cm; and 199-1221C-1H-1, 112 cm, through 1H-4, 134 cm
Depths: 4.61–8.50 mbsf (Hole 1221A); 1.21–3.20 mbsf (Hole 1221B); and 1.12–5.84 mbsf (Hole 1221C)
Age: early Oligocene
Lithology: nannofossil ooze and diatom ooze

Unit II contains interbedded nannofossil and diatom oozes with varying amounts of radiolarians, clay, and volcanic glass. Interbedding is present on the scale of tens of centimeters with gradational boundaries between lithologies. The nannofossil ooze ranges in color from dark yellowish brown (10YR 4/4) to yellowish brown (10YR 5/4); the diatom ooze ranges from yellowish brown (10YR 5/4) to dark brown (10YR 3/3). Large (~5 cm) very pale brown (10YR 8/2 and 10YR 8/3) mottles are common. The drilling disturbance at the top of the cores from this site affects the continuity of the upper portion of Unit II as well as the sediments of Unit I.

Unit III

Intervals: 199-1221A-1H-6, 100 cm, through 13X-CC; 199-1221B-1H-3, 20 cm, through 2H-CC; 199-1221C-1H-4, 134 cm, through 10X-CC; and 199-1221D-2X-CC, 0 cm, through 3X-CC
Depths: 8.5–115.6 mbsf (Hole 1221A); 3.2–14.2 mbsf (Hole 1221B); 5.8–150.4 mbsf (Hole 1221C); and 132.0–144.8 mbsf (Hole 1221D)
Age: middle to late Eocene
Lithology: radiolarian ooze and chert

Unit III is siliceous in character and is divided into two subunits based on lithology. Subunit IIIA is radiolarian ooze and radiolarian ooze with clay, and Subunit IIIB is dominated by chert.

Subunit IIIA

Intervals: 199-1221A-1H-6, 100 cm, through 12H-CC; 199-1221B-1H-3, 20 cm, through 2H-CC; and 199-1221C-1H-4, 134 cm, through 6X-CC
Depths: 8.5–110.6 mbsf (Hole 1221A); 3.2–14.2 mbsf (Hole 1221B); and 5.8–112.1 mbsf (Hole 1221C)
Age: late Eocene
Lithology: radiolarian ooze and radiolarian ooze with clay

Subunit IIIA contains a 104.7-m sequence dominated by dark brown radiolarian ooze with lighter-colored mottles. The uppermost 4 m of Subunit IIIA is dominated by a dark brown (10YR 3/3) to very dark brown (7.5YR 2.5/2) zeolitic clay that contains radiolarians, Fe-Mn oxides, and opaques. Colors of the radiolarian ooze range from very dark brown (7.5YR 2.5/3) to strong brown (7.5YR 4/6). The mottles are usually very pale brown (10YR 8/3) to light brown (7.5YR 6/4), although occasionally darker mottles are present. Intervals of dark brown (10YR 3/3) zeolitic clay are present within the radiolarian ooze. Mn nodules, pumice, and a one centimeter-sized fish tooth (Section 199-1221A-6H-1, 14 cm) are also present.

Subunit IIIB

Intervals: 199-1221A-13X-CC, 0–14 cm; 199-1221C-7X-CC, 0 cm, through 10X-CC; and 199-1221D-2X-CC, 0 cm, through 3X-CC
Depths: 110.6–115.6 mbsf (Hole 1221A); 112.1–150.4 mbsf (Hole 1221C); and 132.0–144.8 mbsf (Hole 1221D)
Age: early to middle Eocene
Lithology: chert

Recovery of Subunit IIIB was poor in all holes and consists of chert fragments and drilling breccia. The chert is generally black (N1), and larger fragments often exhibit banding ranging from dark yellowish brown (10YR 4/4) to white (10YR 8/1); the banding is interpreted as flattened burrows and mottles later replaced by silica.

Unit IV

Intervals: 199-1221C-11X-1, 0 cm, through 12X-CC, 8 cm; and 199-1221D-4X-1, 0 cm, through 4X-CC, 17 cm
Depths: 150.40–156.20 mbsf (Hole 1221C) and 151.00–153.18 mbsf (Hole 1221D)
Age: late Paleocene to early Eocene
Lithology: calcareous chalk, nannofossil chalk, and zeolitic clay

Unit IV is dominated by calcareous and nannofossil chalk and contains an interval of zeolitic clay with dramatic color variations (Fig. F4). The upper portion of the unit contains very pale brown (10YR 8/2 to 10YR 7/3) to light reddish brown (5YR 6/4) calcareous chalk with nannofossils and clay and dark yellowish brown (10YR 4/4) nannofossil chalk. The middle portion of the unit is a zeolitic clay exhibiting exten-

F4. P/E boundary intervals, p. 28.

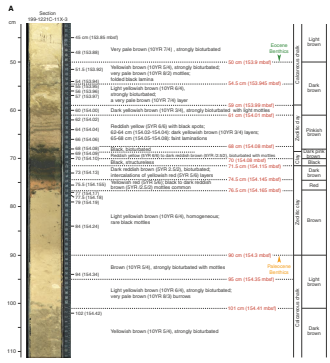

sive color banding with millimeter- to centimeter-scale laminations and layering. The lower portion of the unit contains a very pale brown (10YR 7/4 and 10YR 8/4) to brown (10YR 4/3) calcareous chalk. Some chert fragments and occasional microfaulting were observed in Unit IV.

Sediment of the P/E Boundary Interval

The P/E boundary lies within Unit IV (see **"Biostratigraphy,"** p. 9), and was recovered twice (intervals 199-1221C-11X-3, 50–90 cm, and 199-1221D-4X-2, 70–125 cm). The two intervals are very similar, with the interval in Hole 1221D appearing slightly expanded relative to that in Hole 1221C and exhibiting more disturbance (i.e., microfaults in interval 199-1221D-4X-2, 80–86 cm, and folded laminations in intervals 199-1221D-4X-2, 17–26 and 54–56 cm). A detailed lithologic stratigraphy of these two P/E boundary intervals is presented in Figure **F4** and summarized below.

The first temporal occurrence of Eocene benthic foraminifers is at 50 cm in Section 199-1221C-11X-3 (see **"Benthic Foraminifers,"** p. 12, in "Biostratigraphy") in the transition between a very pale brown (10YR 7/4) to yellowish brown (10YR 5/4) calcareous chalk. A similar lithologic transition occurs in Section 199-1221D-4X-2 at 70.5 cm; however, no biostratigraphic samples were taken from Hole 1221D. This chalk is strongly bioturbated, as evidenced by common light brown (10YR 7/3) burrows and mottles.

Below the chalk is a zeolitic clay interval (intervals 199-1221C-11X-3, 59–69 cm, and 199-1221D-4X-2, 79–96.5 cm), which darkens downcore from reddish yellow (5YR 6/6) to dark brown (10YR 2/2). The downcore decrease of light yellowish brown (10YR 6/4) burrows indicates that bioturbation is strong at the top of the clay and moderate toward the bottom; laminations of color, if not in lithology, are observed in intervals 199-1221C-11X-3, 65–68 cm, and 199-1221D-4X-2, 84–87 cm.

Beneath the zeolitic clay interval lies a narrow band of clay (intervals 199-1221C-11X-3, 69–71.5 cm, and 199-1221D-4X-2, 96.5–97.5 cm), which is dark reddish brown (5YR 2.5/2) to black (10YR 2/1). It is generally structureless, with faint dark mottling present in the top of the clay in Hole 1221C.

Underlying the clay is another zeolitic clay (intervals 199-1221C-11X-3, 71.5–90 cm, and 199-1221D-4X-2, 97.5–126 cm), which lightens downcore from dark brown (5YR 2.5/2 and 10YR 2/2) to light brown (10YR 6/4 and 10YR 6/6). Common to minor mottling and burrowing is present in the upper portion of the zeolitic clay; the lower portion is generally homogeneous in appearance. A prominent yellowish red (5YR 5/6) horizon is present near the top of this zeolitic clay (Sections 199-1221C-11X-3, 74.5–76.5 cm, and 199-1221D-4X-2, 101.5–106 cm). This yellowish red color band is very similar to one described in the same stratigraphic position at Site 1220.

The last temporal occurrence of Paleocene benthic foraminifers is at the base of this zeolitic clay (Sections 199-1221C-11X-3, 90 cm, and 199-1221D-4X-2, 126 cm), where it gradually changes to a calcareous chalk over a span of several centimeters. This lowermost chalk interval is very pale brown (10YR 7/4 and 10YR 6/4) and exhibits moderate bioturbation in the form of light colored burrows.

Unit V

Interval: 199-1221D-4X-CC, 17–22 cm
Depth: 153.18–153.23 mbsf
Age: late Paleocene
Lithology: basalt

Two 3-cm-sized fragments of partially weathered basalt were recovered at the bottom of Hole 1221D. The basalts are fine grained and phaneritic.

Discussion/Summary

At Site 1221, Paleocene seafloor basalt is overlain by 156 m of pelagic sediment. The lowermost sedimentary unit, Unit IV, contains a dramatically colored P/E boundary interval consisting of reddish yellow zeolitic clay beneath a black, oxide-rich clay. The clay layers are present within calcareous and nannofossil chalks. The color variation is the result of changes in mineralogy and geochemistry (see **"P/E Boundary,"** p. 19, in "Geochemistry"). The sequence is remarkably similar to the P/E boundary interval obtained 206 km to the south, at Site 1220 (see Fig. **F30,** p. 81, in the "Leg Summary" chapter).

The Eocene siliceous sediments of Unit III, radiolarian ooze overlying chert, dominate the lithology of Site 1221. This section of siliceous material is comparable to the radiolarian oozes, cherts, and radiolarites drilled at other sites (e.g., Sites 1216–1220) and may represent a broad zone of low-latitude biological productivity during the middle and late Eocene.

The E/O boundary interval was also recovered near the top of the sediment section at Site 1221. It is present as a gradational transition from siliceous (Unit III) to carbonate sedimentation (Unit II), similar to that observed elsewhere in the region (e.g., Sites 1218, 1219, and 1220). The transition from Eocene siliceous sediments to Oligocene carbonates reflects a deepening of the CCD during the Oligocene (van Andel et al., 1975).

The thin cover of sediments overlying the E/O boundary interval is probably the result of some combination of sediment removal by abyssal processes and declining sedimentation rates as this site moved northward on the Pacific plate during the later Oligocene and Neogene.

BIOSTRATIGRAPHY

The four holes drilled at Site 1221 yielded a sequence of lower Oligocene–lower Eocene radiolarian clay and ooze and a condensed (~16 m) section of upper Paleocene–lower Eocene nannofossil ooze and chalk. Radiolarian and nannofossil biostratigraphy indicate the presence of the E/O boundary in Cores 199-1221A-1H, 199-1221B-2H, and 199-1221C-1H. However, the exact placement of this boundary at Site 1221 cannot be constrained because of the absence of planktonic foraminifers, upon which the E/O boundary is defined. Calcareous microfossils are completely absent in the siliceous sediments between ~8 and ~96 mcd, and biostratigraphic control through this interval is provided entirely by radiolarians. The carbonate content of sediments increases in the basal 17 m of Site 1221, and nannofossil and planktonic foraminiferal biostratigraphy allow basic zonation of a condensed sequence

of lower Eocene nannofossil ooze and chert. Section 199-1221C-11X-3 contains an interval of colorful strata, the base of which, as at Site 1220, corresponds to the extinction of Paleocene benthic foraminifers and, therefore, the P/E boundary. Preservation of calcareous microfossils improves below the P/E boundary, and planktonic foraminifers and nannofossils allow a detailed zonation of upper Paleocene nannofossil ooze and clay, which constitutes the short section recovered in Core 199-1221C-12X. The biostratigraphic results are summarized in Figure **F5** and in Tables **T2** and **T3.**

F5. Calcareous and siliceous biostratigraphy, p. 30.

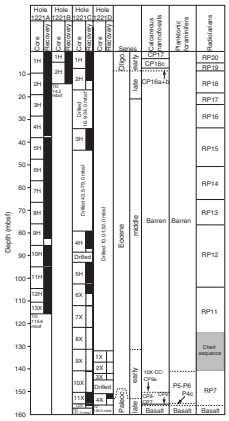

T2. Calcareous nannofossil datum events, p. 51.

T3. Radiolarian zonal boundaries, p. 52.

Calcareous Nannofossils

Lower Oligocene and Eocene–Oligocene Transition

The uppermost carbonate-bearing sediment in the mudline core of Hole 1221B contains abundant nannofossils showing poor preservation. Sample 199-1221B-1H-1, 127 cm, taken immediately below the overlying radiolarian ooze, contains a low-diversity assemblage belonging to Zone CP17 (lower NP23) of the lower Oligocene, which includes *Coccolithus pelagicus, Cyclicargolithus floridanus, Dictyoccites bisectus, Dictyoccoccites hesslandii, Discoaster deflandrei, Discoaster nodifer, Discoaster tanii,* and *Sphenolithus moriformis*. Samples from Section 199-1221B-1H-2 contain apical parts of lower Oligocene sphenoliths, presumably originating from *Sphenolithus predistentus* and *Sphenolithus tribulosus*. The last occurrence of *Reticulofenestra umbilicus* is constrained within a 49 cm interval in Section 199-1221B-1H-2 (Table **T2**), which defines the CP16c/CP17 (NP22/NP23) boundary. Exceptionally large specimens of *D. bisectus* (up to 18 µm) are present in Sample 199-1221B-1H-CC.

The CP16c/CP17 boundary is also observed in Hole 1221A, between Samples 199-1221A-1H-3, 3 cm, and 1H-3, 40 cm. The CP16c/CP16a+b (NP21/22 boundary; defined by the top of *Ericsonia formosa*) is observed between Samples 199-1221A-1H-5, 70 cm, and 1H-6, 40 cm. Calcareous nannofossils in Core 199-1221A-1H are badly dissolved. Isolated, circular, and elliptical distal shield rims that are nonbirefringent between crossed nicols are observed from below the extinction level of *E. formosa*. These rim ghosts are considered to originate from *E. formosa* (circular) and *C. pelagicus* (elliptical). Only elliptical distal shield rims are observed above the assigned range of *E. formosa,* and these rim ghosts undoubtedly originate from *C. pelagicus,* supporting the proposed placement of the top of *E. formosa* and the CP16c/CP16a+b boundary despite the strongly dissolved assemblages in the critical interval.

Subzone CP16a+b (NP21) is recognized through Sample 199-1221A-1H-6, 100 cm. Sample 199-1221A-1H-1, 110 cm, is barren of calcareous nannofossils. The E/O boundary is formally defined by the extinction of the planktonic foraminifer genus *Hantkenina*. But planktonic foraminifers are completely dissolved throughout Core 199-1221A-1H. The exact placement of the E/O boundary at Site 1221, therefore, will remain unresolved, perhaps until the problem can be addressed by analysis of nannofossil stable isotopes.

Paleocene–Eocene Transition and Lower Eocene

Eocene radiolarian ooze prevails from Sample 199-1221A-1H-1, 110 cm, through Sample 199-1221C-10X-CC. Several samples were investigated from the core catcher of Core 199-1221C-10X-CC. This core has a total recovery of 27 cm, with chert pieces overlying nannofossil ooze. A

smear slide, made from ooze stuck to a piece of chert, yielded mixed lower Eocene assemblages representing Subzones CP9b (NP11) and CP9a (NP10), with common *Rhomboaster* spp., *Tribrachiatus contortus, Tribrachiatus orthostylus, Discoaster diastypus, Discoaster multiradiatus,* and lower Eocene placoliths.

Sample 199-1221C-10X-CC, 14 cm, from the ooze underlying the cherts continues an assemblage from the lowermost part of Subzone CP9a (NP10), judging from the presence of both rare *Tribrachiatus bramlettei* and forms transitional between *Rhomboaster* spp. and *Tribrachiatus* spp. Secondary calcite overgrowth blurs the morphological details in the evolution of the *Rhomboaster-Tribrachiatus* lineage in virtually all lower Eocene samples investigated from Leg 199 sediments, including those from Site 1221. Sample 199-1221C-11X-1, 20 cm, contains an assemblage from Zone CP8 (upper NP9), implying that the base of Zone CP9 (NP10) falls in the gap between Cores 199-1221C-10X and 11X.

The Benthic Extinction Event (BEE) and, thus, the P/E boundary is located in Sample 199-1221C-11X-3, 91 cm. The pattern of nannofossil abundance and preservation in the colorful strata immediately overlying the P/E boundary layer is similar to the corresponding interval at Site 1220. A 30-cm barren interval, or one with only rare nannofossils, is present between Samples 199-1221C-11X-3, 60 cm, and 11X-3, 90 cm. The fasciculiths disappear between Samples 199-1221C-11X-2, 97 cm, and 11X-2, 110 cm, ~1.4 m above the benthic foraminfer extinction. The assemblages are poorly preserved below the boundary. Preservation improves above the colorful strata in Section 199-1221C-11X-3.

Upper Paleocene

Core 199-1221C-12X consists of 72 cm of sediment in Section 199-1221C-12X-1 and 8 cm of sediment in the core catcher. Fasciculiths are common to abundant and diverse throughout Core 199-1221C-12X. Preservation is otherwise poor throughout the samples investigated from Section 199-1221C-12X-1, corresponding closely to preservation category 3 of Bukry (1973); "Majority of specimens strongly etched. Many major structures removed. Many centerless specimens and fragmented specimens of questionable identity; low-diversity assemblage."

The base of both *D. multiradiatus* (defines the base of Subzone CP8a/NP9) and *Discoaster nobilis* (defines the base of Zone CP7) are present between Samples 199-1221C-12X-1, 18 cm, and 12X-1, 32 cm, which probably indicates strong condensation or a short hiatus in the carbonate-free dark brown sediment between these two samples. Ray numbers of *D. multiradiatus* are higher here than in younger (Eocene) populations. The large (>9 µm) *Ericsonia robusta* is common together with *D. multiradiatus* in the upper part of Section 199-1221C-12X-1 and disappears in the core gap between Cores 199-1221C-11X and 12X. *Discoaster okadai* is observed in Sample 199-1221C-12X-1, 40 cm.

Sample 199-1221C-12X-CC shows a marked improvement in preservation compared to the overlying samples in Core 199-1221A-12X and contains a diverse assemblage representing Zone CP6 (NP8) of the upper Paleocene. These taxa include *Bomolithus elegans, Chiasmolithus bidens, Coccolithus pelagicus, Cruciplacolithus frequens, Cruciplacolithus latipons, Discoaster mohleri, Ellipsolithus macellus, E. robusta, Ericsonia* spp. (see Bralower and Mutterlose, 1995; plate 4, figs. 9 and 10), *Fasciculithus involutus, Fascicultihus tympaniformis, Fasciculithus ulii, Heliolithus riedelii, Neochiastozygus* spp., *Prinsius bisulcus, Sphenolithus primus, To-*

weius eminens, Toweius pertusus, and *Zygodiscus plectopons*. Isolated rims and rim fragments are abundant in this core catcher sample.

Sample 199-1221C-12X-CC represents sediment resting immediately on the underlying basalt. This sample has an age range between 56.5 and 57.3 Ma, being older than the first occurrence of *D. nobilis* and younger than the first occurrence of *H. riedelii*.

Planktonic Foraminifers

The ~152 m of radiolarian clay, radiolarian ooze, and chert recovered at Site 1221 is completely barren of planktonic foraminifers. As at Site 1220, planktonic foraminifers are sporadically present in the upper Paleocene–lower Eocene nannofossil ooze and chalk sequence overlying basaltic basement in Holes 1221C and 1221D. As a result of extremely low recovery, variable states of foraminiferal preservation, and limited sampling through this critical interval (mainly core catcher samples), planktonic foraminiferal biostratigraphic zonation was confined to the Paleocene–Eocene portion of the site.

Sample 199-1221C-10X-CC contained highly dissolved planktonic assemblages characterized by solution-resistant forms such as *Acarinina coalingensis, Acarinina soldadoensis,* and *Morozovella aequa*. These species indicate a Zone P5–P6 age, which is in agreement with the nannofossil Zone NP10 assignment for this sample. A highly dissolved planktonic foraminifer assemblage was also recovered from Core 199-1221C-11X and contains only *A. soldadoensis*. The BEE has been placed at 154.31 mbsf and suggests that Sample 199-1221C-11X-CC is of latest Paleocene age. Sample 199-1221C-12X-CC contains a moderately well preserved and diverse assemblage of Paleocene planktonic foraminifers. Species present in this sample include *A. coalingensis, A. soldadoensis, Acarinina nitida, Morozovella mckannai, M. aequa, Morozovella velascoensis, Morozovella acuta, Morozovella angulata, Igorina albeari, Globanomalina pseudomenardii, Globanomalina ovalis, Subbotina triangularis, Subbotina patagonica,* and *Subbotina velascoensis*. Based on the presence of *G. pseudomenardii, M. aequa,* and *A. soldadoensis,* we assign this sample to Subzone P4c. Sample 199-1221D-4X-CC contains only traces of *A. coalingensis* and cf. *Tenuitella* spp.

A suite of small-volume samples (~1 cm^3) from Section 199-1221C-11X-3 was obtained by scraping the surface of the core with glass microscope slides. These samples are heavily contaminated with plastic fragments derived from sawing through the core liner during core splitting. Planktonic foraminifers are very rare in the scrape samples, consisting only of pieces of acarininids and extremely small specimens of four chambered cf. *Tenuitella* spp. No traces of the P/E boundary "excusion taxa" that are present at Site 1220 were found. However, these sample residues are extremely small and it is possible that larger volumes of sediment may yield greater numbers of planktonic foraminifers.

Benthic Foraminifers

Benthic foraminiferal assemblages from the early Oligocene and most parts of the Eocene at Site 1221 consist of agglutinated species. Samples 199-1221A-1H-CC, 2H-CC, 3H-CC, 5H-CC, 8H-CC, and 10H-CC contain *Recurvoides* sp. *Ammodiscus* sp., *Ammovertellina* sp., *Thalmannammina* sp., and *Spiroplectammina spectabilis*. Preservation of these species is poor, and most specimens show signs of damage. Elongate

tests of *Bathysiphon* sp., *Rhizammina* sp., and *Archimerismus*? sp. are usually fragmented. These assemblages indicate abyssal paleodepths.

Calcareous foraminiferal assemblages are present in Samples 199-1221C-10X-CC through 12X-CC. These assemblages are moderately well preserved, but the presence of small calcite microcrystals on the surfaces of the tests indicates some diagenetic alteration. Sample 199-1221C-10X-CC is characterized by a high abundance of *Nuttallides truempyi* and *Abyssamina quadrata*. Also present are *Anomalinoides spissiformis, Globocassidulina globosa,* small pleurostomellids, and stilostomellids. This assemblage is also characterized by low species diversity, which is suggestive of the early Eocene (Tjalsma and Lohmann, 1983). In contrast, high diversity assemblages are found in Samples 199-1221C-11X-CC and 12X-CC. These assemblages contain the Velascotype species such as *Gavelinella beccariiformis, Bulimina midwayensis, Gyroidinoides globosus, Pullenia coryelli, Nuttallinella florealis, Anomalinoides praeacuta, Aragonia velascoensis, Neoeponides hillebrandti, Neoflabellina semireticulata,* and *Dorothia trochoides,* indicating a Paleocene age and placement of the P/E boundary above Sample 199-1221C-11X-CC.

Ten samples scraped from the surface of Section 199-1221C-11X-3 were analyzed to precisely locate the P/E boundary. The foraminiferal assemblages in Samples 199-1221C-11X-3, 23–31 cm; 11X-3, 31–38 cm; 11X-3, 38–45 cm; and 11X-3, 45–53 cm, are composed mainly of *A. quadrata, Nuttalides truempyi,* and *G. globosa*. The high abundance of these species is diagnostic of the early Eocene (Tjalsma and Lohmann, 1983). Benthic foraminifers are rare and very poorly preserved in Samples 199-1221C-11X-3, 53–60 cm; 11X-3, 60–68 cm; and 11X-3, 68–76 cm. However, the main constituents of the assemblage are recognizable and are similar to the assemblage above these samples. Sample 199-1221C-11X-3, 76–83 cm, is barren of benthic foraminifers. Sample 199-1221C-11X-3, 83–91 cm, contains a few poorly preserved specimens of *N. truempyi* and *A. spissiformis praeacuta*. Samples 199-1221C-11X-3, 91–98 cm, and 11X-3, 98–106 cm, are characterized by *A. velascoensis, Gyroidinoides globosus,* and *G. beccariiformis,* which constitute the Velascotype assemblage. The P/E boundary is probably present near 154.31 mbsf (Section 199-1221C-11X-3, 91 cm), using the BEE as criterion for boundary definition (see **"P/E Boundary,"** p. 9, in "Biostratigraphy" in the "Explanatory Notes" chapter).

Radiolarians

A continuous sequence of radiolarian-bearing sediments, ranging in age from earliest Oligocene to early middle Eocene (Zone RP11), was recovered from Hole 1221A. Poorly recovered chert horizons in Cores 199-1221C-8X and 9X are barren of radiolarians. However, a small amount of radiolarian ooze in Sample 199-1221C-10X-CC contains radiolarians indicative of Zone RP7. Cores 199-1221C-11X and 12X are barren of radiolarians. With the exception of Core 199-1221A-1H and the upper sections of 2H, the radiolarian fauna is abundant and well preserved. Radiolarian zonal assignments are presented in Table **T3.**

Despite considerable reworking of middle Eocene forms, numerous diatoms, and some ash, it was possible to place the RP20/RP19 zonal boundary between Samples 199-1221A-1H-5, 45–47 cm, and 1H-6, 45–47 cm. Using data from Hole 1221B it is possible to further constrain this boundary and place it between Samples 199-1221A-1H-5, 45–47 cm, and 199-1221B-2H-3, 22–24 cm. Zone RP19 spans the E/O boundary. A combination of reworking and poor preservation made it equally

difficult to place the boundary between Zones RP19 and RP18. However, by removing poorly preserved samples from consideration, using data from Hole 1221B, and integrating information from the magnetostratigraphic record (see **"Paleomagnetism,"** p. 15), the RP19/RP18 boundary can be placed between Samples 199-1221A-1H-6, 45–47 cm, and 199-1221B-2H-4, 7–9 cm.

Subsequent zonal boundaries are clearly defined because of an increase in preservation of the radiolarians below the E/O boundary. The Eocene sediments maintained a uniformly brown color with a sugarlike texture. Although not abundant, the first occurrence of *Calocyclas bandyca* clearly defines the Zone RP18 and Zone RP17 boundary between Samples 199-1221A-2H-7, 43–45 cm, and 2H-CC. The RP17 and RP16 zonal boundary is equally well defined by the first occurrence of *Cryptocarpium azyx* between Samples 199-1221A-3H-3, 46–48 cm, and 3H-4, 46–48 cm. The series of middle Eocene zones defined by the evolution of species belonging to the genus *Podocyrtis* are all present and contain a rich and abundant faunal assemblage. The RP16/RP15 zonal boundary lies between Samples 199-1221A-4H-5, 45–47 cm, and 4H-6, 45–47 cm; the RP15/RP14 boundary is between Samples 199-1221A-6H-3, 45 cm, and 6H-4, 45 cm; the RP14/RP13 boundary is between Samples 199-1221A-7H-6, 45–47 cm, and 7H-CC; and the RP13/RP12 boundary is between Samples 199-1221A-9H-1, 45–47 cm, and 9H-2, 45–47 cm. The first occurrence of *Sethochytris triconiscus* is a useful and easily recognizable datum within Zone RP14. The earliest clearly defined boundary is between Zones RP12 and RP11 between Samples 199-1221A-11H-6, 45–47 cm, and 11H-7, 45–47 cm, and between Sections 199-1221C-4H-CC and 5H-CC. The lowermost Zone RP11 assemblages are found in Samples 199-1221A-12H-CC and 199-1221C-6X-CC.

An older assemblage, found only in Hole 1221C and belonging to Zone RP7, was recovered. Radiolarian Zone RP7 spans the lower/middle Eocene boundary. In Section 199-1221C-10X-CC, a small amount of the typically brown sugarlike sediment was found between the overlying chert and underlying calcareous material belonging to nannofossil Zone NP10. The fauna is well preserved and abundant.

Table **T3** summarizes newly determined zonal boundary ages calibrated using the paleomagnetic reversals from Site 1220. Figure **F6** compares the calculated ages with those estimated by Sanfilippo and Nigrini (1998; SN98) (see **"Radiolarian Zonal Scheme and Taxonomy,"** p. 11, in "Biostratigraphy" in the "Explanatory Notes" chapter). The age estimates of Sanfilippo and Nigrini (1998) are based on an unpublished catalog and chart constructed from a reexamination of all Paleogene low- and middle-latitude Deep Sea Drilling Project/Ocean Drilling Program sites from Legs 1–135 where there is a recognizable radiolarian fauna. The published information was reevaluated using current uniform species concepts and integrated, where possible, with published nannofossil and paleomagnetic data. Sanfilippo and Nigrini (1998) cautioned that their chronology of Paleogene radiolarian zonal boundary events is, at best, a good approximation. However, tested against a direct paleomagnetic record it can be seen that the estimates are fairly accurate. The largest discrepancies are present at the Zone RP15/RP14 boundary with a Site 1220 age that is 1.89 m.y. older than the SN98 age (from Sanfilippo and Nigrini, 1998). The fact that this boundary is defined by the evolutionary transition of *Podocyrtis mitra* to *P. chalara* rather than a more objective morphological first or last occurrence may account for some of this discrepancy. There is also a relatively large discrepancy for the boundary between Zones RP12 and RP11, where the

F6. Comparison of estimated zonal boundary ages, p. 31.

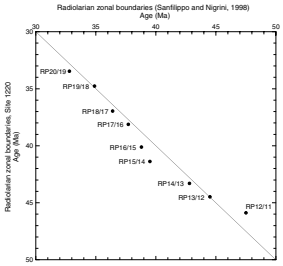

SN98 age is 1.61 m.y. older than the Site 1220 age. In this case, the paleomagnetic record is not well constrained in Site 1220. The Site 1220 age for the boundary between Zones RP16 and RP15 is 1.32 m.y. older than the SN98 age. The RP15/16 boundary event is marked by the first occurrence of *Podocyrtis goetheana,* which is easily recognizable but not particularly abundant in the Site 1221 material.

PALEOMAGNETISM

As in previous Leg 199 sites, all APC cores from Holes 1221A and 1221B that did not show large drilling-related disturbances were measured on the shipboard pass-through cryogenic magnetometer. The natural remanent magnetization (NRM) was measured at 5-cm intervals in each core section, followed by three steps of alternating-field (AF) demagnetization up to a maximum peak field of 20 mT. The XCB cores were not measured with the exception of Sections 199-1221C-11X-1 through 11X-3 and 199-1221D-4X-2, which contained apparently undisturbed sediment. In addition to whole-core measurements, numerous discrete samples were taken from Hole 1221A to carry out more detailed progressive demagnetization.

As in most of the siliceous sediments cored at previous sites, the NRM magnetization intensities were in the order of 10^{-1} to 10^{-2} A/m and decreased to ~10^{-3} A/m after partial AF demagnetization (Fig. **F7**). The drilling-induced overprint was mostly removed by AF demagnetization at 10 mT. Some magnetic directions did not reach a stable point at 20 mT and, despite the high grouping of antipodal directions, magnetization directions of most cores did not pass a reversal test, suggesting that the characteristic remanent magnetization (ChRM) has not been fully isolated in these samples. Further shore-based stepwise demagnetization is thus required to isolate the primary magnetization, particularly if a precise estimate of paleolatitudinal changes in the Paleogene is desired for Site 1221. Samples from XCB cores show paleomagnetic inclinations much steeper than expected for this near-equatorial site. For this reason, data from these cores were excluded when interpreting the polarity reversals. The cause of the steep inclinations is unclear and might be indicative of an unrecognized deformation during the drilling process or of a stronger drilling-induced overprint not removed by AF demagnetization. The latter could require a progressive thermal demagnetization to isolate the ChRM.

Data obtained from Site 1221 have a lower signal-to-noise ratio as compared to results from previous sites, particularly in the lower half of the section. This problem, together with the discontinuous recovery, makes the interpretation of the magnetic reversals more problematic.

Correlation of the magnetic stratigraphy to the geomagnetic polarity timescale is shown in Figure **F8.** We were able to identify polarity Chrons C15n to C20n (late–middle Eocene). The uppermost sediments from which we obtained reliable data (~40 mcd) were thus deposited during Chron C13r, near the E/O boundary. Below 80 mcd, the polarity record is more difficult to interpret because the record is not continuous and there is a large scatter in the virtual geomagnetic pole latitudes.

F7. Magnetization intensities after AF demagnetization, p. 32.

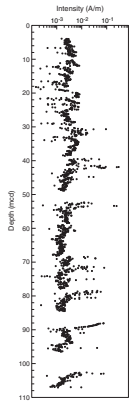

F8. Composite magnetic stratigraphy, p. 33.

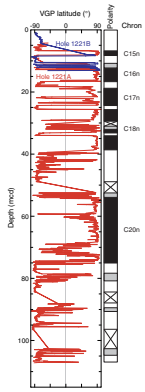

COMPOSITE DEPTHS

Site 1221 extended to a total depth of 156.20 mbsf (Core 199-1221C-12X), but it was not possible to construct a complete composite depth scale for the site. We encountered severe flow-in problems in the uppermost ~20 mbsf, probably related to large heave motions of the ship. Below ~110 mbsf, commonly occurring chert layers prevented recovery. In the remaining intervals, the often soupy nature of the sediment (radiolarian ooze) resulted in MST data that were not suitable for correlation purposes, with the exception of the P/E boundary interval in the lowermost part of the recovered interval (see "Lithostratigraphy," p. 5).

At Site 1221, magnetic susceptibility (MS) and color reflectance data were collected at 2-cm intervals and gamma ray attenuation (GRA) bulk density at 4-cm intervals. *P*-wave velocity data were collected at 2-cm intervals in those cores that were recovered by APC coring. Readings from the natural gamma ray (NGR) instrument showed only background radiation levels, apart from the P/E boundary interval in Core 199-1221D-4X. Over the Paleocene–Eocene interval, GRA bulk density and MS data were collected at 1-cm intervals. Disturbed intervals, as determined by visual inspection of split cores, are listed in Table **T4.** Data from these intervals were removed prior to correlation work. Table **T5** lists the offsets that were applied to cores from each hole to create a partial composite depth record.

Cores from Site 1221 overlap and form a continuous sedimentary sequence only down to 19.5 mcd (base of Core 199-1221A-2H) (Table **T6**). Figure **F9** shows the GRA bulk density, MS, and color reflectance data for the upper 20 mcd plotted on the resulting composite depth scale after removing disturbed intervals according to Table **T4.** Deeper in the section, it may be possible to correlate Cores 199-1221A-4H and 5H with Core 199-1221C-3H, using other records such as paleomagnetic intensity data. This correlation was not attempted aboard ship. In the composite framework for Site 1221, a depth shift of 0.5 m was applied to Cores 199-1221A-3H, 4H, 8H, and 9H in order to avoid overlap of data associated with the >100% recovery often encountered with APC coring. Between ~150.5 and 155 mcd (the P/E boundary), cores from Hole 1221B and 1221C contained correlative features and were depth shifted. However, for the remaining intervals there is no overlapping record from multiple cores. Furthermore, the lack of correlative features in the data collected from the soupy radiolarian ooze precluded the construction of a convincing correlation. Because of correlation problems and the lack of overlap between holes, the remaining data (primarily from Hole 1221A) were only appended in the composite depth framework according to the depth at which they were recovered.

The flow-in encountered in Core 199-1221A-1H resulted in an artificially longer section than what was actually cored. Thus, when features in the undisturbed lower portion of this core were correlated to equivalent sections in Holes 1221B and 1221C, the composite construction resulted in an upward (negative) shift in the mcd offset for Core 1H. Such a shift artificially places some sediment within this core above the sediment/water interface. However, this sediment is flow-in and does not represent in situ material. All undisturbed material in Core 1H remains below the sediment/water interface in the composite depth framework.

T4. Core disturbance intervals, p. 53.

T5. Core composite depth offsets, p. 54.

T6. Splice tie points, p. 55.

F9. GRA bulk density, magnetic susceptibility, and color reflectance data for the upper 20 mcd plotted vs. composite depth, p. 34.

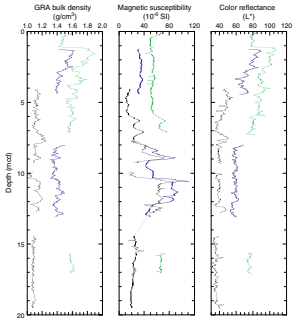

SEDIMENTATION AND ACCUMULATION RATES

The principal biostratigraphies, plus a set of 12 paleomagnetic reversals (Tables T7, T8), are defined primarily in Holes 1221A, 1221B, and 1221C. Paleomagnetic reversals are used to calculate the average linear sedimentation rates (LSRs) for Site 1221 through the upper part of the section; however, the disturbed nature of many of the cores required reliance on all the principal biostratigraphies in order to achieve a detailed picture of the LSR through the section (Fig. F10). To this end, we have calibrated radiolarian events and the magnetic record at Site 1220 (see "Biostratigraphy," p. 9) and have used these events through the middle and upper Eocene. In the lower Eocene, the nannofossil events and the BEE provide the stratigraphic control. The first reliable paleomagnetic reversals are found in Core 199-1221A-1H, along with the youngest radiolarian and nannofossil events. The paleomagnetic stratigraphy extends through the section recovered by APC coring (0–102.5 mcd). The age of the base of the hole is based on the identification of the BEE in Section 199-1221C-11X-3 (Tables T7, T8) and on four nannofossil events.

Based on a simple linear interpolation through the uppermost stratigraphic events (Tables T7, T8), the calcareous and siliceous ooze of lithologic Units I and II (see "Lithostratigraphy," p. 5) have an LSR near 3.4 m/m.y. The density records from the lowermost 7 m of piston Core EW9709-14P (Lyle, 2000) taken in the survey area can be correlated to those from Hole 1221A (Fig. F11). This correlation is supported by the ages of the radiolarian assemblages from the bottom of Core EW9709-14P and the uppermost cores of Site 1221. The comparison between these two records indicates that the uppermost 5 m of clays collected in the piston core is missing at the location of Site 1221 (Fig. F11).

Within Core 199-1221A-1H, the radiolarians, nannofossils, and paleomagnetic reversals (see Tables T7, T8) indicate that there is a break in deposition just above the level of the top of Chron C15n (6.67 mcd). This break is near the top of Zone RP19, which spans the E/O boundary. Samples at the base of Core 199-1221A-1H are poorly preserved and contain a mixture of Eocene species. At the top of Core 199-1221A-2H, the radiolarians are from Zone RP18, well within the upper Eocene (see "Biostratigraphy," p. 9). Together these data suggest that the lower part of the Oligocene (Chron C13n) and part of the upper Eocene are missing at this site (Fig. F10).

The LSR at Site 1221 gradually increases in the siliceous ooze of lithologic Units II and III, reaching nearly 19 m/m.y. in the middle Eocene part of the section (Fig. F10). This relatively high sedimentation rate exceeds the maximum LSR encountered in the middle Eocene of Site 1220 by about a factor of two; however, the overall mid-Eocene LSR at Site 1221 is only slightly higher at Site 1220 (Fig. F10) (see also Fig. F15, p. 49, in the "Site 1220" chapter). The LSR at Site 1221 apparently drops to ~6 m/m.y. near the top of the lower Eocene with the appearance of the first significant chert layers (see "Lithostratigraphy," p. 5). In the lowermost section of chalk, the LSR appears to decrease to ~1.3 m/m.y. This low rate may indicate the presence of hiatuses in the part of the section just above basement.

LSR values may be combined with the dry bulk density (DBD) data from porosity measurements on individual samples (see "Physical Properties," p. 20) (Table T13) to determine the bulk mass accumulation rates (MARs) of the sediments (Table T9). Sediment with an LSR

T7. Paleomagnetic horizons, p. 56.

T8. Nannofossil, foraminifer, and radiolarian datums, p. 57.

F10. LSRs and chronostratigraphic markers, p. 35.

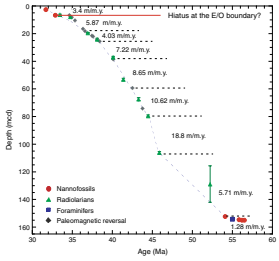

F11. Density record of site survey piston Core EW9709-14P compared to density record of Site 1221, p. 36.

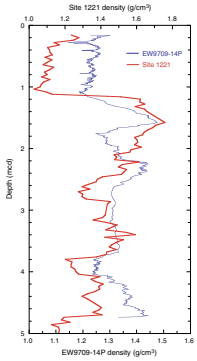

T9. Depths, ages, rates, and fluxes of sediments, p. 58.

of 1.0 cm/k.y. and a DBD of 1.0 g/cm3 will have an MAR value of 1.0 g/cm²/k.y. The observed values are rarely this high, so we report the data in milligrams per square centimeter per thousand years (mg/cm²/k.y.). MAR values are essentially zero above the Oligocene carbonate oozes, reflecting the widespread nondeposition in this part of the Pacific (Fig. F12). Lithologic Unit III, dominated by the radiolarian oozes, accumulated at 200–500 mg/cm²/k.y., with the maximum flux rates exceeding 600 mg/cm²/k.y. Unit IV, the basal chalks that contain the P/E boundary horizon, accumulated at a rate of ~160 mg/cm²/k.y.

F12. MAR of sediments, p. 37.

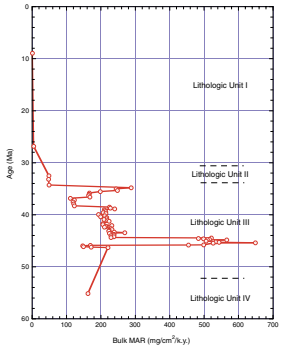

GEOCHEMISTRY

Interstitial Water Geochemistry

We collected interstitial waters from eight samples in Hole 1221A at intervals of approximately one sample every core for the first six cores and every third core thereafter, at depths ranging from 4.45 to 108.95 mbsf (Table T10; Fig. F13).

T10. Interstitial water data, p. 59.

F13. Interstitial water data, p. 38.

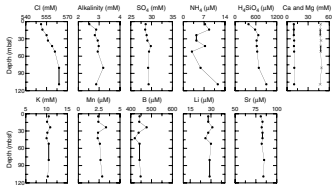

Chlorinity, as measured by titration, increases with depth from 551 mM at 4.45 mbsf to 564 mM at 108.95 mbsf (Fig. F13). The lower than average seawater value of interstitial water at shallow sediment depth (4.45 mbsf) at this site is consistent with the chlorinity of modern Pacific bottom waters (~542 mM). Sodium concentrations determined by charge balance increase with depth from 485 mM at 4.45 mbsf to 501 mM at 108.95 mbsf (Table T10). Salinity, as measured by a handheld refractometer, increases with depth from 34.5 at 4.45 mbsf to 35.5 at 108.95 mbsf.

Alkalinity generally increases with depth from 2.53 mM at 4.45 mbsf to a maximum of 3.20 mM at 80.41 mbsf and subsequently decreases to 2.86 mM at 108.95 mbsf.

The pH varies between 7.21 and 7.40. Like all other Leg 199 sites, average sulfate concentrations are high (29.1 mM) and ammonium concentrations are low (≤12 µM), indicating little oxidation of organic matter.

Dissolved silica concentrations increase with depth, from 388 µM at 4.45 mbsf to ~900 µM at 108.95 mbsf. These high interstitial water silica values are consistent with dissolution of biogenic silica throughout the sediment.

Site 1220 calcium, magnesium, potassium, and lithium profiles are similar to those seen at all other Leg 199 sites except Site 1219 and show little evidence for exchange with basalt and subsequent diffusion. Calcium and potassium concentrations are relatively constant at ~10 mM (about seawater concentration), magnesium concentrations are relatively constant at 48 mM, and lithium pore water values are slightly higher than that of seawater (27 µM).

Strontium concentrations (81 µM) are slightly lower than seawater value (87 µM) at the top of the hole and do not show much increase with depth, consistent with the lack of carbonate at this site. Dissolved manganese averages ~2.6 µM and boron averages ~444 µM, slightly above seawater value (416 µM). Dissolved barium concentrations are below the detection limit.

In summary, the pore water profiles from Site 1220 primarily reflect minor organic matter degradation and the dissolution of biogenic silica. Most of the dissolved chemical constituents show a lack of gradient with depth and values similar to or slightly higher than seawater. Overall, the profiles from Site 1221 are very similar to the profiles from Site

1215, except lithium, which is elevated at the base of the hole at Site 1215.

Solid-Phase Geochemistry

We collected bulk-sediment samples in every other section, adjacent to the interval sampled for physical properties (see "Physical Properties," p. 20) at Site 1221, resulting in a sampling resolution of approximately three samples per core. The resulting depth profile is based primarily on data from sediments in Hole 1221A (Table T11; Fig. F14). We also analyzed continuous scrapings (31 samples of 2.5–5 cm in width) from the P/E boundary section (in Section 199-1221C-11X-3, between 153.50 and 154.91 mbsf), discussed separately below.

Bulk-sediment geochemistry does not show much variation. It is difficult to resolve Unit I (clay) from Unit II (diatom-radiolarian-nannofossil ooze), although the radiolarian ooze (Subunit IIIA) and nannofossil chalk (Unit IV) are distinctive (Fig. F14).

Silicon is <20 wt% in Units I–II, increases to ~30 wt% in Unit III, and decreases to 2 wt% in Unit IV (Fig. F14). Aluminum and titanium concentrations show little variation and are generally <2 and <0.10 wt%, respectively. Iron, manganese, and magnesium contents show similar trends to each other (Fig. F14). Iron, manganese, and magnesium concentrations are relatively constant throughout Unit II at levels of 1.5, 0.3, and 1.3 wt%, respectively.

Levels of calcium and strontium are highest in the more carbonate-rich lithologies, ~10–30 wt% for calcium and ~700–1200 ppm for Sr (Units II and IV). Calcium and strontium are <1 wt% and <100 ppm, respectively, in the radiolarian ooze (Subunit IIIA). Phosphorus concentrations are generally <0.5 wt%, and barium concentrations are generally <3000 ppm.

Calcium carbonate ($CaCO_3$; in weight percent) was determined by coulometric methods for two to three samples per core from 5.23 to 103.23 mbsf for Hole 1221A and for one sample each from Holes 1221B (2.23 mbsf) and 1221C (104.73 mbsf) (Table T12; Fig. F15). $CaCO_3$ is variable in Units I and II (20–60 wt%) and is low in Subunit IIIA (<1 wt%). $CaCO_3$ values calculated from Ca inductively coupled plasma–atomic emission spectroscopy data (in weight percent) and salt-fraction data (in weight percent) yielded similar trends to $CaCO_3$ measured via coulometer, except at high $CaCO_3$ values, when the calculated values overestimate carbonate, and at values <1 wt%, when calculated values underestimate carbonate (see "Geochemistry," p. 20, in the "Explanatory Notes" chapter). Organic carbon (C_{ORG}; in weight percent) determined for one sample per core is uniformly low (<0.2 wt%) for the samples measured.

In summary, the bulk geochemistry of the sediments from Site 1221 reflect the shifts in lithology between sediments dominated by silica and carbonate.

P/E Boundary

Changes of both shape and absolute concentration in bulk geochemistry seen across the P/E boundary of Site 1221 (Section 199-1221C-11X-3) are similar to those seen at Site 1220 (Table T11; Fig. F16). Silicon, aluminum, and magnesium have elevated concentrations (~20, 5, and 0.3 wt%, respectively) above their Unit IV background concentra-

T11. Bulk-sediment data, p. 60.

F14. Bulk-sediment data, p. 39.

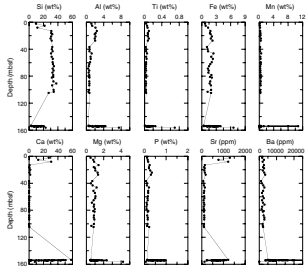

T12. $CaCO_3$ and C_{org} data, p. 61.

F15. $CaCO_3$ data, p. 40.

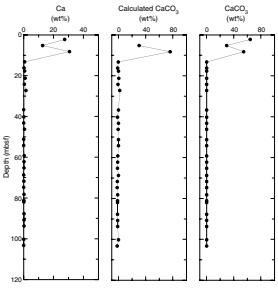

F16. Bulk-sediment geochemical data for the P/E boundary, p. 41.

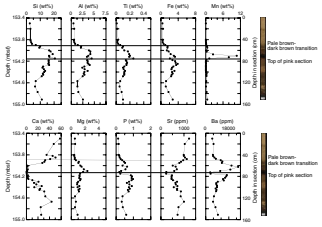

tions. Over the same interval, calcium is below its Unit IV background concentration, as low as 0.1 wt%. Strontium generally decreases downsection and has a distinct minima centered at interval 199-1221C-11X-3, 72.5–77.5 cm. Strontium levels in the carbonate lithology at the base of the section generally increase downsection (between 154.15 and 154.91 mbsf), possibly reflecting a decrease in the extent of carbonate recrystallization. Iron concentrations peak at ~4 wt% at interval 199-1221C-11X-3, 85–87.5 cm, and titanium concentrations peak at 0.25 wt% at interval 199-1221C-11X-3, 75–77.5 cm, in the section. Manganese concentrations are low overall but show a single peak (11 wt%) at interval 199-1221C-11X-3, 70–72.5 cm, corresponding to the darkest sediments in the section. Phosphorus and barium concentrations show similar trends to each other. Unlike Site 1220 where the maxima were coincident, the barium maximum is at interval 199-1221C-11X-3, 62.5–67.5 cm, and the phosphorus maximum is at interval 199-1221C-11X-3, 85–87.5 cm.

Calcium is extremely high (35–58 wt%) between 10 and 50 cm in this section. Calcium values higher than 35.9% are out of the range of the standards (see **"Geochemistry,"** p. 20, in the "Explanatory Notes" chapter for more discussion).

PHYSICAL PROPERTIES

Physical properties at Site 1221 were measured on whole cores, split cores, and discrete samples. MST measurements (bulk density, MS, *P*-wave velocity, and natural gamma radiation) and thermal conductivity comprised the whole-core measurements. Compressional wave velocity measurements on split cores and moisture and density (MAD) analyses on discrete core samples were made at a frequency of one per undisturbed section in Hole 1221A. Samples from cores in Holes 1221B and 1221C were used to supplement intervals that were disturbed by drilling or not recovered in Hole 1221A. Light absorption spectroscopy (LAS) analyses were performed on the MAD samples as well as an additional one sample per section (located ~50 cm from the MAD sample).

Density and Porosity

Two methods were used to evaluate the wet bulk density at Site 1221. GRA provided an estimate from whole cores. MAD samples gave a second, independent measure of wet bulk density, along with providing DBD, grain density, water content, and porosity from discrete samples (Table **T13**). The GRA and MAD wet bulk densities are a close match in the clays and nannofossil oozes of lithologic Unit I (0–1.12 mbsf) and Unit II (1.12–7.40 mbsf), but the MAD densities are consistently 0.10 g/cm³ greater than the GRA density in the radiolarian ooze of Subunit IIIA (7.40–112.00 mbsf) (Fig. **F17**). The GRA bulk density was the primary density measurement made on the P/E boundary sections contained in Cores 199-1221C-11X and 199-1221D-4X (see **"Sediment of the P/E Boundary Interval,"** p. 8, in "Lithostratigraphy"). In both Holes 1221C and 1221D, the calcareous chalk above and below the boundary is characterized by bulk densities of ~1.60 to 1.75 g/cm³ (Fig. **F18**). In Hole 1221C, the GRA bulk densities of the multicolored clays directly above the boundary are ~0.30 g/cm³ lower (~1.40 g/cm³) than the densities above and below the clays. In Hole 1221D, the bulk density in the multicolored clays, which ranges from 1.20 to 1.40 g/cm³, is

T13. Moisture and density measurements, p. 62.

F17. MAD measurements, p. 42.

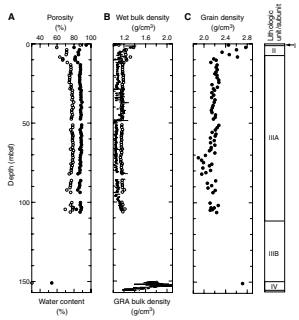

F18. Magnetic susceptibility and GRA bulk density and the P/E boundary, p. 43.

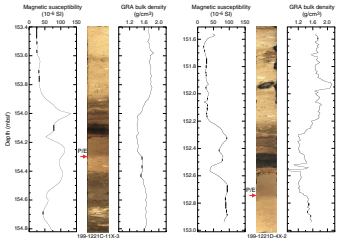

lower and less uniform than in Hole 1221C. Section 199-1221D-4X-2 contains a chert nodule at 151.93 mbsf that has a bulk density of 2.13 g/cm³. The two low density spikes in the section, at 152.52 and 152.56 mbsf, coincide with small voids in the core.

GRA bulk densities for Cores 199-1221A-4H and 5H (28.5–47.5 mbsf) appear to be displaced to values 0.10–0.15 g/cm³ greater than adjacent GRA densities (Fig. F17). As at Site 1220, where GRA densities display a similar displacement over short intervals, the offset is an electronic artifact in the MST data acquisition. The correlation between the MAD and GRA densities (excluding the questionable GRA data from Cores 199-1221A-4H and 5H) is not as strong at Site 1221 as it is at other Leg 199 sites because of the limited range in densities (Fig. F19). In both the regression of GRA density with wet bulk density and GRA density with DBD, the regression coefficients are 0.86.

The MAD wet bulk density varies over a narrow range for sediments at Site 1221 (Fig. F17). Bulk density of the clay and radiolarian ooze in Unit I is 1.10 g/cm³ at 0.75 mbsf. Density increases in Unit II to a maximum of 1.38 g/cm³ at 2.25 mbsf in an interval of nannofossil ooze. Below this depth, density decreases in conjunction with LAS-indicated increasing opal content (Fig. F20). The highest wet bulk density in Unit III (1.32 g/cm³) is at 8.25 mbsf, near the clay-rich top of the unit. Density decreases as the clay content of the sediment rapidly decreases downhole. The average density for the radiolarian ooze of Subunit IIIA is 1.14 g/cm³. The nannofossil chalk of lithologic Unit IV (150.50–156.00 mbsf) was sampled at 150.88 mbsf and has a wet bulk density of 1.81 g/cm³.

Grain density is low for most of the interval cored at Site 1221, reflecting the abundance of radiolarians. The highest grain density (2.78 g/cm³) occurs in the nannofossil ooze at 2.25 mbsf in Unit II. At the top of Subunit IIIA, grain density rapidly decreases to 2.20 g/cm³ at 18.86 mbsf as a result of the decrease in nannofossils. The high concentration of radiolarians in Subunit IIIA is reflected by the low average grain density for the unit (2.17 g/cm³). Grain density of the Unit IV nannofossil chalk is 2.72 g/cm³.

The porosity near the seafloor (0.75 mbsf) is 94%. It decreases rapidly to 80% in the nannofossil ooze at 2.25 mbsf. Porosity then increases slightly downhole as radiolarian content increases. The average porosity for the radiolarian ooze of Subunit IIIA is 84%. Porosity of the nannofossil chalk at 150.88 mbsf in Unit IV is 54%.

LAS

LAS studies were conducted on sediments from Cores 199-1221A-1H through 11H and Sections 199-1221B-1H-1 through 1H-3 at a frequency of two samples per undisturbed section (see **Vanden Berg and Jarrard**, this volume, for a discussion of the LAS technique). Samples were not collected below 105 mbsf because of poor core recovery. Semiquantitative mineral concentrations were calculated from the collected spectra, assuming a four-component system: calcite, opal, smectite, and illite (Table T14). The results of the LAS analyses correlate well with the major lithologic boundaries (Fig. F20) and are described below in terms of lithologic units.

The upper 8 cm of Site 1221 contains an illite-rich (60%) clay, which abruptly changes to radiolarian ooze that characterizes the rest of lithologic Unit I below 0.08 mbsf. Unit II contains calcite-rich (75%) nanno-

F19. Wet and dry bulk density plotted with GRA density, p. 44.

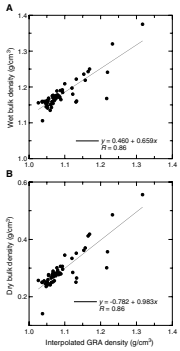

F20. LAS mineralogy determinations, p. 45.

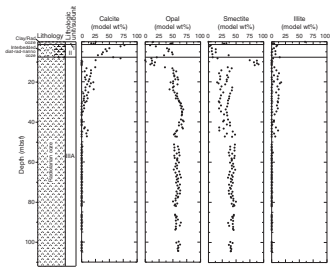

T14. LAS-based mineralogy, p. 63.

fossil ooze between 1.7 and 2.3 mbsf, an interval of opal-rich (48%) radiolarian and diatom ooze between 3.2 and 6.8 mbsf, and a lower thin interval of calcite-rich (65%) nannofossil ooze between 7.7 and 8.3 mbsf. The upper 4.3 m of lithologic Unit III is a smectite-rich (75%–90%) clay layer, which overlies 100.7 m of opal-rich radiolarian ooze. Opal and smectite concentrations average 58% and 37%, respectively, throughout Unit III (excluding the upper clay layer). The illite–smectite transition at this site is difficult to determine precisely with LAS because of the high concentrations of biogenic material in the uppermost sediments.

Compressional Wave Velocity

Compressional wave velocity was measured by the *P*-wave logger (PWL) on all whole cores from Holes 1221A and 1221B and Cores 199-1221C-1H through 6X. The contact probe system was used to measure velocities on split cores from Hole 1221A and Sections 199-1221B-1H-1 through 1H-3, 199-1221C-6X-1 through 6X-3, and 199-1221C-11X-1 (Table **T15**). Agreement between PWL and split-core velocities is poor, and the two data sets show an offset of ~30 m/s (Fig. **F21**). Velocities in Unit I decrease from 1531 m/s at the seafloor to 1488 m/s at 1.3 mbsf. This low-velocity interval correlates with a thin layer of nannofossil ooze as recorded in the LAS mineralogy data (Fig. **F20**). Below 1.3 mbsf, velocities increase to 1525 m/s in the radiolarian and diatom oozes of Unit II before decreasing again to ~1500 m/s between 9.3 and 12.4 mbsf in a clayey interval. In the radiolarian ooze between 12.4 and 114.0 mbsf, velocities gradually increase downcore from ~1530 to ~1550 m/s. A velocity of 1610 m/s was measured in the nannofossil chalk of Unit IV at 150.89 mbsf.

T15. Split-core velocity measurements, p. 64.

F21. Compressional wave velocity, p. 46.

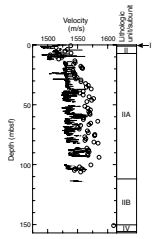

Thermal Conductivity

Thermal conductivity was measured on the third section of all undisturbed cores from Hole 1221A and Cores 199-1221B-1H and 2H (Table **T16**). The conductivity was only measured on cores in lithologic Unit II and Subunit IIIA. The average thermal conductivity for these units is 0.73 W/(m·K). This value is comparable to the other high-porosity (80%–90%) radiolarian oozes cored during Leg 199. The conductivity does not vary as a function of porosity or display a trend in variation downhole at Site 1221.

T16. Thermal conductivity, p. 65.

Natural Gamma Radiation

Natural gamma radiation was measured on all whole cores in Holes 1221A, 1221B, 1221C, and 1221D (Fig. **F22**). The highest NGR value (38 counts per second [cps]) is present in clay-rich lithologic Unit I. NGR values rapidly decrease downhole in the radiolarian ooze of Unit III, coinciding with a downhole decrease in clay content. The values are essentially at zero below 25 mbsf. In the P/E boundary section in Sections 199-1221C-11X-3 and 199-1221D-4X-2 (see **"Sediment of the P/E Boundary Interval,"** p. 8, in "Lithostratigraphy"), NGR values rise from background levels in the calcareous chalk to 17 cps in the multicolored clay above the boundary.

F22. Natural gamma radiation, p. 47.

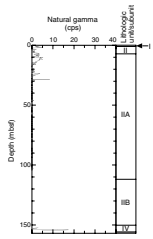

MS

Whole-core MS measurements were made on all cores from Holes 1221A, 1221B, 1221C, and 1221D (Fig. F23). MS for lithologic Unit I is 25×10^{-6} SI at the seafloor and decreases to 9×10^{-6} SI at the base of the unit. Unit II is characterized by a small increase in susceptibility to 18×10^{-6} SI at 3.4 mbsf and another decrease to values of 9×10^{-6} SI at 4.2 mbsf. The susceptibility minima in Units I and II correspond to intervals of calcite-rich nannofossil ooze, whereas the maxima correspond to regions of more clay- and radiolarian-rich sediments (see "Unit I," p. 6, and "Unit II," p. 6, both in "Lithostratigraphy").

The top of Lithologic Unit III is marked by an increase in susceptibility to ~72×10^{-6} SI. The high MS correlates with a region of clay-rich sediments between 7.4 and 11.7 mbsf. This interval is also characterized by higher NGR values and low porosities and velocities. Between 9.8 and 114.2 mbsf in the radiolarian-rich Unit III, MS decreases to an average of 17×10^{-6} SI. The lower susceptibility values (~6×10^{-6} SI at 69.1 mbsf) correlate with the lowest grain densities in Unit III.

The P/E boundary sections, Sections 199-1221C-11X-3 and 199-1221D-4X-2, were well documented by the MS detector (Fig. F18). The transition from nannofossil chalk to the metal oxide–rich clay is marked by an increase from ~25×10^{-6} SI to 119×10^{-6} SI at 154.02 mbsf in Hole 1221C and 25×10^{-6} SI to 92×10^{-6} SI at 152.32 mbsf in Hole 1221D. This difference is comparable to the change at the boundary between the radiolarian ooze of Unit II and the upper clay interval of Unit III but occurs over a much narrower interval. Below this peak, susceptibility decreases to minima of 53×10^{-6} SI in Hole 1221C and 38×10^{-6} SI in Hole 1221D, which coincides with the reddish brown layer (154.16 mbsf in Hole 1221C and 152.56 mbsf in Hole 1221D). In Hole 1221C, a second broad susceptibility peak of 112×10^{-6} SI at 154.26 mbsf lies just above the P/E boundary (Fig. F18). Hole 1221D is characterized by the same broad peak (94×10^{-6} SI at 152.69 mbsf) but fails to return to the same low values as in Hole 1221C. Susceptibility and GRA bulk density in the three recovered P/E boundary sections (two from Site 1221 and one from Site 1220) correlate well with one another. The susceptibility peaks also correlate well with zones of metal enrichment, as seen in the geochemical analyses (see "P/E Boundary," p. 19, in "Geochemistry").

F23. Magnetic susceptibility, p. 48.

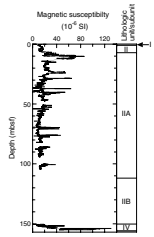

REFERENCES

Bralower, T.J., and Mutterlose, J., 1995. Calcareous nannofossil biostratigraphy of Site 865, Allison Guyot, Central Pacific Ocean: a tropical Paleogene reference section. *In* Winterer, E.L., Sager, W.W., Firth, J.V., and Sinton, J.M. (Eds.), *Proc. ODP, Sci. Results,* 143: College Station, TX (Ocean Drilling Program), 31–74.

Bukry, D., 1973. Coccolith stratigraphy, eastern equatorial Pacific, Leg 16, Deep Sea Drilling Project. *In* van Andel, T.H., Heath, G.R., et al., *Init. Repts. DSDP,* 16: Washington (U.S. Govt. Printing Office), 653–711.

Cande, S.C., LaBrecque, J.L., Larson, R.L., Pitmann, W.C., III, Golovchenko, X., and Haxby, W.F., 1989. *Magnetic Lineations of the World's Ocean Basins*. AAPG Map Ser., 13.

Engebretson, D.C., Cox, A., and Gordon, R.G., 1985. *Relative Motions Between Oceanic and Continental Plates in the Pacific Basin*. Spec. Pap.—Geol. Soc. Am., 206.

Gripp, A.E., and Gordon, R.G., 1990. Current plate velocities relative to the hotspots incorporating the NUVEL-1 global plate motion model. *Geophys. Res. Lett.,* 17:1109–1112.

Lyle, M., 2000. Data submission to ODP Pollution Prevention and Safety Panel: proposed drill sites for ODP Leg 198—a Paleogene equatorial APC transect. *BSU-CGISS Tech Rept.,* 2000-03.

Sanfilippo, A., and Nigrini, C., 1998. Code numbers for Cenozoic low latitude radiolarian biostratigraphic zones and GPTS conversion tables. *Mar. Micropaleontol.,* 33:109–156.

Tjalsma, R.C., and Lohmann, G.P., 1983. *Paleocene–Eocene Bathyal and Abyssal Benthic Foraminifera from the Atlantic Ocean.* Spec. Publ.—Micropaleontology, 4.

van Andel, T.H., Heath, G.R., and Moore, T.C., Jr., 1975. *Cenozoic History and Paleoceanography of the Central Equatorial Pacific Ocean: A Regional Synthesis of Deep Sea Drilling Project Data.* Mem.—Geol. Soc. Am., 143.

Figure F1. Location of Site 1221 in the Leg 199 transect. The top map shows Site 1221 on the regional bathymetry. The bottom map shows the transect target crust. In the lower panel, gray shading = seafloor depths >5000 mbsl, red shading = approximate position of the nominal target crust of the 56-Ma transect. FZ= fracture zone.

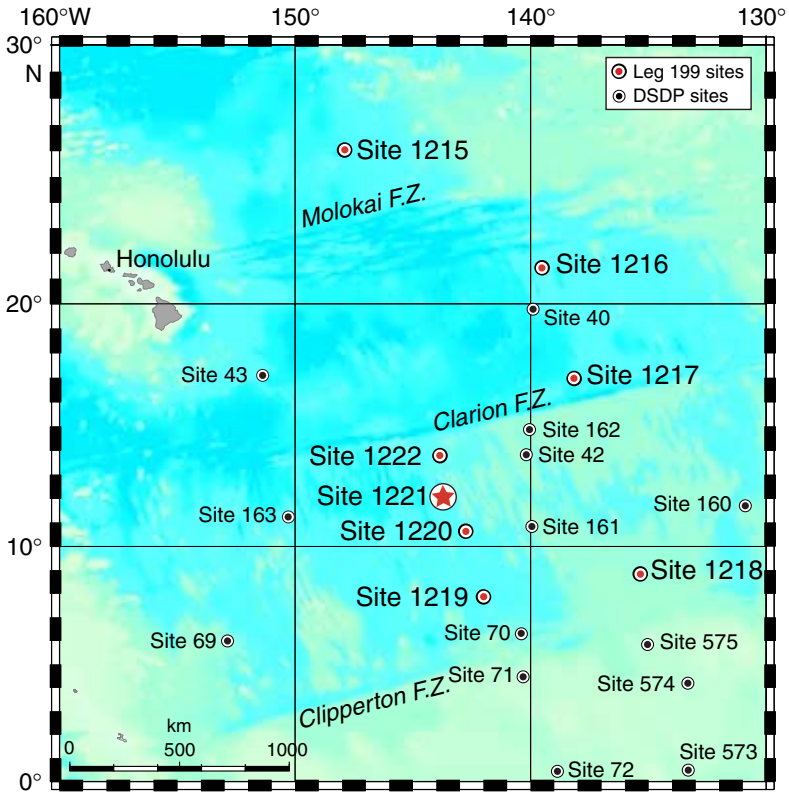

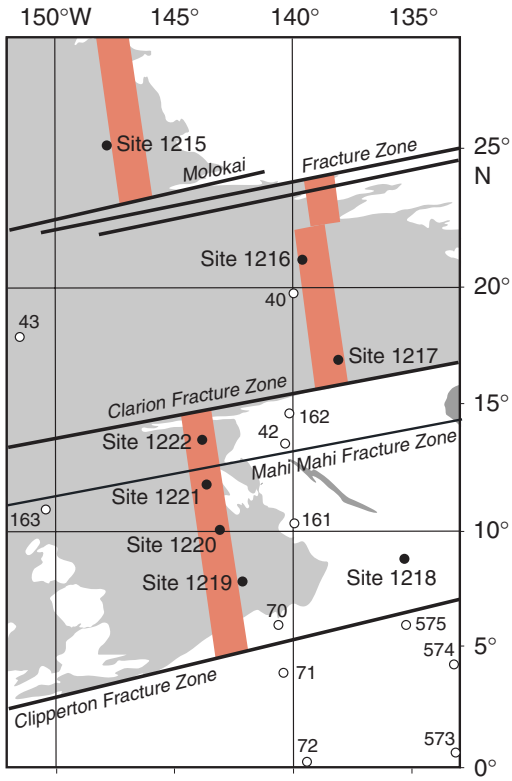

Figure F2. Seismic reflection profile across Site 1221. The sedimentary section is marked by a weakly reflective unit between the seafloor and ~20 ms two-way traveltime (TWT) below the seafloor, which is assumed to be clays. On the basis of drilling results from Sites 1219 and 1220, the next notable reflector (~40 ms TWT mbsf P3?) is interpreted to mark the contact between a thin sequence of Oligocene nannofossil ooze and thick underlying upper–middle Eocene radiolarian ooze. In turn, P2 marks the inferred boundary between radiolarian ooze and a thin sequence of lower Eocene chalk and chert atop basement (~190 ms TWT mbsf) (see **Lyle et al.,** this volume).

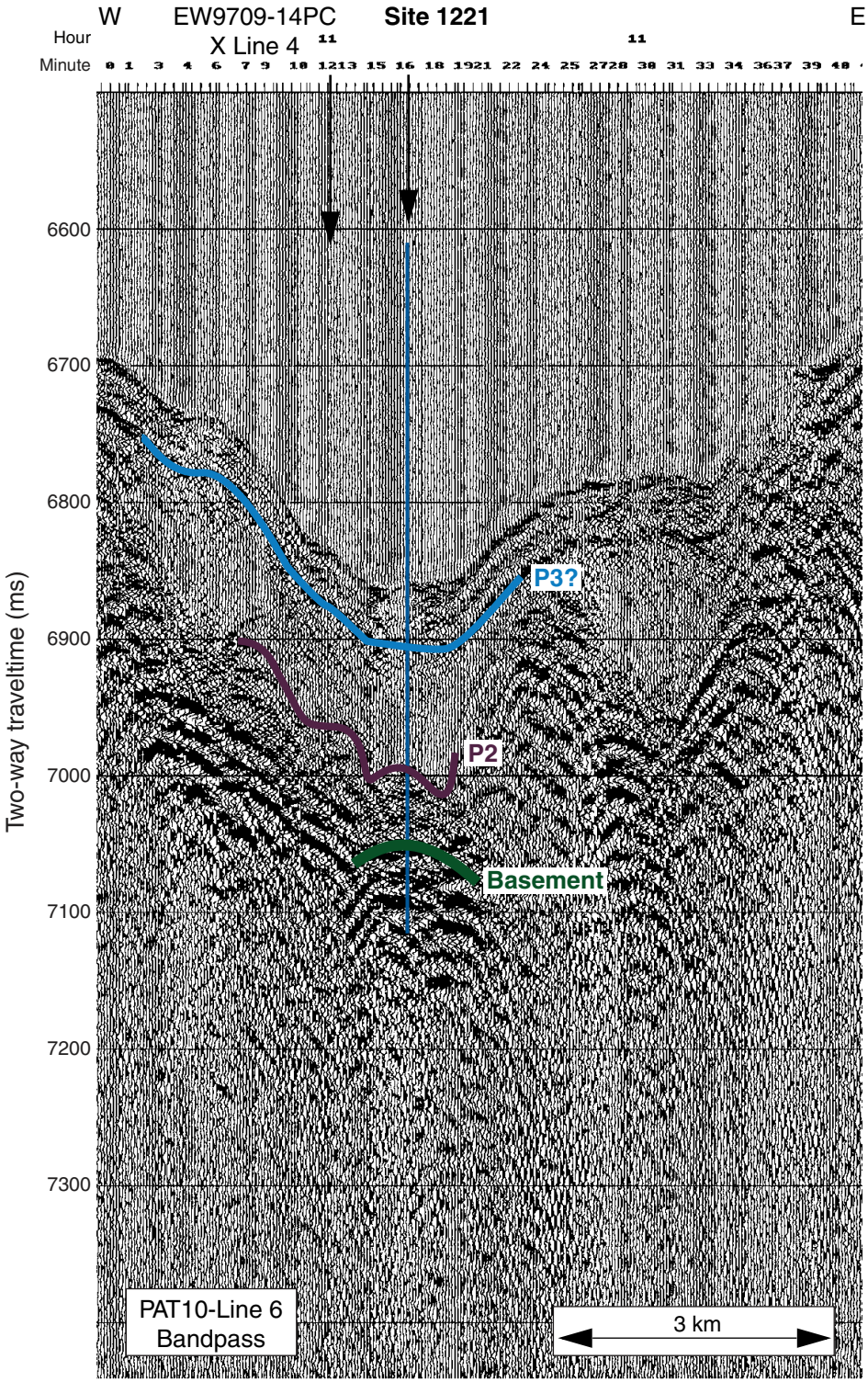

Figure F3. Lithologic summary for Site 1221. LAS = light absorption spectroscopy, TD = total depth.

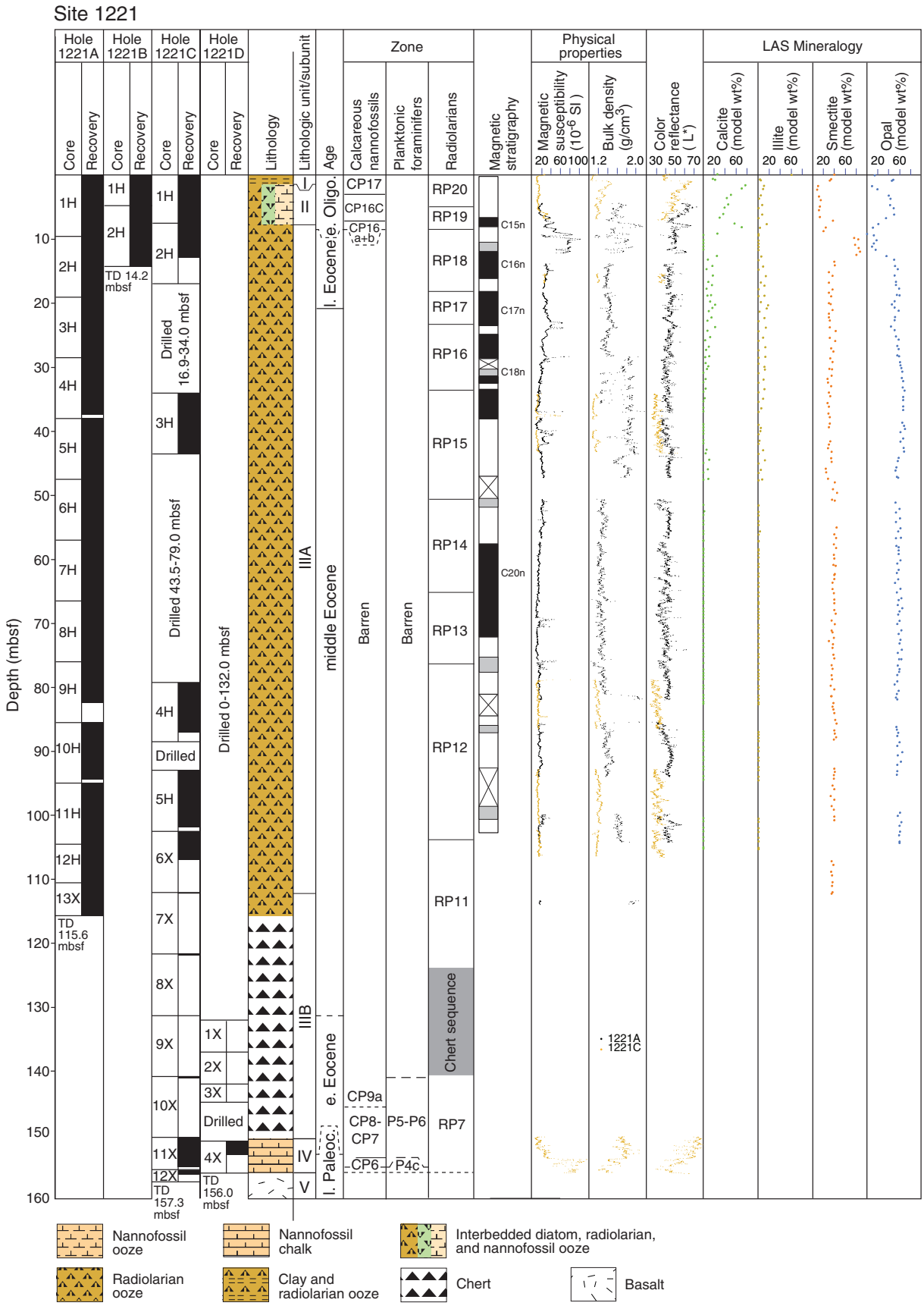

Figure F4. Close-up digital core photographs of the dramatically colored P/E boundary intervals recovered at Site 1221. **A.** Section 199-1221C-11X-3. (Continued on next page.)

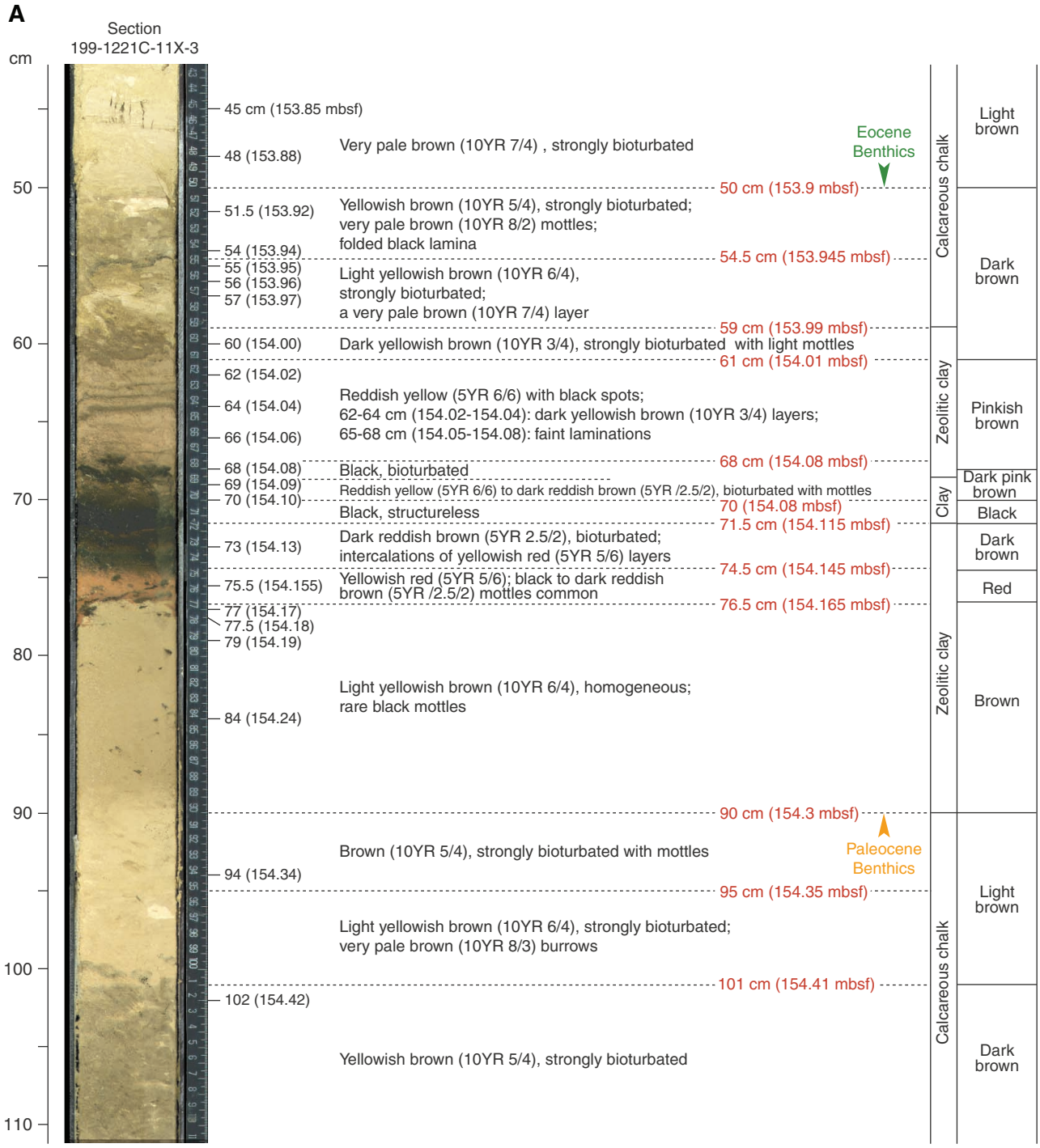

Figure F4 (continued). B. Section 199-1221D-4X-2.

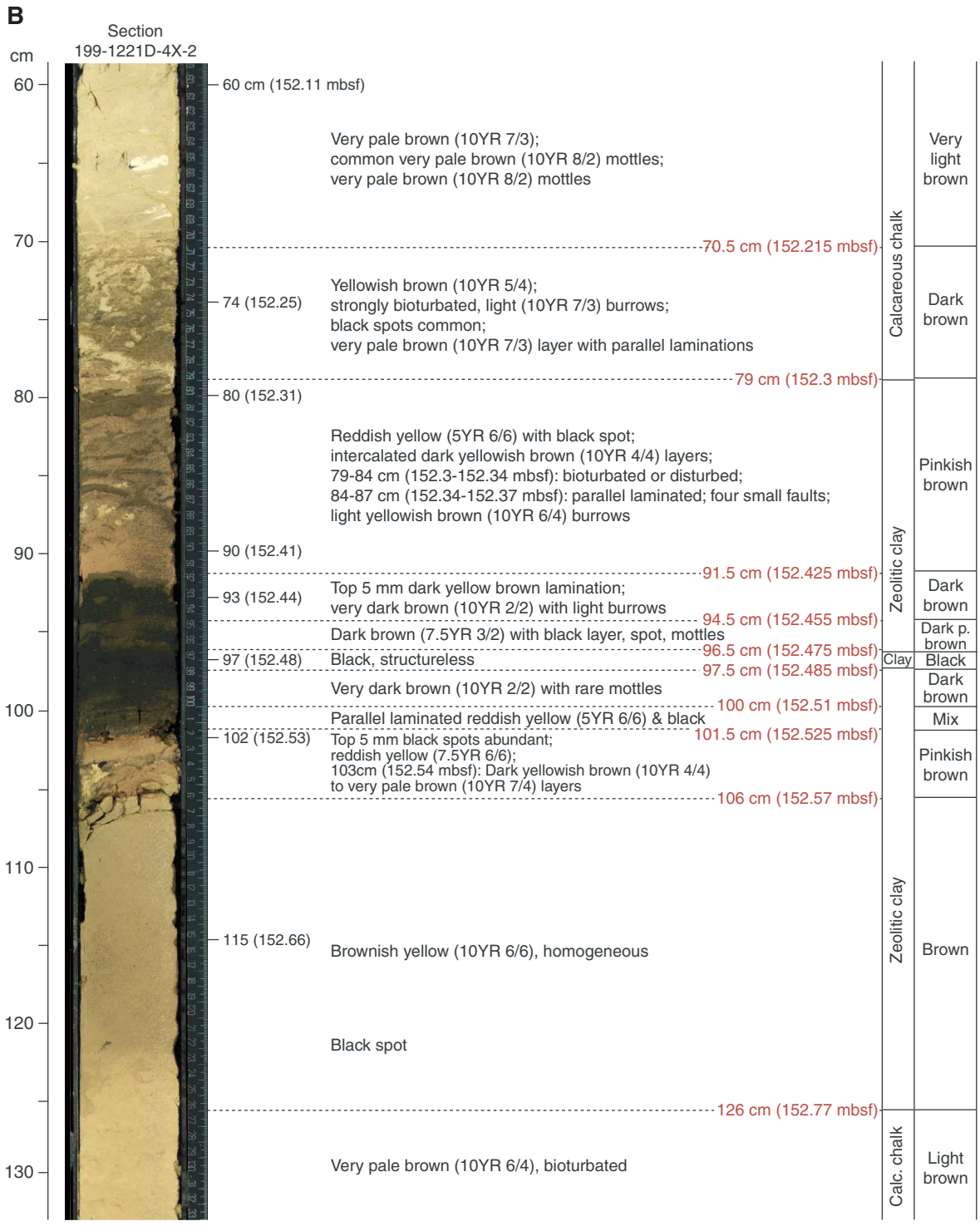

Figure F5. Calcareous and siliceous biostratigraphy for Site 1221. Gray shaded bar indicates an interval for which no zonation could be assigned with confidence. Horizontal dashed lines indicate that a boundary can only be approximated by available biostratigraphy. TD = total depth.

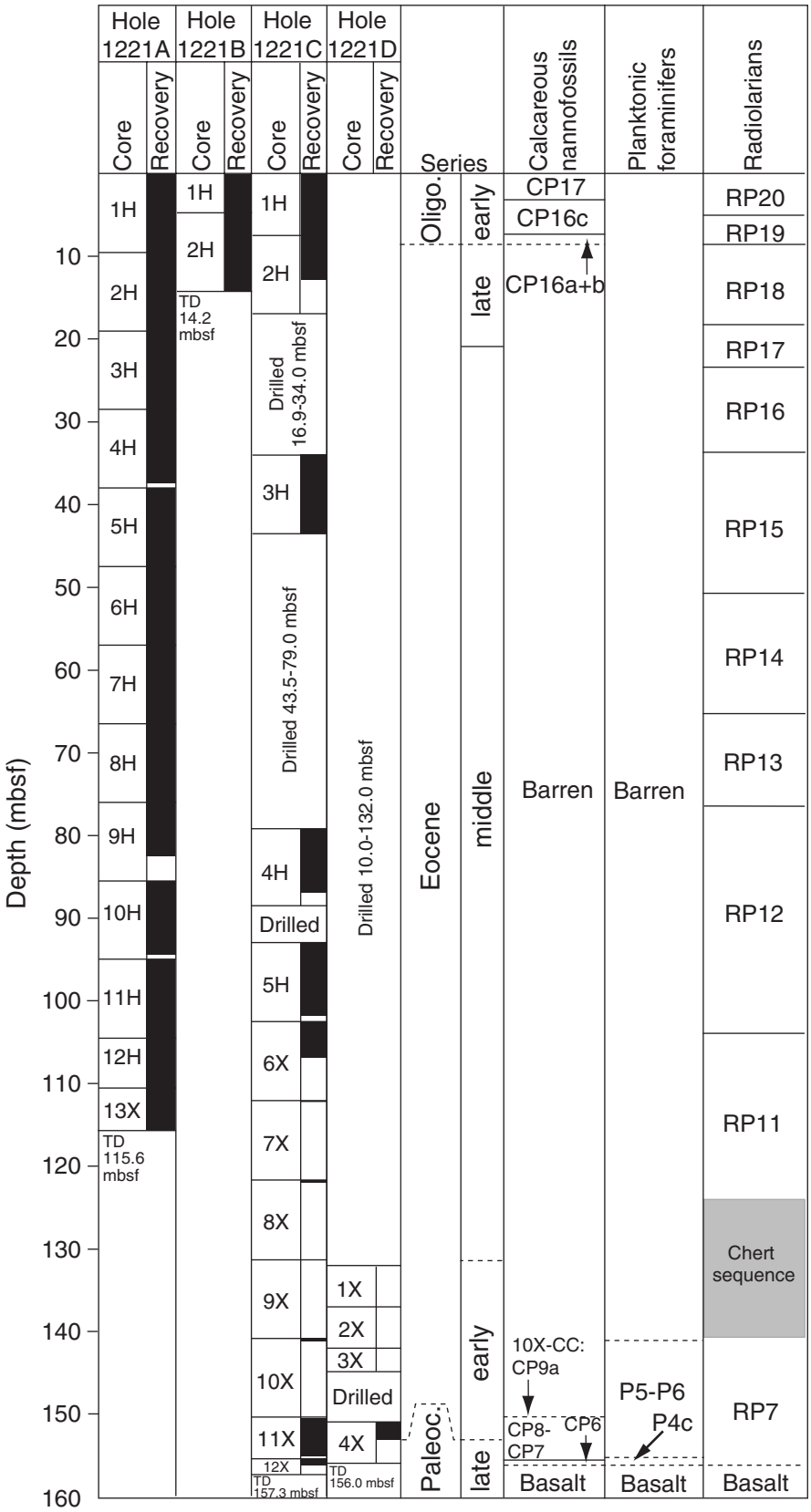

Figure F6. Comparison of estimated zonal boundary ages from Sanfilippo and Nigrini (1998) and newly calibrated ages derived from geomagnetic reversals at Site 1220 (see **"Paleomagnetism,"** p. 15).

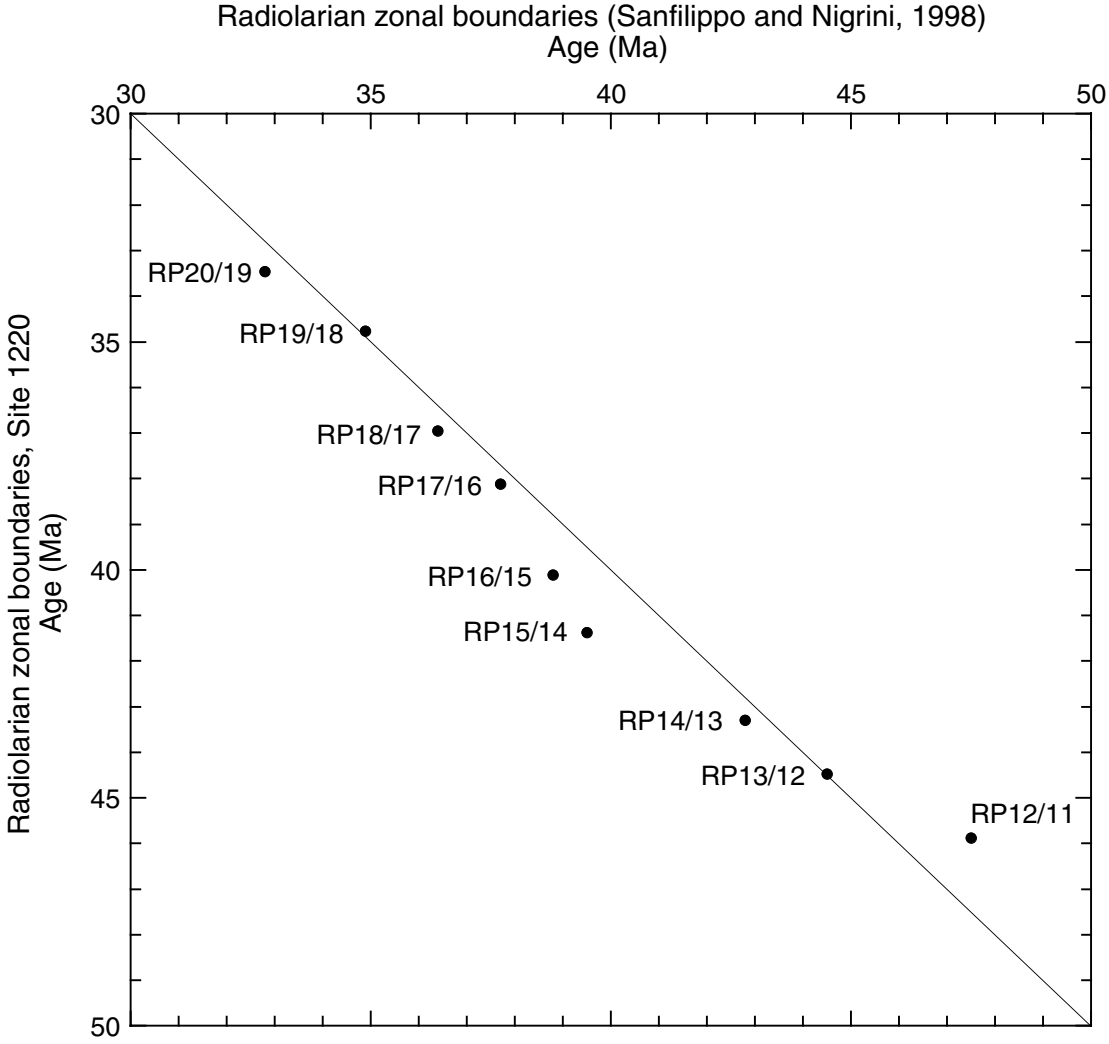

Figure F7. Archive-half magnetization intensities after AF demagnetization at a peak field of 20 mT from Hole 1221A.

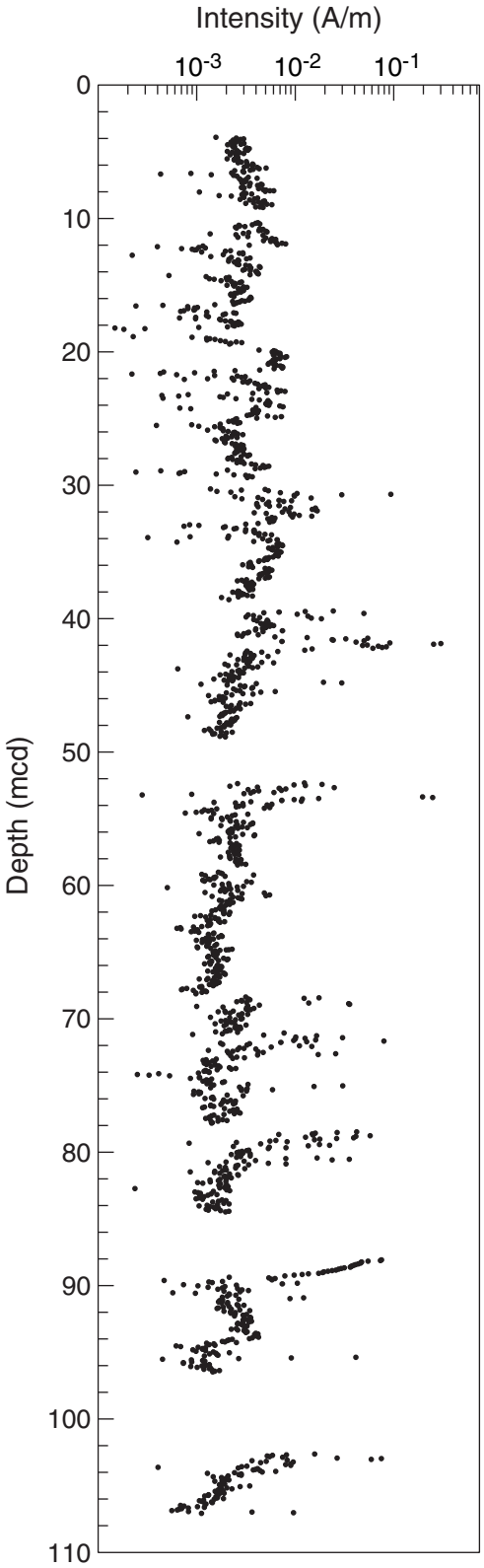

Figure F8. Composite magnetic stratigraphy for Site 1221. Virtual geomagnetic pole (VGP) latitudes were obtained after partial AF demagnetization of continuous measurements at a peak field of 20 mT. Polarity column shows interpreted zones of normal (black) and reversed (white) magnetization, gray intervals indicate zones with no polarity interpretation. Hole 1221A is in red, and Hole 1221B is in black.

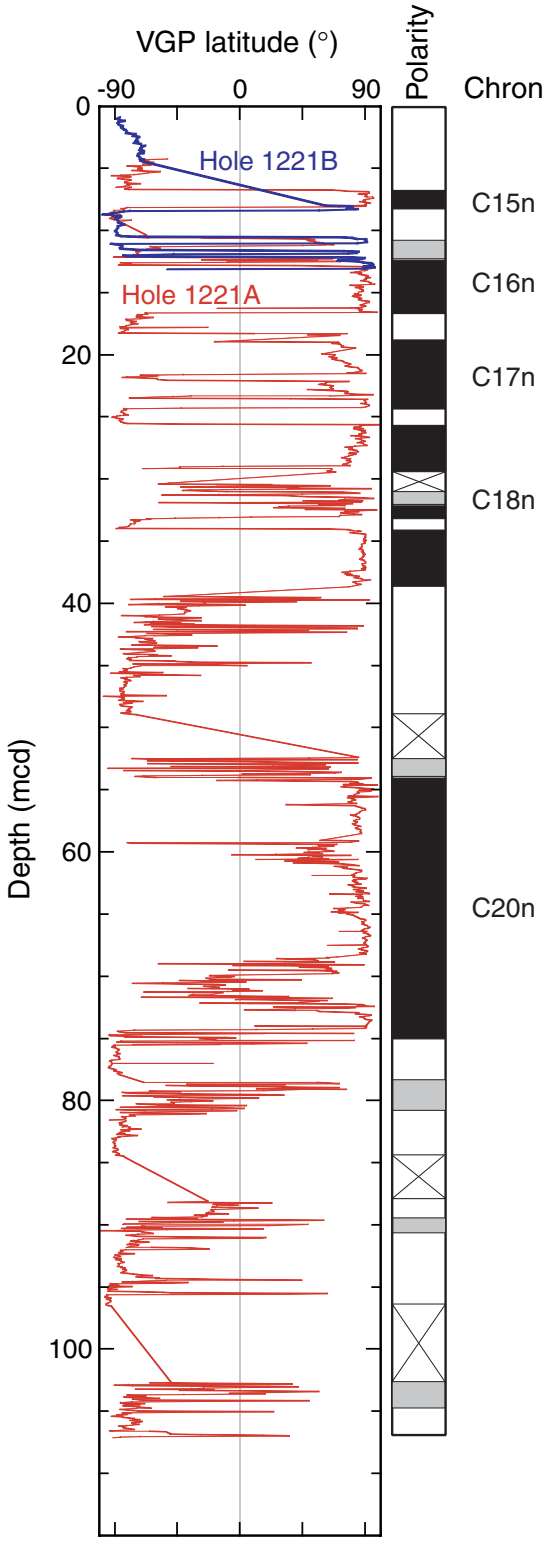

Figure F9. Gamma ray attenuation (GRA) bulk density, magnetic susceptibility, and color reflectance (L*) data for the upper 20 mcd in Holes 1221A (black; left curve in each panel), 1221B (blue; middle curve in each panel), and 1221C (green; right curve in each panel) plotted vs. composite depth. The data from Holes 1221B and 1221C are offset by constants for illustration purposes. All data sets are smoothed with a nine-point Gaussian filter. Intervals with obvious flow-in or drilling disturbance are removed from the data sets (see Table **T4**, p. 53).

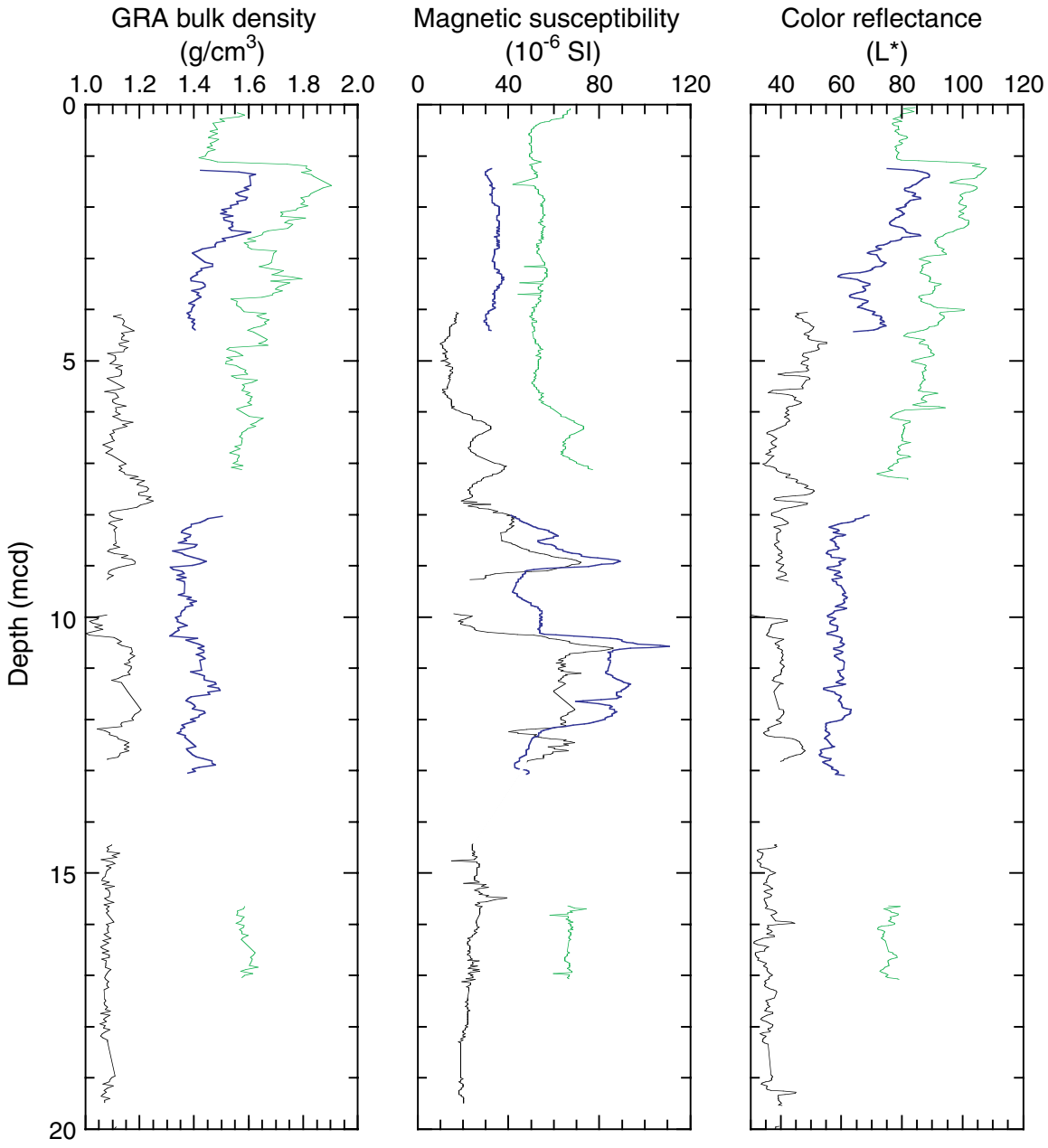

Figure F10. LSRs and chronostratigraphic markers for Site 1221.

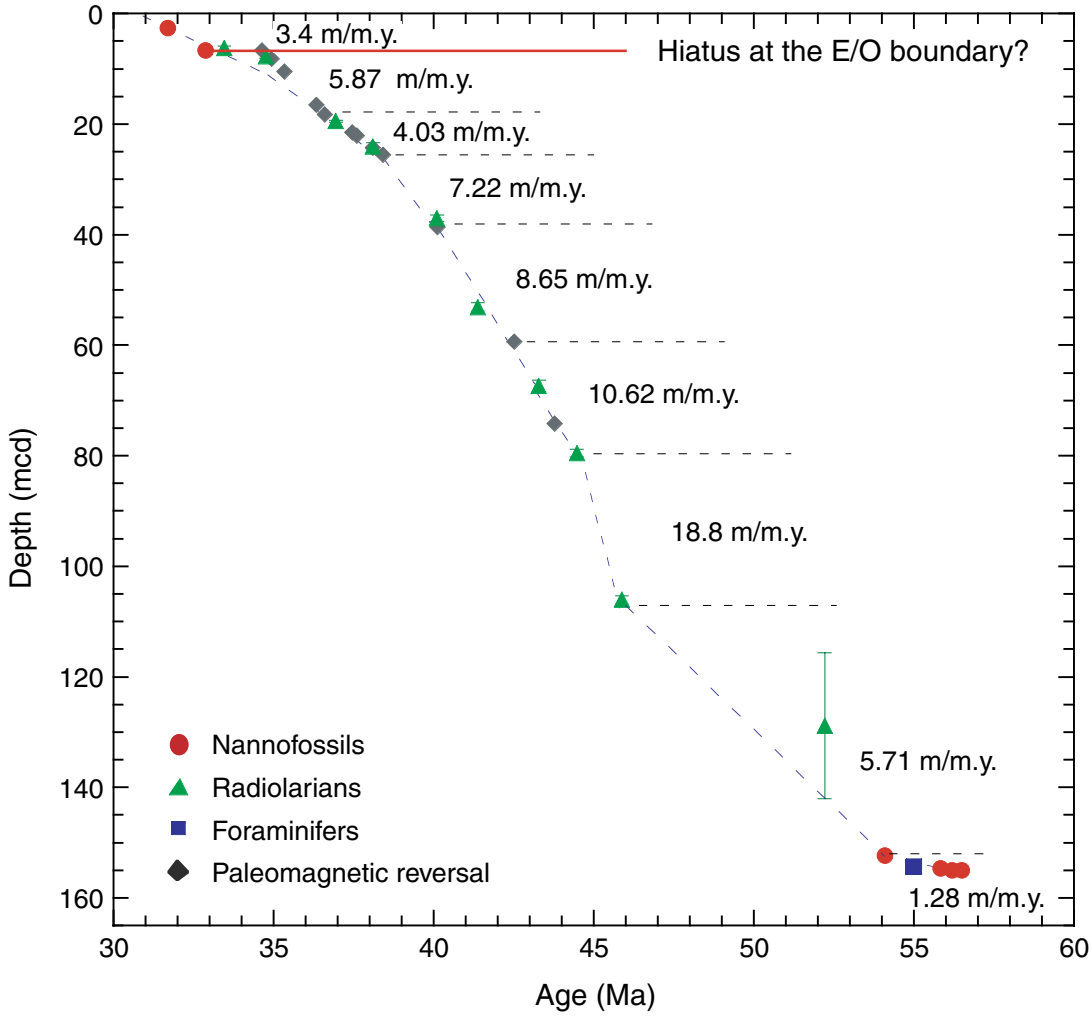

Figure F11. Density record of lowermost 5-m site survey piston Core EW9709-14P (red, thick line) compared to density record of Site 1221 (blue, thin line).

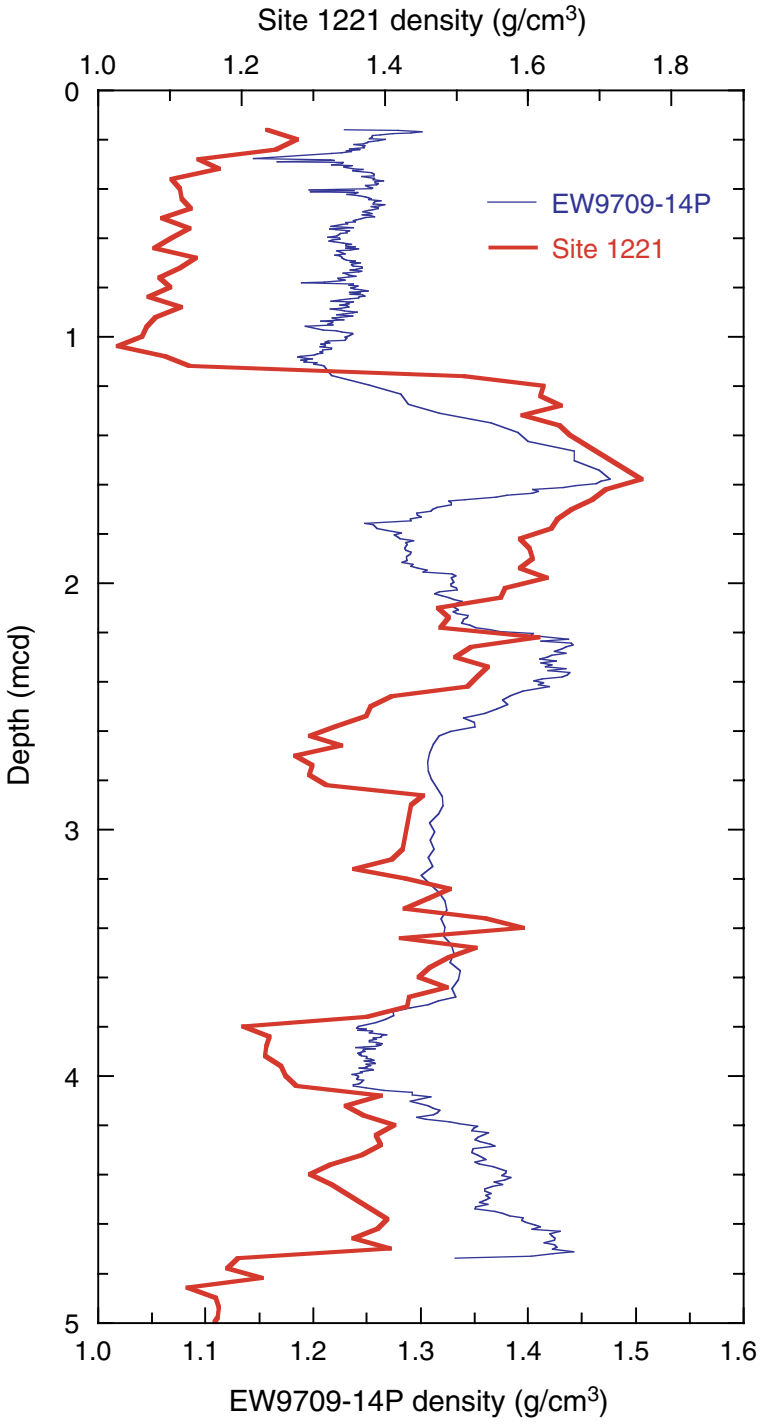

Figure F12. Bulk mass accumulation rates (MARs) of sediments from Site 1221.

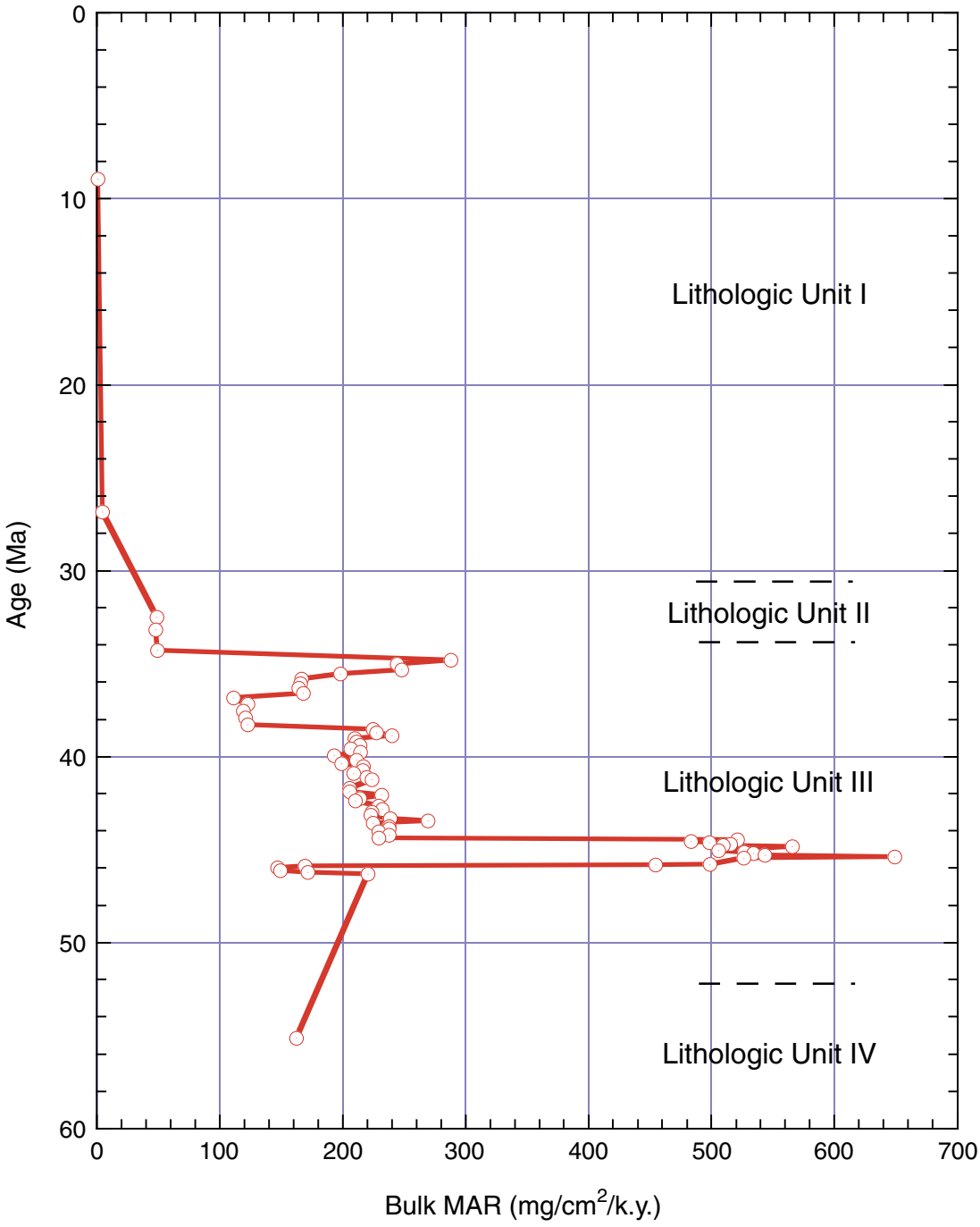

Figure F13. Interstitial water data from Site 1221. Solid circles = Ca, crosses = Mg.

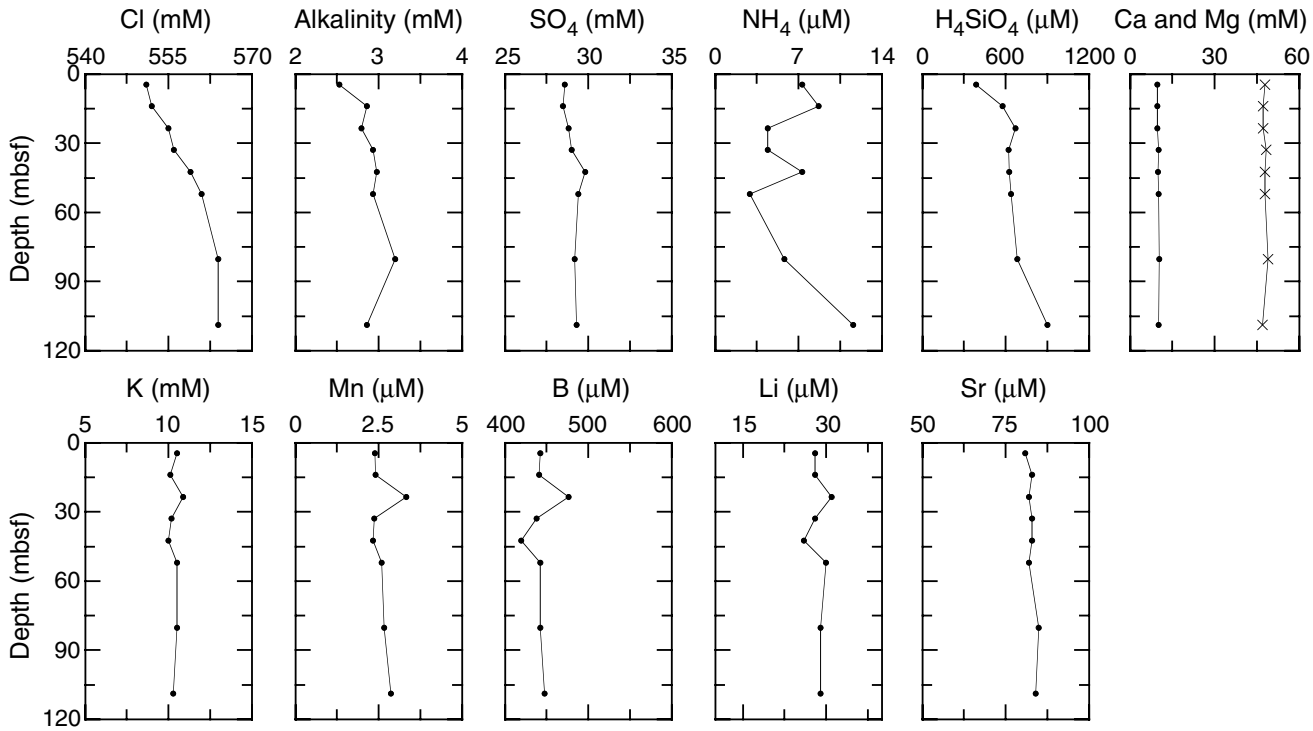

Figure F14. Bulk-sediment data from Site 1221. Calcium values higher than 35.9 wt% are out of the range of the standards (see "Geochemistry," p. 20, in the "Explanatory Notes" chapter).

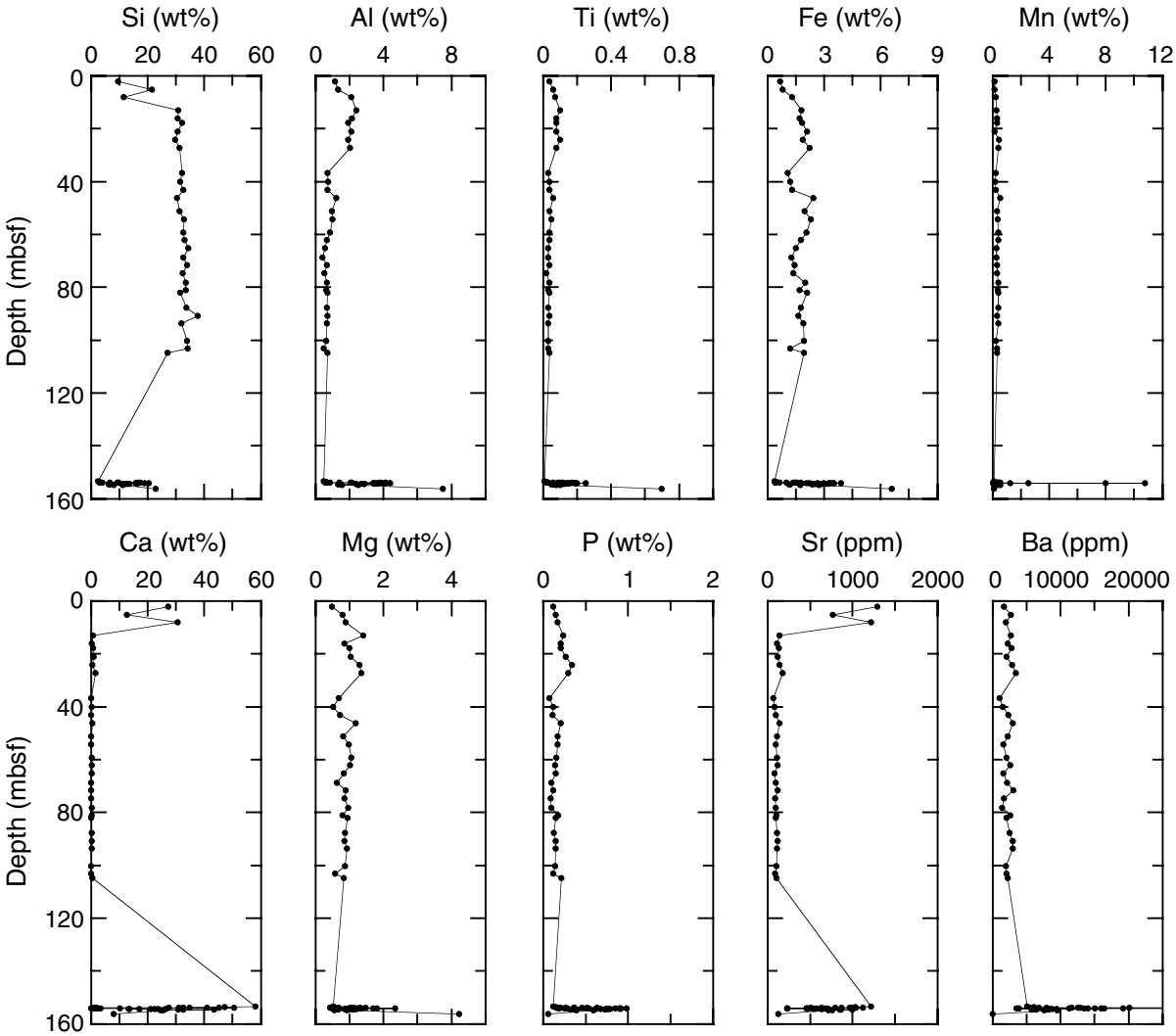

Figure F15. $CaCO_3$ data from Site 1221.

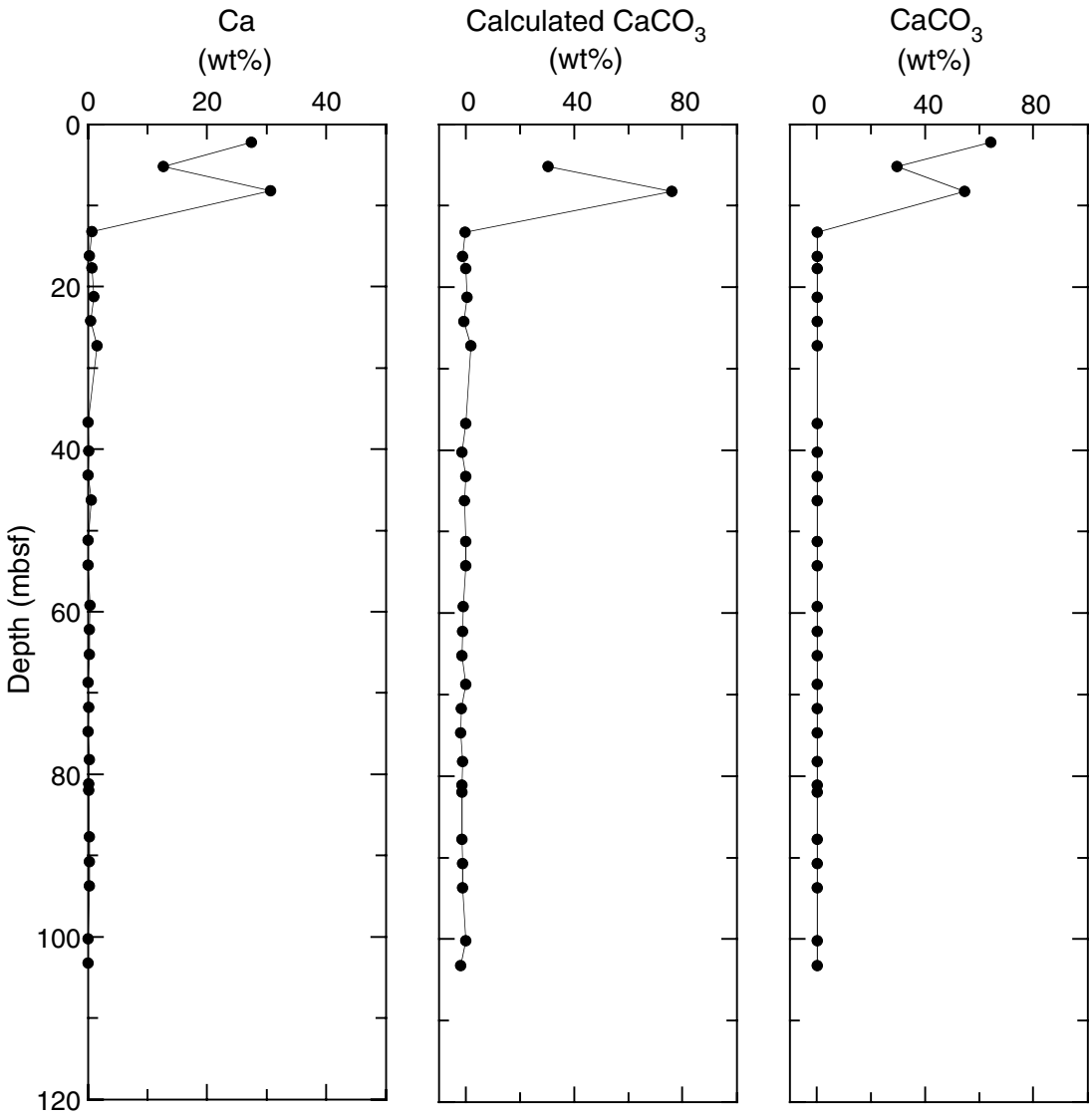

Figure F16. Bulk-sediment geochemical data for the P/E boundary from Site 1221. Horizontal lines = stratigraphic interval with most prominent color variation in lithology. Calcium values higher than 35.9 wt% are out of the range of the standards (see **"Geochemistry,"** p. 20, in the "Explanatory Notes" chapter).

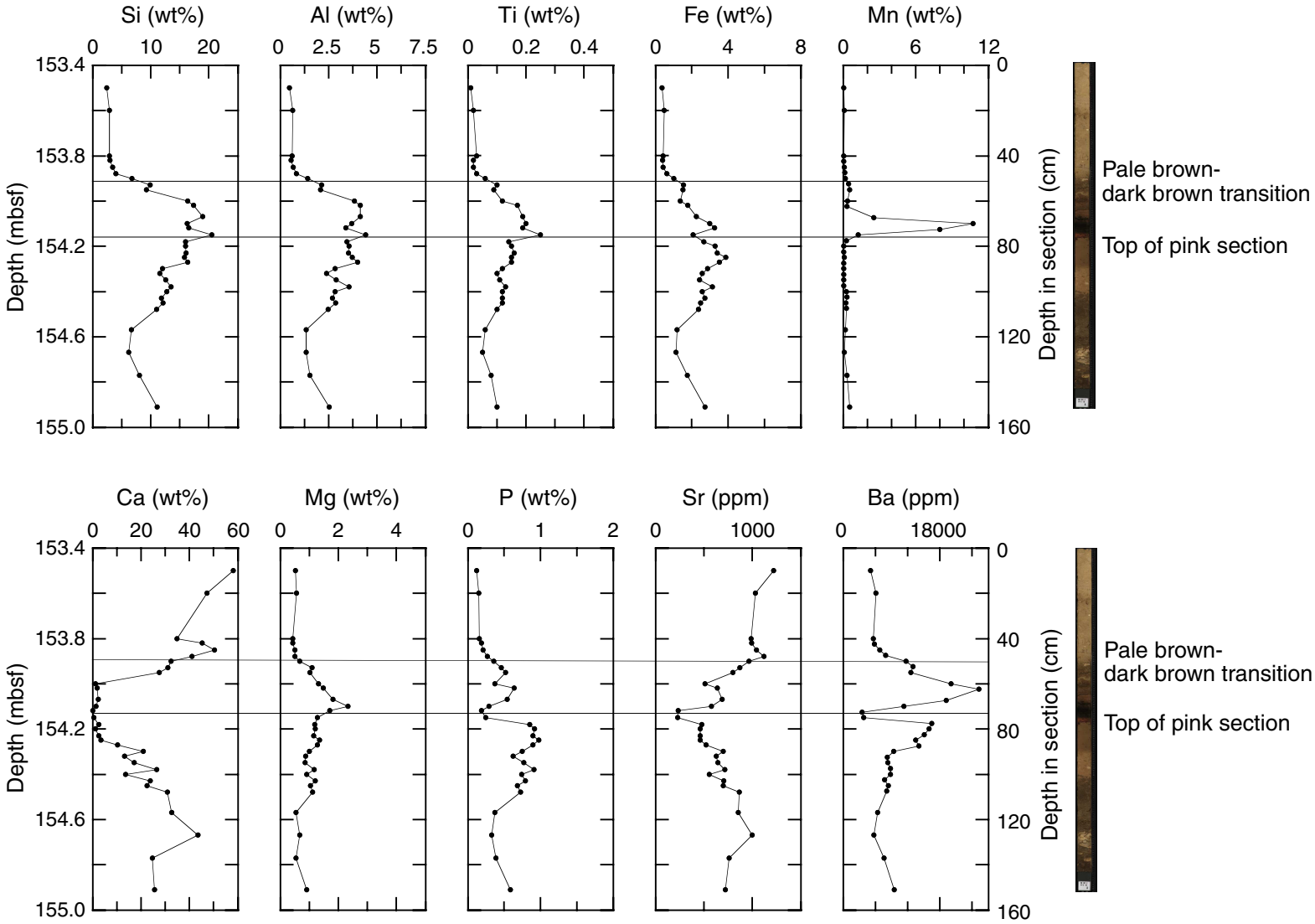

Figure F17. MAD measurements for Hole 1221A and Cores 199-1221B-1H and 199-1221C-6X. **A.** Porosity (solid symbols) and water content (open symbols). **B.** Discrete-sample wet bulk density (open symbols) and gamma ray attenuation (GRA) bulk density (line). **C.** Grain density. Lithologic Units I–IV are noted on the right side of the figure.

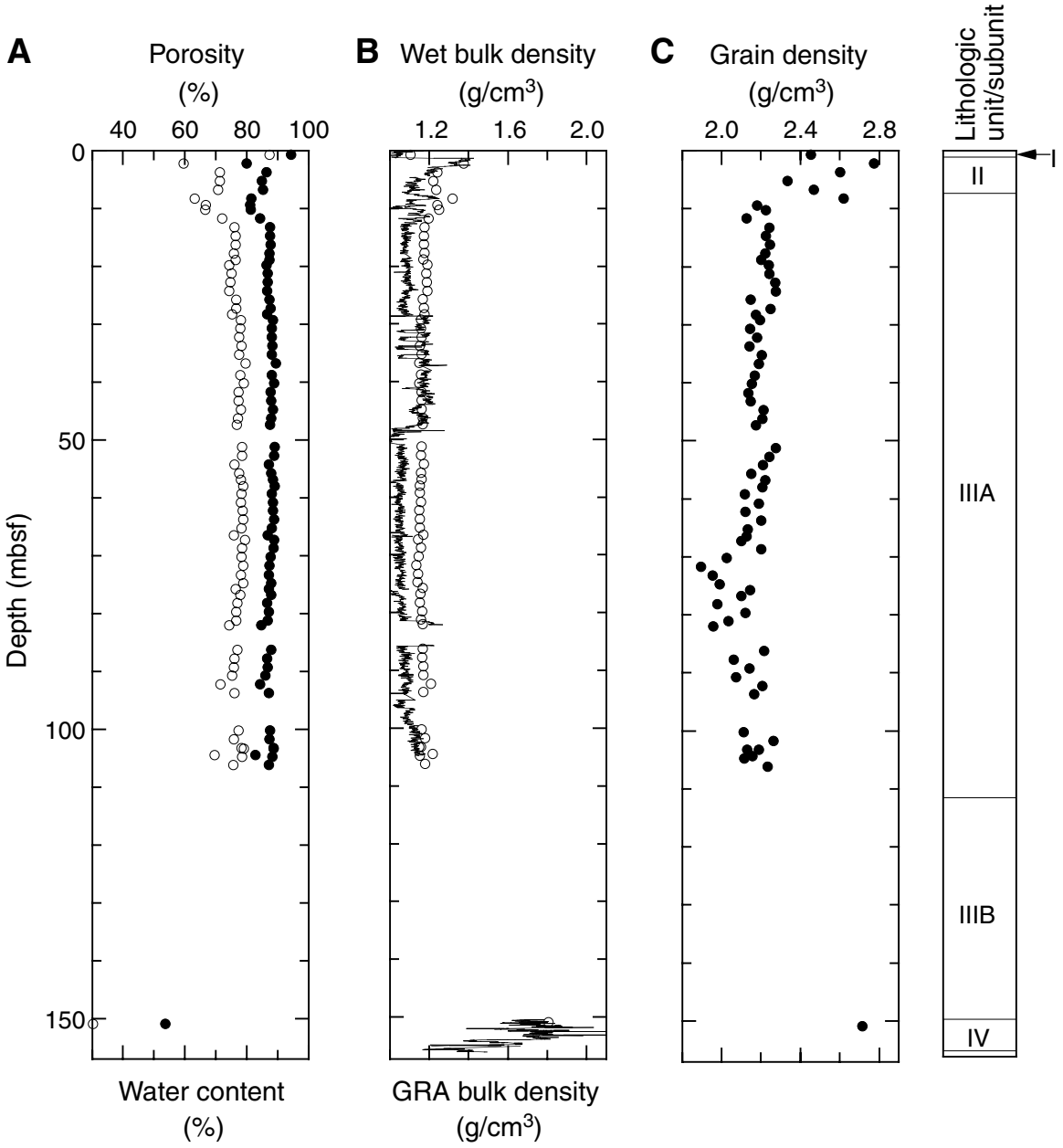

Figure F18. Comparison of magnetic susceptibility and gamma ray attenuation (GRA) bulk density with the digital core images from Sections199-1221C-11X-3 and 199-1221D-4X-2. The red arrows denote the P/E boundary.

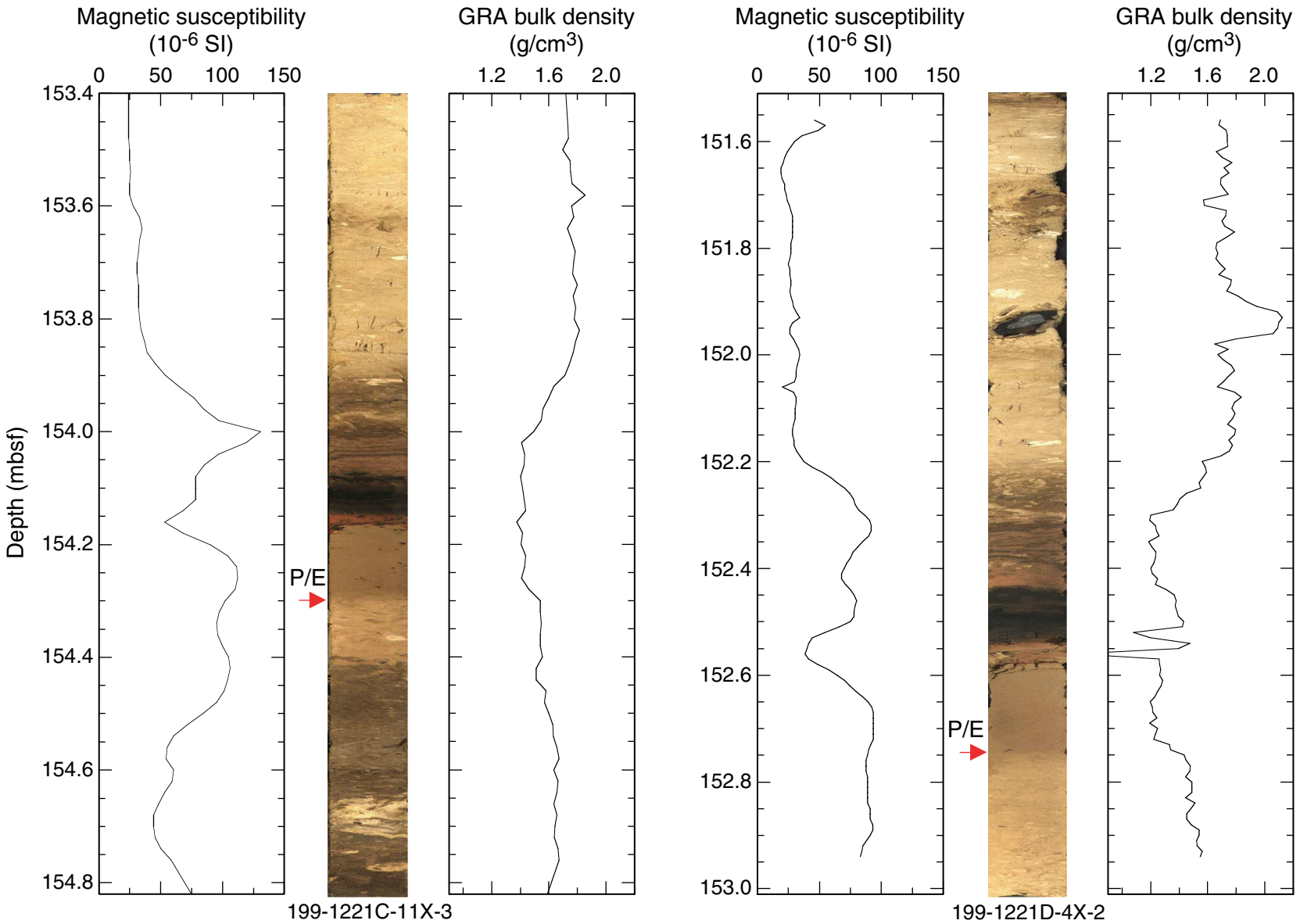

Figure F19. (**A**) Wet and (**B**) dry bulk density from discrete samples from Cores 199-1221A-1H through 3H, 6H through 11H, and 199-1221B-1H plotted with gamma ray attenuation (GRA) bulk density interpolated with a 20-cm-wide Gaussian window. GRA bulk densities from Cores 199-1221A-4H and 5H, which appear to be offset by an electronic artifact in MST data acquisition, are not included in the comparison.

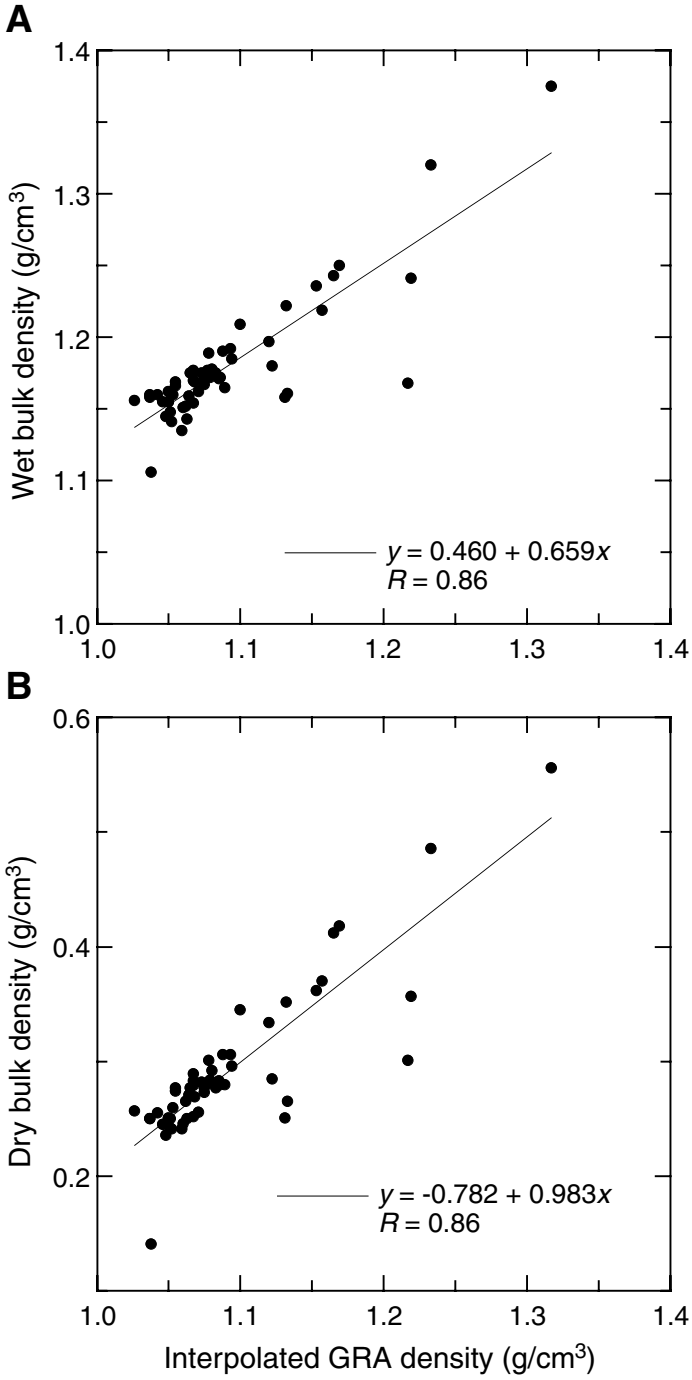

Figure F20. LAS mineralogy determinations for Hole 1221A and Sections 199-1221B-1H-1 through 1H-3. Lithologic Units I–IIIA are noted to the left of the figure. Diat = diatom, rad = radiolarian, nanno = nannofossil.

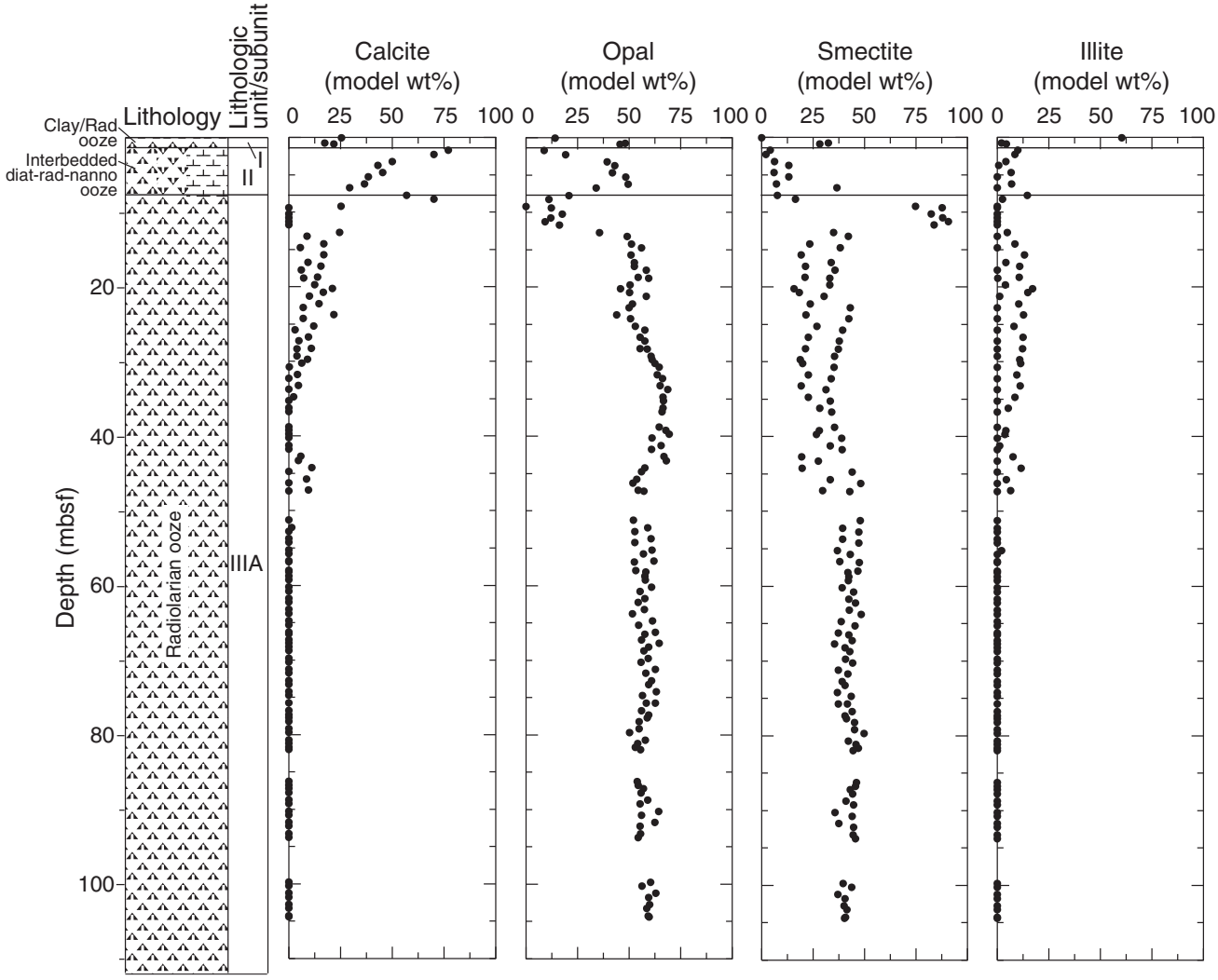

Figure F21. Compressional wave velocity from the PWL (line) and transverse velocity measured with the contact probe system (circles) for Hole 1221A and Cores 199-1221B-1H and 199-1221C-6X and 11X. Lithologic Units I–IV are noted on the right side of the figure.

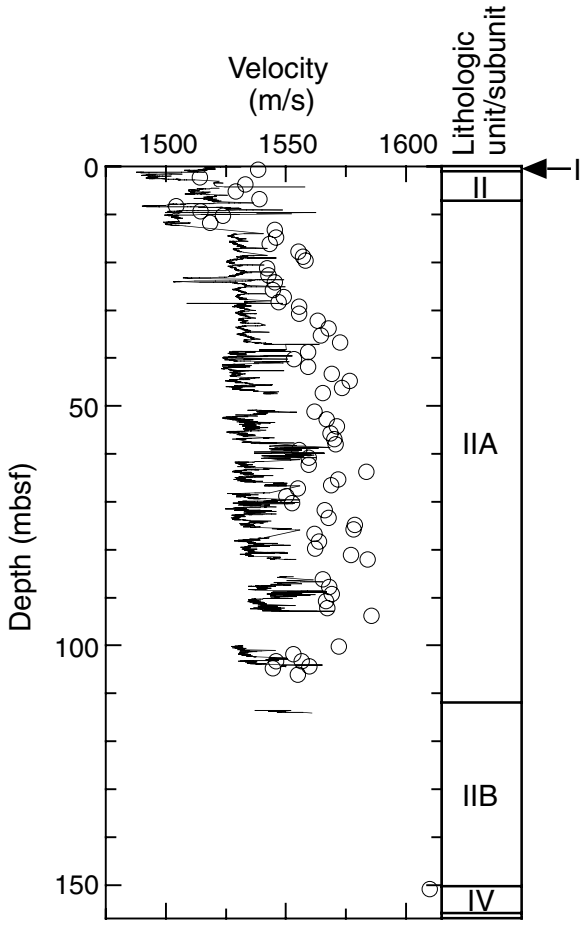

Figure F22. Natural gamma radiation for Hole 1221A and Cores 199-1221B-1H (0–4.2 mbsf) and 199-1221C-11X (150.6–154.6 mbsf). Most data below 25 mbsf are at or near background levels. Lithologic Units I–IV are noted on the right side of the figure. cps = counts per second.

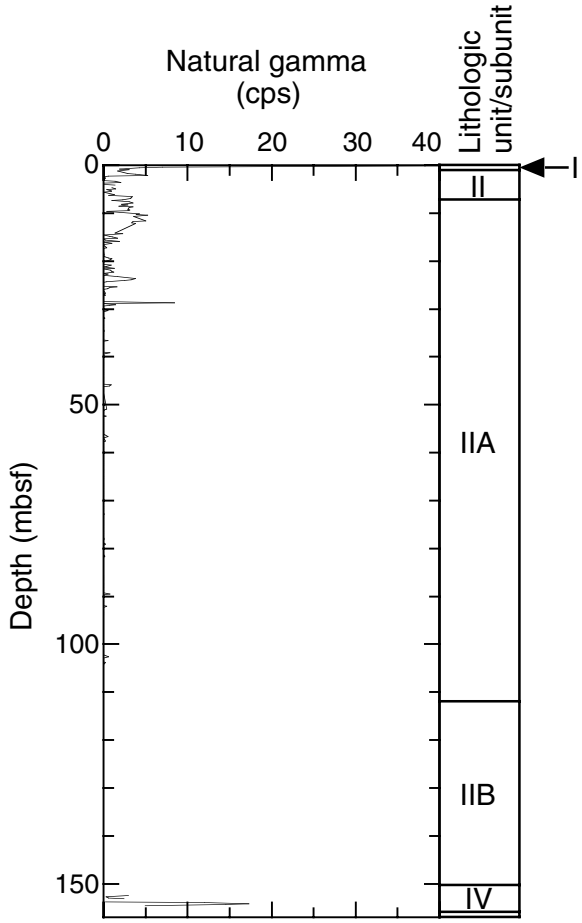

Figure F23. Magnetic susceptibility for Hole 1221A and Cores 199-1221B-1H and 199-1221C-11X.

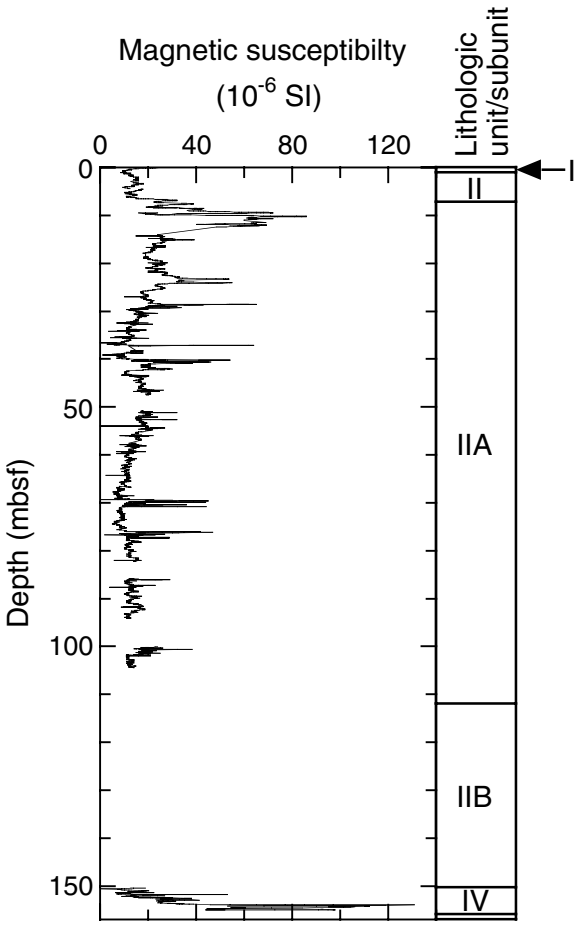

Table T1. Coring summary, Site 1221. (See table note. Continued on next page.)

Hole 1221A
Latitude: 12°1.9987′N
Longitude: 143°41.6514′W
Time on site (hr): 113.75 (0315 hr, 5 Dec–2100 hr, 9 Dec 2001)
Time on hole (hr): 47 (0315 hr, 5 Dec–0215 hr, 7 Dec 2001)
Seafloor (drill pipe measurement from rig floor, mbrf): 5186.6
Distance between rig floor and sea level (m): 11.3 m
Water depth (drill pipe measurement from sea level, m): 5175.3
Total depth (drill pipe measurement from rig floor, mbrf): 5302.2
Total penetration (meters below seafloor, mbsf): 115.6
Total length of cored section (m): 115.6
Total core recovered (m): 113.81
Core recovery (%): 98.4
Total number of cores: 13
Total number of drilled intervals: 0

Hole 1221B
Latitude: 12°1.9880′N
Longitude: 143°41.6524′W
Time on hole (hr): 12.83 (0215 hr, 7 Dec–1505 hr, 7 Dec 2001)
Seafloor (drill pipe measurement from rig floor, mbrf): 5186.4
Distance between rig floor and sea level (m): 11.3
Water depth (drill pipe measurement from sea level, m): 5175.1
Total depth (drill pipe measurement from rig floor, mbrf): 5200.6
Total penetration (meters below seafloor, mbsf): 14.2
Total length of cored section (m): 14.2
Total core recovered (m): 14.53
Core recovery (%): 102.3
Total number of cores: 2
Total number of drilled intervals: 0

Hole 1221C
Latitude: 12°1.9873′N
Longitude: 143°41.6513′W
Time on hole (hr): 24.42 (1505 hr, 7 Dec–1530 hr, 8 Dec 2001)
Seafloor (drill pipe measurement from rig floor, mbrf): 5185.70
Distance between rig floor and sea level (m): 11.3
Water depth (drill pipe measurement from sea level, m): 5174.4
Total depth (drill pipe measurement from rig floor, mbrf): 5343.0
Total penetration (meters below seafloor, mbsf): 157.3
Total length of cored section (m): 100.2
Total length of drilled intervals (m): 57.1
Total core recovered (m): 54.07
Core recovery (%): 54.0%
Total number of cores: 12
Total number of drilled intervals: 3

Hole 1221D
Latitude: 12°1.9762′N
Longitude: 143°41.6519′W
Time on hole: 29.5 (1530 hr, 8 Dec –2100 hr, 9 Dec 2001)
Seafloor (drill pipe measurement from rig floor, mbrf): 5185.7
Distance between rig floor and sea level (m): 11.3
Water depth (drill pipe measurement from sea level, m): 5174.4
Total depth (drill pipe measurement from rig floor, mbrf): 5341.7
Total penetration (meters below seafloor, mbsf): 156.0
Total length of cored section (m): 17.8
Total length of drilled intervals (m): 138.2
Total core recovered (m): 2.28
Core recovery (%): 12.8
Total number of cores: 4
Total number of drilled intervals: 2

Core	Date (Dec 2001)	Local time (hr)	Depth (mbsf) Top	Depth (mbsf) Bottom	Length (m) Cored	Length (m) Recovered	Recovery (%)
199-1221A-							
1H	5	1500	0.0	9.5	9.5	10.11	106.4
2H	5	1620	9.5	19.0	9.5	9.86	103.8
3H	5	1735	19.0	28.5	9.5	9.89	104.1
4H	5	1855	28.5	38.0	9.5	9.03	95.1

Table T1 (continued).

Core	Date (Dec 2001)	Local time (hr)	Depth (mbsf) Top	Depth (mbsf) Bottom	Length (m) Cored	Length (m) Recovered	Recovery (%)
5H	5	2010	38.0	47.5	9.5	9.80	103.2
6H	5	2120	47.5	57.0	9.5	9.87	103.9
7H	5	2240	57.0	66.5	9.5	10.12	106.5
8H	5	2345	66.5	76.0	9.5	9.86	103.8
9H	6	0115	76.0	85.5	9.5	6.41	67.5
10H	6	0255	85.5	95.0	9.5	8.91	93.8
11H	6	0655	95.0	104.5	9.5	9.93	104.5
12H	6	0850	104.5	110.6	6.1	9.88	162.0
13X	7	0245	110.6	115.6	5.0	0.14	2.8
				Cored totals:	115.6	113.81	98.4
199-1221B-							
1H	7	1435	0.0	4.7	4.7	4.68	99.6
2H	7	1545	4.7	14.2	9.5	9.85	103.7
				Cored totals:	14.2	14.53	102.3
199-1221C-							
1H	7	1710	0.0	7.4	7.4	7.40	100.0
2H	7	1830	7.4	16.9	9.5	9.84	103.6
			*****Drilled from 16.9 to 34.0*****				
3H	7	2015	34.0	43.5	9.5	9.75	102.6
			*****Drilled from 43.5 to 79.0*****				
4H	7	2225	79.0	88.5	9.5	7.91	83.3
			*****Drilled from 88.5 to 93.0*****				
5H	7	2355	93.0	102.5	9.5	8.83	93.0
6X	8	0135	102.5	112.1	9.6	4.35	45.3
7X	8	0325	112.1	121.7	9.6	0.03	0.3
8X	8	0555	121.7	131.3	9.6	0.15	1.6
9X	8	0750	131.3	140.8	9.5	0.04	0.4
10X	8	0945	140.8	150.4	9.6	0.27	2.8
11X	8	1145	150.4	155.4	5.0	4.70	94.0
12X	8	1410	155.4	157.3	1.9	0.80	42.1
				Cored totals:	100.2	54.07	54.0
				Drilled total:	57.1		
				Total:	157.3		
199-1221D-							
			*****Drilled from 0.0 to 132.0 mbsf*****				
1X	9	0025	132.0	137.0	5.0	0.00	0.0
2X	9	0230	137.0	142.0	5.0	0.03	0.6
3X	9	0455	142.0	144.8	2.8	0.02	0.7
			*****Drilled from 144.8 to 151.0 mbsf*****				
4X	9	0945	151.0	156.0	5.0	2.23	44.6
				Cored totals:	17.8	2.28	12.8
				Drilled total:	138.2		
				Total:	156.0		

Note: The expanded coring summary table is available in ASCII (see the "Supplementary Material" contents list).

Table T2. Calcareous nannofossil datums, Site 1221.

Core, section, interval (cm)		Marker species	Age (Ma)	Depth (mbsf)	
Top	Bottom			Midpoint	±
199-1221A-	199-1221A-				
1H-3, 3	1H-3, 40	T *Reticulofenestra umbilicus* ≥14 µm	31.7	3.22	0.19
1H-5, 70	1H-6, 40	T *Ericsonia formosa*	32.9	7.30	0.60
199-1221C-	199-1221C-				
11X-2, 97	11X-2, 110	T *Fascicultihus* spp.*	54.1	152.94	0.06
199-1221C-	199-1221C-				
11X-CC	12X-1, 3	T *Ericsonia robusta*†	55.9	155.27	0.16
12X-1, 18	12X-1, 32	B *Discoaster multiradiatus*	56.2	155.65	0.07
12X-1, 18	12X-1, 32	B *Discoaster nobilis*	56.5	155.65	0.07

Notes: T = top, B = bottom. * = age estimate in need of revision; event occurs 1.38 m above the P/E boundary (199-1221C-11X-3, 91 cm). † = age estimate derived from Site 1215 data. This table is also available in **ASCII.**

Table T3. Radiolarian zonal boundaries, Site 1221.

Zonal boundaries	Age (Ma)	Hole, core, section, interval (cm)		Depth (mbsf)		Depth (mcd)	
		Top	Bottom	Midpoint	±	Midpoint	±
		199-	199-				
RP20/19	33.47	1221A-1H-5, 45	1221B-2H-3, 22	7.19	0.74	6.29	0.40
RP19/18	34.77	1221A-1H-6, 45	1221B-2H-4, 7	8.61	0.66	7.71	0.32
RP18/17	36.96	1221A-2H-7, 43	1221A-2H-CC	19.13	0.20	19.51	0.20
RP17/16	38.12	1221A-3H-3, 46	1221A-3H-4, 46	23.21	0.75	24.09	0.75
RP16/15	40.12	1221A-4H-5, 45	1221A-4H-6, 45	35.70	0.75	37.08	0.75
RP15/14	41.39	1221A-6H-3, 45	1221A-6H-4, 45	51.70	0.75	53.08	0.75
RP14/13	43.30	1221A-7H-6, 45	1221A-7H-CC	66.02	1.07	67.40	1.07
RP13/12	44.48	1221A-9H-1, 45	1221A-9H-2, 45	77.18	0.73	79.56	0.73
RP12/11	45.89	1221A-11H-6, 45	1221A-11H-7, 45	103.70	0.75	106.08	0.75
RP8/7	52.22	1221A-12H-CC	1221C-10X-CC	127.68	13.35	128.87	12.16

Notes: * = new ages calibrated from geomagnetic reversals at Site 1220. This table is also available in **ASCII.**

Table T4. Core disturbance, Holes 1221A, 1221B, and 1221C.

Core, section, interval (cm)	Depth (mbsf) Top	Depth (mbsf) Bottom	Comments
199-1221A-			
1H-1, 0–150	0.00	1.50	Flow-in
1H-2, 0–150	1.50	3.00	Flow-in
1H-3, 0–150	3.00	4.50	Flow-in
1H-4, 0–11	4.50	4.61	Flow-in
1H-CC, 0–22	9.89	10.11	Flow-in
2H-1, 0–40	9.50	9.90	Flow-in
2H-2, 10–40	11.10	11.40	Crack
2H-3, 0–150	12.50	14.00	Flow-in
3H-CC, 9–16	28.76	28.83	Disturbed
5H-1, 0–14	38.00	38.14	Soupy
6H-1, 0–150	47.50	49.00	Soupy
6H-2, 0–150	49.00	50.50	Soupy
6H-3, 0–34	50.50	50.84	Soupy
7H-1, 0–57	57.00	57.57	Soupy
10H-1, 0–15	85.50	85.65	Soupy
10H-1, 25–26.5	85.75	85.77	Crack
10H-CC, 0–15	94.21	94.36	Disturbed
11H-1, 0–150	95.00	96.50	Flow-in
11H-2, 0–150	96.50	98.00	Flow-in
11H-3, 0–124	98.00	99.24	Flow-in
11H-3, 124–150	99.24	99.50	Disturbed
11H-4, 0–57	99.50	100.07	Disturbed
12H-1, 0–150	104.50	106.00	Flow-in
12H-2, 0–150	106.00	107.50	Flow-in
12H-3, 0–150	107.50	109.00	Flow-in
12H-4, 0–150	109.00	110.50	Flow-in
12H-5, 0–150	110.50	112.00	Flow-in
12H-6, 0–150	112.00	113.50	Flow-in
199-1221B-			
1H-1, 0–150	0.00	1.50	Soupy
1H-1, 90–125	0.90	1.25	Cracks
2H-1, 0–150	4.70	6.20	Flow-in
2H-2, 0–150	6.20	7.70	Flow-in
2H-3, 0–150	7.70	9.20	Flow-in
199-1221C-			
2H-1, 0–150	7.40	8.90	Flow-in
2H-2, 0–150	8.90	10.40	Flow-in
2H-3, 0–150	10.40	11.90	Flow-in
2H-4, 0–150	11.90	13.40	Flow-in
2H-5, 0–100	13.40	14.40	Flow-in
2H-5, 100–150	14.40	14.90	Flow-in
2H-6, 0–72	14.90	15.62	Flow-in?
2H-7, 0–12	16.40	16.52	Flow-in?
3H-1, 0–40	34.00	34.40	Soupy
3H-1, 81–82	34.81	34.82	Void
3H-3, 13–16	37.13	37.16	Void
3H-4, 0–150	38.50	40.00	Core liner debris

Notes: Data from these intervals were removed from the GRA bulk density, MS, color reflectance, natural gamma, and *P*-wave velocity data sets prior to construction of the composite section. This table is also available in **ASCII.** [**N1**]

Table T5. Composite depths, Site 1221.

Core	Length (m)	Depth (mbsf)	Offset (m)	Depth (mcd)
199-1221A-				
1H	9.5	0.00	–0.56	–0.56
2H	9.5	9.50	0.38	9.88
3H	9.5	19.00	0.88	19.88
4H	9.5	28.50	1.38	29.88
5H	9.5	38.00	1.38	39.38
6H	9.5	47.50	1.38	48.88
7H	9.5	57.00	1.38	58.38
8H	9.5	66.50	1.88	68.38
9H	9.5	76.00	2.38	78.38
10H	9.5	85.50	2.38	87.88
11H	9.5	95.00	2.38	97.38
12H	6.1	104.50	2.38	106.88
199-1221B-				
1H	4.7	0.00	0.00	0.00
2H	9.5	4.70	–1.24	3.46
199-1221C-				
1H	7.4	0.00	0.00	0.00
2H	9.5	7.40	0.00	7.40
3H	9.5	34.00	0.00	34.00
4H	9.5	79.00	0.00	79.00
5H	9.5	93.00	0.00	93.00
6X	9.6	102.50	0.00	102.50
11X	5.0	150.40	0.00	150.40
12X	1.9	155.40	0.00	155.40
199-1221D-				
4X	5.0	151.00	1.63	152.63

Note: This table is also available in **ASCII.**

Table T6. Splice tie points, Holes 1221A, 1221B, and 1221C.

Hole, core, section, interval (cm)	Depth (mbsf)	Depth (mcd)		Hole, core, section, interval (cm)	Depth (mbsf)	Depth (mcd)
199-				199-		
1221C-1H-4, 32	4.82	4.82	Tie to	1221A-1H-4, 88	5.38	4.82
1221A-1H-7, 48	9.48	8.92	Tie to	1221B-2H-4, 96	10.16	8.92
1221B-2H-5, 94	11.64	10.40	Tie to	1221A-2H-1, 52	10.02	10.40
1221A-2H-7, 62	19.12	19.50	Append to	1221A-3H-1, 0	19.00	19.88
1221A-3H-7, 62	28.62	29.50	Append to	1221A-4H-1, 0	28.50	29.88
1221A-4H-6, 130	37.30	38.68	Append to	1221A-5H-1, 0	38.00	39.38
1221A-5H-7, 48	47.48	48.86	Append to	1221A-6H-1, 0	47.50	48.88
1221A-6H-7, 48	56.98	58.36	Append to	1221A-7H-1, 0	57.00	58.38
1221A-7H-7, 88	66.88	68.26	Append to	1221A-8H-1, 0	66.50	68.38
1221A-8H-7, 54	76.04	77.92	Append to	1221A-9H-1, 0	76.00	78.38
1221A-9H-5, 72	82.18	84.56	Append to	1221A-10H-1, 0	85.50	87.88
1221A-10H-6, 118	94.18	96.56	Append to	1221A-11H-1, 0	95.00	97.38
1221A-11H-7, 48	104.48	106.86	Append to	1221C-11X-1, 0	150.40	150.40
1221C-11X-CC, 26	155.08	155.08	Append to	1221C-12X-1, 0	155.40	155.40
1221C-12X-CC, 6	156.18	156.18				

Note: This table is also available in **ASCII.**

Table T7. Paleomagnetic events, Site 1221.

Chron/ Subchron	Age (Ma)	Depth (mcd)
T C15n	**34.655**	**6.67**
B C15n	34.940	8.21
T C16n.1n	**35.343**	**10.57**
B C16n.2n	36.341	16.60
T C17n.1n	**36.618**	**18.31**
B C17n.1n	37.473	21.56
T C17n.2n	**37.604**	**22.09**
B C17n.3n	38.113	24.34
T C18n.1n	**38.426**	**25.58**
B C18n.2n	40.130	38.60
T C20n	**42.536**	**59.38**
B C20n	43.789	74.29

Notes: T = top, B = bottom. Bold type = control points for LSR calculation in Figure **F10,** p. 35. This table is also available in **ASCII.**

Table T8. Nannofossil, foraminifer, and radiolarian events, Site 1221.

Marker species/ Zonal boundaries	Age (Ma)	Midpoint (mcd)	± (m)
Nannofossil events:			
T *Reticulofenestra umbilicus* ≥14 µm	**31.70**	**2.66**	0.19
T *Ericsonia formosa*	32.90	6.74	0.60
T *Fascicultihus* spp.*	**54.10**	**152.94**	0.06
T *Ericsonia robusta*	55.90	155.27	0.16
B *Discoaster multiradiatus*	**56.20**	**155.65**	0.07
B *Discoaster nobilis*	56.50	155.65	0.07
Foraminifer events:			
Benthic extinction event	55.00	154.31	0.01
Radiolarian events:			
RP20/19	33.47	6.29	0.40
RP19/18	34.77	7.71	0.32
RP18/17	36.96	19.51	0.20
RP17/16	38.12	23.59	0.75
RP16/15	40.12	35.89	0.56
RP15/14	41.39	52.08	0.75
RP14/13	43.30	**66.33**	**1.00**
RP13/12	44.48	**77.56**	0.73
RP12/11	45.89	**104.08**	0.75
RP8/7	52.22	127.86	13.16

Notes: T = top, B = base. * = age estimate in need of revision; event occurs 1.38 m above the P/E boundary (199-1221B-11X-3, 91 cm). Bold type = control point for LSR calculations in Figure **F10,** p. 35. This table is also available in **ASCII.** [**N1**]

Table T9. Depths, ages, rates, and fluxes of sediments, Site 1221.

Depth (mcd)	Age (Ma)	LSR (m/m.y.)	DBD (g/cm^3)	MAR (mg/cm^2/k.y.)
0.75	8.95	0.08	0.141	1
2.25	26.86	0.08	0.556	5
3.75	32.51	1.36	0.357	48
4.69	33.20	1.36	0.350	48
6.19	34.30	1.36	0.360	49
7.69	34.83	5.93	0.490	288
8.88	35.03	5.93	0.410	244
10.63	35.32	5.93	0.420	248
12.13	35.58	5.93	0.330	198
13.63	35.83	5.93	0.280	167
15.13	36.08	5.93	0.280	165
16.63	36.33	5.93	0.280	164
18.13	36.59	5.93	0.280	168
19.24	36.85	4.02	0.280	111
20.63	37.19	4.02	0.310	123
22.13	37.57	4.02	0.300	119
23.63	37.94	4.02	0.300	121
25.13	38.31	4.02	0.310	123
26.63	38.55	8.22	0.270	225
28.13	38.74	8.22	0.280	228
29.21	38.87	8.22	0.290	240
30.63	39.04	8.22	0.260	210
32.13	39.22	8.22	0.260	211
33.63	39.40	8.22	0.260	214
35.13	39.59	8.22	0.250	206
36.63	39.77	8.22	0.260	215
38.13	39.95	8.22	0.240	193
40.13	40.20	8.22	0.260	211
41.63	40.38	8.22	0.240	199
43.13	40.56	8.22	0.260	217
44.63	40.74	8.22	0.260	216
46.13	40.92	8.22	0.250	209
47.63	41.11	8.22	0.270	220
48.73	41.24	8.22	0.270	224
52.63	41.72	8.22	0.250	206
54.13	41.90	8.22	0.250	206
55.63	42.08	8.22	0.280	232
57.13	42.26	8.22	0.260	214
58.23	42.40	8.22	0.260	211
60.64	42.67	9.10	0.250	229
62.18	42.84	9.10	0.260	232
63.63	43.00	9.10	0.250	224
65.15	43.17	9.10	0.250	223
66.66	43.33	9.52	0.250	239
67.88	43.46	9.52	0.280	269
69.13	43.59	9.52	0.240	225
70.63	43.75	9.52	0.250	238
72.13	43.91	9.52	0.250	238
73.63	44.07	9.52	0.240	229
75.16	44.23	9.52	0.250	238
76.63	44.38	9.52	0.240	229
77.63	44.48	18.81	0.280	521
79.13	44.56	18.81	0.260	483
80.59	44.64	18.81	0.270	498
82.09	44.72	18.81	0.270	515
83.54	44.80	18.81	0.270	510
84.39	44.84	18.81	0.300	566
88.65	45.07	18.81	0.270	506
90.13	45.15	18.81	0.280	527
91.63	45.23	18.81	0.280	534
93.13	45.31	18.81	0.290	544
94.63	45.39	18.81	0.350	649
96.13	45.47	18.81	0.280	526
102.63	45.81	18.81	0.270	499
103.28	45.85	18.81	0.242	455
104.13	45.90	5.95	0.280	169
104.75	46.00	5.95	0.247	147
105.63	46.15	5.95	0.250	149
106.17	46.24	5.95	0.288	172
106.79	46.35	5.95	0.370	220
153.5	55.15	1.29	1.257	163

Notes: LSR = linear sedimentation rate, DBD = dry bulk density, MAR = mass accumulation rate. This table is also available in **ASCII.**

Table T10. Interstitial water data, Hole 1221A.

Core, section, interval (cm)	Depth (mbsf)	pH	Alkalinity (mM)	Salinity	Cl (mM)	Na (mM)	K (mM)	Ca (mM)	Mg (mM)	SO_4 (mM)	NH_4 (μM)	H_4SiO_4 (μM)	Sr (μM)	Li (μM)	Mn (μM)	B (μM)
199-1221A-																
1H-3, 145–150	4.45	7.36	2.53	34.5	551	485	10.5	9.7	47.9	28.6	7.3	388	81	28	2.39	442
2H-3, 145–150	13.95	7.40	2.86	34.5	552	488	10.1	9.8	47.2	28.5	8.7	580	83	28	2.42	441
3H-3, 145–150	23.45	7.32	2.79	34.5	555	490	10.9	9.7	47.3	28.8	4.4	670	82	31	3.32	476
4H-3, 145–150	32.95	7.31	2.93	35.0	556	489	10.2	10.0	48.4	29.0	4.4	623	83	28	2.38	438
5H-3, 145–150	42.45	7.21	2.98	35.5	559	496	10.0	9.9	47.8	29.8	7.3	626	83	26	2.33	420
6H-3, 145–150	51.95	7.33	2.93	35.5	561	496	10.5	10.0	47.9	29.4	2.9	642	82	30	2.58	442
9H-3, 145–150	80.41	7.33	3.20	35.5	564	496	10.5	10.3	49.0	29.2	5.8	684	85	29	2.66	443
12H-3, 145–150	108.95	7.30	2.86	35.5	564	501	10.3	10.0	47.1	29.3	11.6	902	84	29	2.87	448

Note: This table is also available in **ASCII.**

Table T11. Bulk sediment data, Holes 1221A, 1221B, and 1221C.

Core, section, interval (cm)	Depth (mbsf)	Si (wt%)	Al (wt%)	Ti (wt%)	Fe (wt%)	Mn (wt%)	Ca (wt%)	Mg (wt%)	P (wt%)	Sr (ppm)	Ba (ppm)
199-1221A-											
1H-4, 73–74	5.23	21.62	1.34	0.06	0.79	0.16	12.67	0.79	0.15	768.14	2,656.52
1H-6, 73–74	8.23	11.57	2.10	0.07	1.29	0.25	30.69	0.89	0.17	1,219.78	1,940.34
2H-3, 73–74	13.23	30.84	2.40	0.10	1.81	0.29	0.69	1.41	0.24	144.28	2,725.65
2H-5, 73–74	16.23	30.61	2.15	0.08	1.70	0.31	0.29	0.85	0.21	114.25	2,234.13
2H-6, 73–75	17.73	32.13	1.94	0.08	1.85	0.30	0.73	1.01	0.21	131.99	2,780.81
3H-2, 73–74	21.23	30.63	2.12	0.08	2.09	0.16	0.97	1.04	0.27	119.48	2,055.01
3H-4, 73–74	24.23	29.86	1.94	0.10	1.88	0.44	0.46	1.29	0.34	141.44	2,852.72
3H-6, 73–74	27.23	31.26	2.04	0.08	2.24	0.40	1.53	1.36	0.30	176.02	3,426.53
4H-6, 73–74	36.73	32.24	0.72	0.03	1.07	0.23	BD	0.68	0.08	71.54	1,022.65
5H-2, 73–74	40.23	31.44	0.74	0.04	1.21	0.19	0.20	0.53	0.12	83.74	1,469.09
5H-4, 73–74	43.23	32.71	0.73	0.04	1.31	0.25	BD	0.73	0.11	101.40	2,374.21
5H-6, 73–74	46.23	30.34	1.22	0.06	2.43	0.54	0.55	1.18	0.21	142.22	2,939.45
6H-3, 74–75	51.24	31.37	0.97	0.04	1.97	0.34	BD	0.82	0.17	109.33	2,230.85
6H-5, 74–75	54.24	32.79	1.01	0.05	2.29	0.35	BD	0.99	0.17	98.40	1,557.82
7H-2, 74–75	59.24	32.59	0.86	0.04	2.05	0.39	0.36	1.05	0.16	114.65	2,053.01
7H-4, 74–75	62.24	33.12	0.69	0.04	1.76	0.40	0.29	1.03	0.14	121.94	2,635.53
7H-6, 77–78	65.27	34.40	0.57	0.03	1.52	0.26	0.24	0.83	0.15	82.55	1,631.48
8H-2, 73–74	68.73	32.57	0.40	0.03	1.28	0.28	BD	0.63	0.10	95.98	2,134.26
8H-4, 73–74	71.73	33.99	0.68	0.04	1.42	0.33	0.12	0.90	0.12	118.14	3,063.30
8H-6, 73–74	74.73	32.39	0.53	0.02	1.38	0.30	0.00	0.86	0.09	86.29	1,727.79
9H-2, 73–74	78.19	33.46	0.66	0.04	2.01	0.40	0.31	0.96	0.10	97.38	1,415.17
9H-4, 69–70	81.15	33.43	0.64	0.03	1.69	0.35	0.19	0.80	0.18	104.68	2,591.08
9H-5, 54–55	82.00	31.40	0.71	0.04	2.11	0.40	0.18	0.94	0.15	100.30	2,069.89
10H-2, 73–74	87.73	33.63	0.68	0.03	1.77	0.39	0.23	0.88	0.13	111.18	2,507.31
10H-4, 73–74	90.73	37.84	0.71	0.04	1.65	0.31	0.30	0.86	0.15	118.21	2,990.71
10H-6, 72–73	93.72	31.88	0.68	0.03	1.91	0.39	0.29	0.93	0.15	111.77	2,965.64
11H-4, 73–74	100.23	33.95	0.64	0.03	1.95	0.25	BD	0.88	0.14	102.07	1,991.65
11H-6, 73–74	103.23	34.16	0.50	0.03	1.21	0.32	0.02	0.58	0.12	87.27	2,044.20
199-1221B-											
1H-2, 73–74	2.23	9.65	1.16	0.04	0.67	0.15	27.40	0.49	0.12	1,295.80	1,691.35
199-1221C-											
6X-2, 73–74	104.73	27.02	0.70	0.04	1.92	0.30	0.41	0.84	0.22	103.05	2,259.67
11X-3, 10–12.5	153.50	2.45	0.47	0.01	0.36	0.08	58.16*	0.53	0.12	1,222.24	5,088.92
11X-3, 20–22.5	153.60	2.88	0.64	0.02	0.48	0.09	47.24*	0.56	0.15	1,034.76	6,122.57
11X-3, 40–42.5	153.80	2.87	0.61	0.03	0.43	0.07	34.76	0.44	0.16	990.86	5,665.19
11X-3, 42.5–45	153.82	2.95	0.56	0.02	0.40	0.08	45.27*	0.43	0.19	993.98	5,807.29
11X-3, 45–47.5	153.85	3.43	0.69	0.02	0.42	0.10	50.49*	0.50	0.21	1,044.09	6,868.51
11X-3, 47.5–50	153.88	4.02	0.84	0.03	0.64	0.13	41.10*	0.51	0.27	1,120.83	7,955.54
11X-3, 50–52.5	153.90	6.74	1.42	0.06	1.01	0.20	32.50	0.68	0.36	967.13	11,673.13
11X-3, 52.5–55	153.93	9.87	2.15	0.10	1.55	0.48	31.13	1.10	0.46	873.48	12,995.66
11X-3, 55–57.5	153.95	9.26	2.09	0.09	1.51	0.56	27.57	1.03	0.52	798.11	12,568.04
11X-3, 60–62.5	154.00	16.34	3.82	0.12	1.37	0.38	1.13	1.31	0.37	509.12	20,098.18
11X-3, 62.5–67.5	154.02	17.35	4.13	0.17	1.78	0.32	1.84	1.49	0.64	637.38	25,308.22
11X-3, 67.5–70	154.07	18.94	4.14	0.19	2.24	2.53	2.28	1.81	0.54	690.11	19,220.07
11X-3, 70–72.5	154.10	16.25	3.69	0.20	2.99	10.76	1.34	2.34	0.29	577.98	11,276.49
11X-3, 72.5–75	154.12	16.55	3.39	0.19	3.26	7.98	0.16	1.71	0.19	234.36	3,570.02
11X-3, 75–77.5	154.15	20.49	4.41	0.25	2.08	1.26	0.53	1.28	0.25	231.79	3,847.46
11X-3, 77.5–80	154.18	15.98	3.44	0.14	2.67	0.30	2.57	1.19	0.85	476.39	16,482.49
11X-3, 80–82.5	154.20	16.04	3.56	0.15	3.29	0.07	1.26	1.20	0.92	459.64	15,956.11
11X-3, 82.5–85	154.23	16.13	3.54	0.16	3.42	0.08	2.47	1.16	0.90	463.43	15,108.48
11X-3, 85–87.5	154.25	15.84	3.72	0.15	3.89	0.10	3.46	1.35	0.98	460.88	13,513.79
11X-3, 87.5–90	154.27	16.39	4.00	0.15	3.54	0.05	10.31	1.28	0.90	523.78	14,064.87
11X-3, 90–92.5	154.30	12.07	2.85	0.12	2.89	0.05	21.04	1.00	0.75	701.99	9,415.39
11X-3, 92.5–95	154.32	11.57	2.39	0.10	2.58	0.04	13.27	0.88	0.62	630.76	8,175.47
11X-3, 95–97.5	154.35	12.55	2.89	0.11	2.42	0.05	17.13	0.86	0.77	643.37	8,280.41
11X-3, 97.5–100	154.38	13.55	3.55	0.13	3.15	0.08	26.52	1.17	0.91	716.65	8,784.96
11X-3, 100–102.5	154.40	12.81	2.84	0.12	2.58	0.29	13.55	0.92	0.74	557.99	8,804.62
11X-3, 102.5–105	154.43	11.88	2.69	0.12	2.73	0.33	23.82	1.21	0.79	708.30	7,744.29
11X-3, 105–107.5	154.45	12.11	2.86	0.12	2.49	0.25	22.34	1.04	0.68	698.18	8,395.05
11X-3, 107.5–110	154.48	11.04	2.48	0.10	2.38	0.26	30.87	1.12	0.73	863.68	8,117.07
11X-3, 117–119.5	154.57	6.73	1.35	0.06	1.20	0.18	32.63	0.54	0.37	854.51	6,407.11
11X-3, 127–129.5	154.67	6.22	1.35	0.05	1.13	0.09	43.43*	0.67	0.33	998.86	5,720.42
11X-3, 137–139.5	154.77	8.10	1.54	0.08	1.75	0.32	24.71	0.55	0.39	759.56	7,624.00
11X-CC, 9–11.5	154.91	11.14	2.53	0.10	2.74	0.53	25.63	0.92	0.59	721.14	9,494.12
12X-CC, 3–3	156.15	22.82	7.50	0.70	6.57	0.12	7.94	4.24	0.06	126.68	15.52

Notes: * = calcium values higher than 35.9 wt% are out of range of the standards (see **"Geochemistry,"** p. 20, in the "Explanatory Notes" chapter). BD = below detection limit. This table is also available in **ASCII.** [**N1**]

Table T12. $CaCO_3$ and C_{org}, Holes 1221A, 1221B, and 1221C.

Core, section, interval (cm)	Depth (mbsf)	$CaCO_3$ (wt%)	Organic C (wt%)	$CaCO_3$ (wt%)*
199-1221A-				
1H-4, 73–74	5.23	29.72	0.16	30.30
1H-6, 73–74	8.23	54.76		76.16
2H-3, 73–74	13.23	0.31		–0.20
2H-5, 73–74	16.23	0.23	0.01	–1.22
2H-6, 73–75	17.73	0.18		–0.09
3H-2, 73–74	21.23	0.23		0.51
3H-4, 73–74	24.23	0.22	0.01	–0.79
3H-6, 73–74	27.23	0.22		1.94
4H-2, 73–74	30.73	0.17		
4H-4, 73–74	33.73	0.21	0.01	
4H-6, 73–74	36.73	0.14		
5H-2, 73–74	40.23	0.21		–1.47
5H-4, 73–74	43.23	0.16	0.01	
5H-6, 73–74	46.23	0.21		–0.58
6H-3, 74–75	51.24	0.22		
6H-5, 74–75	54.24	0.21		
7H-2, 74–75	59.24	0.12		–1.06
7H-4, 74–75	62.24	0.20	0.00	–1.24
7H-6, 77–78	65.27	0.14		–1.37
8H-2, 73–74	68.73	0.09		
8H-4, 73–74	71.73	0.14	0.00	–1.67
8H-6, 73–74	74.73	0.11		–1.98
9H-2, 73–74	78.19	0.13	0.00	–1.18
9H-4, 69–70	81.15	0.20		–1.49
9H-5, 54–55	82.00	0.13		–1.49
10H-2, 73–74	87.73	0.14		–1.37
10H-4, 73–74	90.73	0.13	0.01	–1.2
10H-6, 72–73	93.72	0.17		–1.24
11H-4, 73–74	100.23	0.12	0.02	
11H-6, 73–74	103.23	0.12		–1.93
199-1221B-				
1H-2, 73–74	2.23	64.37		
199-1221C-				
6X-2, 73–74	104.73	0.23		

Notes: * = calculated from Ca (wt%), when Ca (wt%) and salt content data were available. This table is also available in **ASCII.**

Table T13. MAD measurements, Holes 1221A, 1221B, and 1221C.

Core, section, interval (cm)	Depth (mbsf)	Water content (%)	Density (g/cm³)			Porosity (%)
			Wet bulk	Dry bulk	Grain	
199-1221A-						
1H-4, 75–77	5.25	71.2	1.22	0.35	2.34	84.9
1H-5, 75–77	6.75	70.7	1.24	0.36	2.47	85.3
1H-6, 75–77	8.25	63.2	1.32	0.49	2.62	81.5
1H-7, 44–46	9.44	66.8	1.24	0.41	2.18	81.1
2H-1, 75–77	10.25	66.5	1.25	0.42	2.23	81.2
2H-2, 75–77	11.75	72.1	1.20	0.33	2.13	84.3
2H-3, 75–77	13.25	76.1	1.18	0.28	2.24	87.5
2H-4, 75–77	14.75	76.3	1.18	0.28	2.23	87.5
2H-5, 75–77	16.25	76.4	1.18	0.28	2.25	87.7
2H-6, 75–77	17.75	75.9	1.18	0.28	2.22	87.3
2H-7, 36–38	18.86	76.4	1.17	0.28	2.20	87.4
3H-1, 75–77	19.75	74.3	1.19	0.31	2.24	86.4
3H-2, 75–77	21.25	75.0	1.19	0.30	2.24	86.8
3H-3, 75–77	22.75	74.7	1.19	0.30	2.27	86.7
3H-4, 75–77	24.25	74.3	1.19	0.31	2.28	86.5
3H-5, 75–77	25.75	76.6	1.17	0.27	2.15	87.3
3H-6, 75–77	27.25	76.5	1.18	0.28	2.25	87.7
3H-7, 33–35	28.33	75.3	1.18	0.29	2.18	86.6
4H-1, 75–77	29.25	78.0	1.16	0.26	2.20	88.4
4H-2, 75–77	30.75	77.8	1.16	0.26	2.15	88.0
4H-3, 75–77	32.25	77.6	1.16	0.26	2.18	88.1
4H-4, 75–77	33.75	78.3	1.16	0.25	2.14	88.3
4H-5, 75–77	35.25	77.5	1.16	0.26	2.21	88.1
4H-6, 75–77	36.75	79.5	1.15	0.24	2.19	89.3
5H-1, 75–77	38.75	77.9	1.16	0.26	2.17	88.2
5H-2, 75–77	40.25	79.0	1.15	0.24	2.16	88.8
5H-3, 75–77	41.75	77.3	1.16	0.26	2.14	87.7
5H-4, 75–77	43.25	77.4	1.16	0.26	2.15	87.8
5H-5, 75–77	44.75	78.1	1.16	0.25	2.22	88.5
5H-6, 75–77	46.25	77.1	1.17	0.27	2.21	87.9
5H-7, 35–37	47.35	76.7	1.17	0.27	2.18	87.5
6H-3, 75–77	51.25	78.4	1.16	0.25	2.28	89.0
6H-4, 75–77	52.75	78.5	1.16	0.25	2.24	88.9
6H-5, 75–77	54.25	76.0	1.18	0.28	2.21	87.2
6H-6, 75–77	55.75	77.6	1.16	0.26	2.15	87.9
6H-7, 35–37	56.85	78.0	1.16	0.26	2.22	88.5
7H-1, 100–102	58.00	78.9	1.16	0.24	2.21	89.0
7H-2, 76–78	59.26	78.2	1.15	0.25	2.12	88.1
7H-3, 80–82	60.80	78.0	1.16	0.26	2.19	88.4
7H-4, 75–77	62.25	78.6	1.15	0.25	2.12	88.4
7H-5, 77–79	63.77	78.8	1.16	0.25	2.20	88.9
7H-6, 78–80	65.28	78.3	1.16	0.25	2.13	88.2
7H-7, 50–52	66.50	75.9	1.17	0.28	2.13	86.7
8H-1, 75–77	67.25	79.4	1.15	0.24	2.10	88.8
8H-2, 75–77	68.75	78.4	1.16	0.25	2.20	88.6
8H-3, 75–77	70.25	78.2	1.15	0.25	2.03	87.7
8H-4, 75–77	71.75	78.8	1.14	0.24	1.90	87.3
8H-5, 78–80	73.28	78.1	1.14	0.25	1.96	87.2
8H-6, 75–77	74.75	78.8	1.14	0.24	1.99	87.9
8H-7, 25–27	75.75	76.3	1.17	0.28	2.15	87.1
9H-1, 75–77	76.75	77.8	1.16	0.26	2.10	87.8
9H-2, 75–77	78.21	77.0	1.15	0.27	1.98	86.6
9H-3, 75–77	79.71	76.5	1.17	0.27	2.12	87.1
9H-4, 70–72	81.16	76.6	1.16	0.27	2.04	86.7
9H-5, 55–57	82.01	74.2	1.17	0.30	1.96	84.6
10H-1, 77–79	86.27	77.0	1.17	0.27	2.22	87.9
10H-2, 75–77	87.75	76.0	1.17	0.28	2.06	86.5
10H-3, 75–77	89.25	75.8	1.17	0.28	2.14	86.7
10H-4, 75–77	90.75	75.3	1.17	0.29	2.08	86.1
10H-5, 75–77	92.25	71.5	1.21	0.35	2.21	84.4
10H-6, 75–77	93.75	76.1	1.17	0.28	2.17	87.1
11H-4, 75–77	100.25	77.2	1.16	0.27	2.11	87.5
11H-5, 75–77	101.75	75.9	1.18	0.28	2.26	87.4
11H-6, 75–77	103.25	78.3	1.16	0.25	2.19	88.6
11H-7, 41–43	104.41	69.6	1.22	0.37	2.16	82.8
199-1221B-						
1H-1, 75–77	0.75	87.3	1.11	0.14	2.46	94.3
1H-2, 75–77	2.25	59.6	1.37	0.56	2.77	80.0
1H-3, 75–77	3.75	71.2	1.24	0.36	2.60	86.3
199-1221C-						
6X-1, 78–80	103.28	79.0	1.15	0.24	2.13	88.7
6X-2, 75–77	104.75	78.5	1.15	0.25	2.12	88.3
6X-3, 67–69	106.17	75.6	1.18	0.29	2.24	87.1
11X-1, 48–50	150.88	30.4	1.81	1.26	2.72	53.7

Note: This table is also available in **ASCII.** [**N1**]

Table T14. LAS-based mineralogy, Holes 1221A and 1221B.

Core, section, interval (cm)	Depth (mbsf)	Calcite (model wt%)	Opal (model wt%)	Smectite (model wt%)	Illite (model wt%)
199-1221A-					
1H-4, 23–25	4.74	45.46	41.87	5.92	6.75
1H-4, 75–77	5.26	38.44	48.45	13.10	0.00
1H-5, 23–25	6.24	36.51	49.49	7.12	6.89
1H-5, 75–77	6.76	29.36	34.12	36.52	0.00
1H-6, 23–25	7.74	56.86	20.91	7.62	14.60
1H-6, 75–77	8.26	70.10	11.03	16.41	2.46
1H-7, 23–25	9.24	25.32	0.00	74.68	0.00
1H-7, 44–46	9.45	0.00	12.17	87.83	0.00
2H-1, 75–77	10.26	0.00	17.59	82.41	0.00
2H-1, 123–125	10.74	0.00	12.11	87.89	0.00
2H-2, 23–25	11.24	0.00	9.37	90.63	0.00
2H-2, 75–77	11.75	0.00	16.09	83.91	0.00
2H-3, 23–25	12.74	24.64	35.58	34.84	4.94
2H-3, 75–77	13.26	8.74	49.07	42.20	0.00
2H-4, 23–25	14.24	16.79	51.21	23.45	8.55
2H-4, 75–77	14.76	5.66	56.13	38.21	0.00
2H-5, 23–25	15.74	16.88	50.91	19.11	13.10
2H-5, 75–77	16.25	9.26	52.64	33.89	4.21
2H-6, 23–25	17.24	15.43	52.51	21.24	10.81
2H-6, 75–77	17.76	6.00	58.40	35.60	0.00
2H-7, 23–25	18.74	13.93	54.31	21.14	10.62
2H-7, 36–38	18.87	7.26	59.57	33.03	0.13
3H-1, 75–77	19.76	12.41	50.36	33.22	4.01
3H-1, 124–126	20.25	21.15	45.93	15.77	17.15
3H-2, 24–26	20.75	16.74	50.12	18.30	14.84
3H-2, 75–77	21.26	10.07	58.23	30.44	1.26
3H-3, 24–26	22.25	14.60	51.51	23.53	10.35
3H-3, 75–77	22.76	6.96	49.92	43.12	0.00
3H-4, 24–26	23.75	21.82	43.87	21.51	12.79
3H-4, 75–77	24.26	6.91	50.77	42.32	0.00
3H-5, 24–26	25.25	11.97	53.11	26.83	8.10
3H-5, 75–77	25.76	2.91	57.72	39.37	0.00
3H-6, 24–26	26.75	9.59	55.41	22.60	12.41
3H-6, 75–77	27.26	4.75	57.58	37.67	0.00
3H-7, 24–26	28.25	10.94	55.41	21.34	12.31
3H-7, 33–36	28.35	3.83	58.84	37.34	0.00
4H-1, 75–77	29.26	3.95	60.60	35.46	0.00
4H-1, 123–125	29.74	9.14	61.08	18.86	10.92
4H-2, 23–25	30.24	6.18	62.60	19.85	11.36
4H-2, 75–77	30.76	0.14	64.63	35.22	0.00
4H-3, 23–25	31.74	4.16	63.63	22.77	9.44
4H-3, 75–77	32.26	0.00	66.28	33.72	0.00
4H-4, 23–25	33.24	4.57	65.04	19.28	11.11
4H-4, 75–77	33.76	0.00	68.84	31.16	0.00
4H-5, 23–25	34.74	2.33	66.35	22.69	8.63
4H-5, 75–77	35.26	0.00	66.60	33.40	0.00
4H-6, 23–25	36.24	0.00	66.42	28.28	5.29
4H-6, 75–77	36.76	0.00	65.95	34.05	0.00
5H-1, 75–77	38.76	0.00	64.62	35.38	0.00
5H-1, 122–124	39.23	0.00	67.84	28.05	4.11
5H-2, 23–25	39.74	0.00	69.55	26.70	3.75
5H-2, 75–77	40.26	0.00	61.16	38.84	0.00
5H-3, 23–25	41.24	0.00	65.60	33.25	1.15
5H-3, 75–77	41.76	0.00	60.96	39.04	0.00
5H-4, 23–25	42.74	5.86	66.97	19.50	7.67
5H-4, 75–77	43.26	4.56	67.98	27.46	0.00
5H-5, 23–25	44.24	11.03	57.73	19.65	11.59
5H-5, 75–77	44.76	0.00	56.02	43.98	0.00
5H-6, 23–25	45.74	8.66	53.66	33.23	4.45
5H-6, 75–77	46.26	0.00	51.76	48.24	0.00
5H-7, 23–25	47.24	9.52	54.40	29.62	6.45
5H-7, 35–37	47.36	0.01	57.14	42.84	0.00
6H-3, 75–77	51.26	0.00	52.06	47.94	0.00
6H-4, 23–25	52.24	1.45	59.12	39.43	0.00
6H-4, 75–77	52.76	0.00	52.85	47.15	0.00
6H-5, 23–25	53.74	0.00	60.54	39.46	0.00
6H-5, 75–77	54.26	0.00	52.78	47.22	0.00
6H-6, 23–25	55.24	0.00	61.10	36.91	1.99
6H-6, 75–77	55.76	0.00	56.94	43.06	0.00
6H-7, 23–25	56.74	0.00	61.96	38.04	0.00
6H-7, 35–37	56.86	0.00	52.62	47.38	0.00
7H-1, 100–102	58.01	0.00	53.27	46.73	0.00
7H-1, 119–122	58.21	0.00	58.04	41.96	0.00
7H-2, 23–25	58.74	0.00	57.64	42.36	0.00
7H-2, 76–78	59.27	0.00	57.87	42.13	0.00
7H-3, 23–25	60.24	0.00	60.96	39.04	0.00
7H-3, 80–82	60.81	0.00	55.26	44.74	0.00
7H-4, 23–25	61.74	0.00	57.73	42.27	0.00
7H-4, 75–77	62.26	0.00	54.30	45.70	0.00
7H-5, 23–25	63.24	0.00	57.40	42.60	0.00
7H-5, 77–79	63.78	0.00	51.63	48.37	0.00
7H-6, 23–25	64.74	0.00	61.30	38.70	0.00
7H-6, 78–80	65.29	0.00	54.56	45.44	0.00
7H-7, 23–25	66.24	0.00	62.68	37.32	0.00
7H-7, 50–52	66.51	0.00	57.62	42.38	0.00
8H-1, 75–77	67.26	0.00	56.05	43.95	0.00
8H-1, 124–126	67.75	0.00	64.58	35.42	0.00
8H-2, 23–25	68.24	0.00	59.44	40.56	0.00
8H-2, 75–77	68.76	0.00	57.29	42.71	0.00
8H-3, 23–25	69.74	0.00	59.21	40.79	0.00
8H-3, 75–77	70.26	0.00	55.78	44.22	0.00
8H-4, 23–25	71.24	0.00	62.72	37.28	0.00
8H-4, 75–77	71.76	0.00	58.14	41.86	0.00
8H-5, 23–25	72.74	0.00	60.98	39.02	0.00
8H-5, 78–80	73.29	0.00	59.47	40.53	0.00
8H-6, 23–25	74.24	0.00	63.31	36.69	0.00
8H-6, 75–77	74.76	0.00	56.50	43.50	0.00
8H-7, 23–25	75.74	0.00	62.77	37.23	0.00
8H-7, 25–27	75.76	0.00	58.44	41.56	0.00
9H-1, 75–77	76.76	0.00	55.96	44.04	0.00
9H-1, 131–133	77.32	0.00	59.44	40.56	0.00
9H-2, 23–25	77.70	0.00	58.89	41.11	0.00
9H-2, 75–77	78.22	0.00	54.88	45.12	0.00
9H-3, 23–25	79.20	0.00	54.83	45.17	0.00
9H-3, 75–77	79.72	0.00	50.29	49.71	0.00
9H-4, 23–25	80.70	0.00	57.78	42.22	0.00
9H-4, 70–72	81.17	0.00	54.27	45.73	0.00
9H-5, 23–25	81.70	0.00	53.07	46.93	0.00
9H-5, 55–57	82.02	0.00	55.66	44.34	0.00
10H-1, 77–79	86.28	0.00	53.90	46.10	0.00
10H-1, 123–125	86.74	0.00	54.34	45.66	0.00
10H-2, 23–25	87.24	0.00	57.02	42.98	0.00
10H-2, 75–77	87.76	0.00	55.86	44.14	0.00
10H-3, 23–25	88.74	0.00	59.02	40.98	0.00
10H-3, 75–77	89.26	0.00	55.31	44.69	0.00
10H-4, 23–25	90.24	0.00	64.46	35.54	0.00
10H-4, 75–77	90.76	0.00	56.07	43.93	0.00
10H-5, 23–25	91.74	0.00	62.39	37.61	0.00
10H-5, 75–77	92.26	0.00	55.43	44.57	0.00
10H-6, 23–25	93.24	0.00	55.59	44.41	0.00
10H-6, 75–77	93.76	0.00	54.47	45.53	0.00
11H-4, 23–25	99.74	0.00	60.42	39.58	0.00
11H-4, 75–77	100.26	0.00	56.17	43.83	0.00
11H-5, 23–25	101.24	0.00	62.88	37.12	0.00
11H-5, 75–77	101.76	0.00	59.49	40.51	0.00
11H-6, 23–25	102.74	0.00	60.06	39.94	0.00
11H-6, 75–77	103.26	0.00	58.50	41.50	0.00
11H-7, 23–25	104.24	0.00	59.15	40.85	0.00
11H-7, 41–43	104.42	0.00	59.75	40.25	0.00
199-1221B-					
1H-1, 6–8	0.07	25.49	14.16	0.00	60.34
1H-1, 75–77	0.76	17.41	48.20	32.37	2.02
1H-1, 88–90	0.89	21.74	45.54	28.32	4.40
1H-2, 23–25	1.74	77.03	8.83	4.23	9.92
1H-2, 75–77	2.26	70.23	19.13	2.04	8.61
1H-3, 23–25	3.24	50.11	39.38	6.30	4.20
1H-3, 75–77	3.76	43.03	43.11	13.25	0.61

Note: This table is also available in **ASCII.** [**N1**]

Table T15. Split-core velocity measurements, Holes 1221A, 1221B, and 1221C.

Core, section, interval (cm)	Depth (mbsf)	Velocity x* (m/s)
199-1221A-		
1H-1, 76	0.76	1,535
1H-2, 76	2.26	1,516
1H-3, 76	3.76	1,536
1H-4, 76	5.26	1,529
1H-5, 76	6.76	1,539
1H-6, 76	8.26	1,504
1H-7, 45	9.45	1,515
2H-1, 76	10.26	1,524
2H-2, 76	11.76	1,519
2H-3, 76	13.26	1,546
2H-4, 76	14.76	1,546
2H-5, 76	16.26	1,543
2H-6, 76	17.76	1,555
2H-7, 37	18.87	1,557
3H-1, 76	19.76	1,558
3H-2, 76	21.26	1,542
3H-3, 76	22.76	1,543
3H-4, 76	24.26	1,545
3H-5, 76	25.76	1,545
3H-6, 76	27.26	1,549
3H-7, 34	28.34	1,547
4H-1, 76	29.26	1,556
4H-2, 76	30.76	1,556
4H-3, 76	32.26	1,563
4H-4, 76	33.76	1,568
4H-5, 76	35.26	1,565
4H-6, 76	36.76	1,573
5H-1, 76	38.76	1,559
5H-2, 76	40.26	1,554
5H-3, 76	41.76	1,559
5H-4, 76	43.26	1,569
5H-5, 75	44.76	1,577
5H-6, 76	46.26	1,573
5H-7, 36	47.36	1,565
6H-3, 76	51.26	1,562
6H-4, 77	52.77	1,567
6H-5, 76	54.26	1,571
6H-6, 76	55.76	1,569
6H-7, 36	56.86	1,570
7H-1, 101	58.01	1,571
7H-2, 77	59.27	1,556
7H-3, 81	60.81	1,560
7H-4, 76	62.26	1,560
7H-5, 78	63.78	1,584
7H-6, 79	65.29	1,572
7H-7, 52	66.52	1,569
8H-1, 76	67.26	1,555
8H-2, 76	68.76	1,550
8H-3, 76	70.26	1,553
8H-4, 76	71.76	1,566
8H-5, 79	73.29	1,568
8H-6, 76	74.76	1,579
8H-7, 26	75.76	1,578
9H-1, 76	76.76	1,562
9H-2, 77	78.23	1,564
9H-3, 76	79.72	1,562
9H-4, 71	81.17	1,577
9H-5, 56	82.02	1,584
10H-1, 78	86.28	1,565
10H-2, 76	87.76	1,568
10H-3, 76	89.26	1,569
10H-4, 76	90.76	1,567
10H-5, 76	92.26	1,567
10H-6, 76	93.76	1,586
11H-4, 76	100.26	1,572
11H-5, 76	101.76	1,553
11H-6, 76	103.26	1,546
11H-7, 42	104.42	1,560
199-1221B-		
1H-1, 76	0.76	1,539
1H-2, 76	2.26	1,514
1H-3, 76	3.76	1,533
199-1221C-		
6X-1, 79	103.29	1,557
6X-2, 76	104.76	1,545
6X-3, 69	106.19	1,555
11X-1, 49	150.89	16,102†

Notes: * = determined by insertion probe, † = determined by contact probe. This table is also available in **ASCII.**

Table T16. Thermal conductivity, Holes 1221A and 1221B.

Core, section, interval (cm)	Depth (mbsf)	Thermal conductivity (W/[m·K])
199-1221A-		
2H-3, 76	13.26	0.71
3H-3, 76	22.76	0.70
4H-3, 76	32.26	0.68
5H-3, 76	41.76	0.73
6H-3, 56	51.06	0.75
7H-3, 76	60.76	0.79
8H-3, 76	70.26	0.70
9H-3, 76	79.72	0.70
10H-3, 76	89.26	0.76
199-1221B-		
1H-3, 76	3.76	0.76
2H-3, 76	8.46	0.82

Note: This table is also available in **ASCII.**

CHAPTER NOTE

N1. 13 December 2002—After the CD-ROM version of this volume was published, errors were noted in the ASCII versions of Tables T4, T8, T11, T13, and T14. This version contains the corrected ASCII files

*Dates reflect file corrections or revisions.